Journal Pre-proof


# Review of bumper materials for spacecraft shield against orbital debris hypervelocity impact

Siyuan Ren, Pinliang Zhang, Qiang Wu, Qingming Zhang, Zizheng Gong, Guangming Song, Renrong Long, Liangfei Gong, Mingze Wu

PII: S2214-9147(24)00218-6

DOI: https://doi.org/10.1016/j.dt.2024.09.002

Reference: DT 1510

To appear in: *Defence Technology*

Received Date: 7 April 2024

Revised Date: 8 August 2024

Accepted Date: 2 September 2024

# Review of bumper materials for spacecraft shield against orbital debris hypervelocity impact

Siyuan Ren [a], Pinliang Zhang [a,*], Qiang Wu [a], Qingming Zhang [b], Zizheng Gong [a], Guangming Song [a], Renrong Long [b,*], Liangfei Gong [c], Mingze Wu [b]

[a] Beijing Institute of Spacecraft Environment Engineering, China Academy of Space Technology, Beijing 100094, China

[b] State Key Laboratory of Explosion Science and Technology, Beijing Institute of Technology, Beijing 100081, China

[c] School of civil engineering, Chongqing jiaotong university, Chongqing 400074, China

***Corresponding author:** Pinliang Zhang(zhangpinliang620@126.com);
Renrong Long(longrenrong@bit.edu.cn)



* Corresponding author.
E-mail: zhangpinliang620@126.com (PL Zhang); longrenrong@bit.edu.cn (RR Long)

# Review of bumper materials for spacecraft shield against orbital debris hypervelocity impact

**Abstract**

It is widely known that the hypervelocity impact of orbital debris can cause serious damage to spacecraft, and enhancing the impact resistance is the great concern of spacecraft shield design. This paper provides a comprehensive overview of advances in the development of bumper materials for spacecraft shield applications. In particular, the protective mechanism and process of the bumper using different materials against hypervelocity impact are reviewed and discussed. The advantages and disadvantages of each material used in shield were discussed, and the performance under hypervelocity impact was given according to the specific configuration. This review provides the useful reference and basis for researchers and engineers to create bumper materials for spacecraft shield applications, and the contemporary challenges and future directions for bumper materials for spacecraft shield were presented.

**Keywords:** Orbital debris; Spacecraft shield; Hypervelocity impact; Bumper materials; Protective mechanism

## 1. Introduction

In 2023, mankind had carried out 212 space launches. With the substantial increase of space activities, the space environment has deteriorated sharply. In particular, the large-scale development of the LEO (Low Earth Orbit) constellation satellite will increase the probability of explosive growth in the number of the orbital debris [1–3]. Manned spaceflight has developed rapidly. For example, the United States had proposed the Artemis plan to return to the moon, and Chniese space station "Tian Gong" has completed in orbit assembly and entered the operational phase. The hypervelocity impact of micrometeoroid and orbital debris (MMOD) will lead to the failure or even disintegration of manned spacecraft, and it will seriously threaten the safety of manned spaceflight [4]. The James Webb Space Telescope has been impact by many micrometeoroids since its launch, and the impact on the mirror of segment C3 in May 2022 caused an uncorrectable change in its observation results [5]. In December 2022, the Progress MS-22 spacecraft was impacted by space debris, and a small hole with a diameter of about 0.8 mm appeared in the cabin near the solar wing, which led to coolant leakage [6]. The SpaceX Crew-4 mission spent nearly 170 days on the Node 2 zenith docking port of the International Space Station between April 27, 2022 and October 14, 2022. A post-flight inspection was performed on the SpaceX Dragon vehicle after the Crew-4 mission for MMOD damage. Fourteen possible MMOD impact damages were identified on the areas of the vehicle inspected [7]. Space safety has raised great concern, and it is an urgent problem to improve the protective capability of spacecraft against orbital debris [8].

Due to the low detectionable characteristics of centimeter sized debris, it is difficult for spacecraft to maneuver to avoid the impact [9–11]. Centimeter sized debris have high kinetic energy and are difficult to be shattered, which leads to serious damage to spacecraft. Protection against the impact of centimeter sized debris had become the primary aim of the development of spacecraft shield structure and material. The improvement of the protective capability of spacecraft shield depends on the development of new high impact resistant performance materials, and the primary purpose of developing improved shielding is to provide higher levels of spacecraft orbital space protection with less weight. At present, most materials can only resist the impact of projectiles with a size of less than 1 cm, and only a few materials can protect projectiles larger than 1 cm under the limitation of area density.

The impact of the projectile on the bumper will produce shock waves propagating towards the interior of the projectile and the bumper respectively, and the shock wave inside the projectile can be reflected on the back of projectile to form a tensile wave [12, 13]. The projectile will be shattered into small fragments under tensile effect, and the projectile material melts and gasifies due to the temperature rise caused by shock wave loading [14]. The melting and gasification of the material can reduce the damage of the projectile to the rear wall. After the interaction between the projectile and bumper, the fragments of the projectile and the bumper will form the debris cloud, which expands within the spacing between the bumper and the rear wall and moves towards the rear wall with a high velocity [15]. It is worth emphasizing that the primary protective mechanism of the Whipple shield is fragmentation of the projectile caused by the impact of the projectile on the bumper, rather than melting and vaporization. The hypervelocity material that has been melted and gasified will also damage the rear wall of the protective structure. The debris cloud impact a large area on the rear wall, dispersing the energy density and load density of the projectile on the rear wall. The mass distribution and motion characteristics of debris cloud determine its damage to the rear wall [16–18]. The density, strength, modulus, hardness, melting temperature and gasification temperature of bumper materials have an important influence on the projectile-bumper interaction process and subsequent debris cloud. Therefore, the selection of bumper material plays an important role in the research and development of spacecraft shield. With the rapid increase of centimeter sized orbital debris, it is expected that traditional materials will no longer meet the protection requirements. At present, a variety of advanced bumper materials have been developed to improve the shielding performance of the spacecraft shield, especially high performance materials, as shown in Fig. 1.

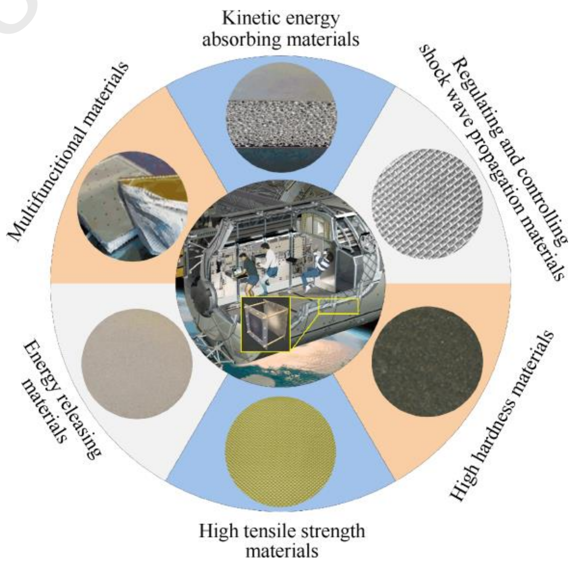


Fig. 1. The advanced bumper materials applied in spacecraft shield.

## 2. Protective structure and concept

The low velocity range is less than 1 km/s, the high velocity range is 1–3 km/s, and the hypervelocity range is ≥3 km/s. The relative impact velocity between space debris and spacecraft is 5–15 km/s, with an average of 10 km/s. In order to enable the projectile to impact the shield structure at the hypervelocity of ≥3 km/s, two-stage light-gas gun (2SLGG) and three-stage light-gas gun (3SLGG) were applied. Initially, the 2SLGG was driven by compressed gas and gunpowder [19]. In order to improve the driving capability, mixed gas detonation driving technology has been developed in recent years to achieve higher launch velocity [20]. At present, the 2SLGG can achieve the launch velocity of 2–8 km/s, while the 3SLGG can achieve the launch velocity of >10 km/s [21]. The development of light-gas gun technology and proliferation of facilities have promoted the progress of bumper materials, including the impact phenomenon caused by higher velocity and the understanding to the response characteristics of materials themselves. High speed camera technique [14, 15], transient optical testing technique [22, 23], and transient magnetic measurement technique [24, 25] can be used in hypervelocity experiments to obtain debris clouds and various radiation signals generated by projectile impacting on bumpers, in order to evaluate the physical properties of bumper materials.

**2.1. Whipple shield**

To protect spacecraft from orbital debris impacts, the Whipple shield [26] was proposed. As shown in Fig. 2, the original Whipple shield is a thin aluminum alloy bumper followed at a distance by the rear wall, and the fragmentation of the projectile depends on the pressure induced by the impact between projectile and bumper. As shown in Fig. 3(a), the shock wave induced by the impact of the projectile on the bumper can cause the projectile to be shattered. The longer duration and higher pressure of the shock wave induced by impact can causes a longer duration and stronger stress tensile wave reflected from the back of the projectile, and the projectile will suffer a longer and stronger tensile effect. The projectile will be shattered into smaller fragments under the longer tensile effect. Then, the projectile fragments and bumper fragments can form the debris cloud with high velocity, as shown in Figs. 3(b) and 3(c). This can cause the kinetic energy of the debris cloud to concentrate in the central area of the rear wall, making the central area of the rear wall bear high load density. The disadvantage of the Whipple shield is that the projectile only experiences single impact load and shatters once, resulting in insufficient fragmentation of the projectile. After the bumper is broken down, the rear wall will be exposed, and the rear wall can be damaged by solid fragments in the debris cloud.

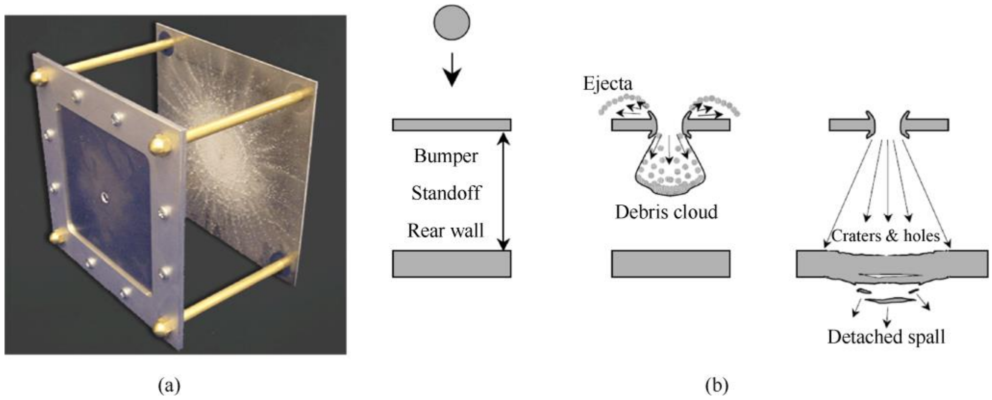


Fig. 2. Whipple shield with aluminum alloy as bumper and protective concept [26]: (a) Whipple shield; (b) Whipple shield protective concept.

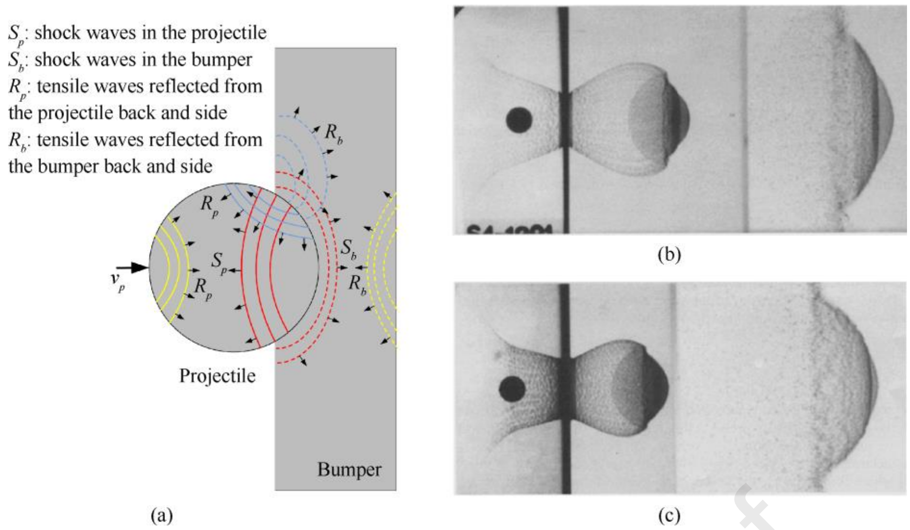


Fig. 3. Views of debris clouds produced by impact of 9.53 mm diameter, 1.275 g, Aluminum spheres with various thicknesses of Al6061 bumper. Impact velocity is 6.6 km/s [15]: (a) Interaction between projectile and bumper; (b) Debris cloud, bumper thickness is 2.225 mm; (c) Debris cloud, bumper thickness is 4.039 mm.

### 2.2. Multi-bumper shield

Although fabric materials provided the new flexible form of shield materials it did not perform any better than an equivalent mass per unit area of aluminum when used as the bumper of Whipple shield. In order to apply the protective structure to flexible fabric materials, Multi-bumper shield (MB shield) [29–31] was presented, as shown in Fig. 4. The total areal density of the bumper is certain, and the projectile is multi-impacted by increasing the layer number of the aluminum alloy bumper. Since the thickness of each layer bumper is very small, the mass of debris cloud generated is very small, and the debris cloud that needs to be intercepted by the subsequent bumper has a small mass. The aluminum alloy multi-bumper shield concept relies on the projectile and bumper fragments from the first impact being re-shocked by the second and subsequent bumpers to raise their thermal states well beyond complete melting. The rear wall deform under the impulsive loading from the final debris cloud of liquid and vapor generated by the multi-impact process, and the failure mode of the bumper under the impulsive load is usually petal tear. As shown in Fig. 5, there will be a lot of craters on the rear wall after projectile impact single aluminum alloy bumper. However, there are molten aluminum residue and vapor deposited on the rear wall after projectile impact multi-bumper with the same impact conditions. This shows that multi-bumper can more effectively shatter, melt and gasify projectile materials [28]. A large number of test results show that the multi-bumper can provide the same protective performance as Whipple shield with 20% to 30% lower weight [32]. The full play of the shielding performance of Multi-bumper shield depends on the long overall spacing available, and short overall spacing can limit the protective capability of Multi-bumper shield.

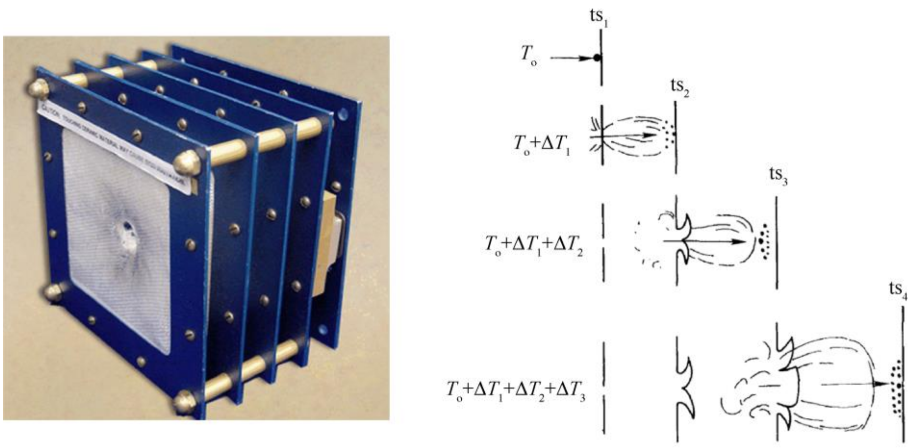


(a) (b)

Fig. 4. Multi-bumper shield with aluminum alloy as bumpers [27]: (a) Multi-bumper shield; (b) Protective mechanism of Multi-bumper shield.

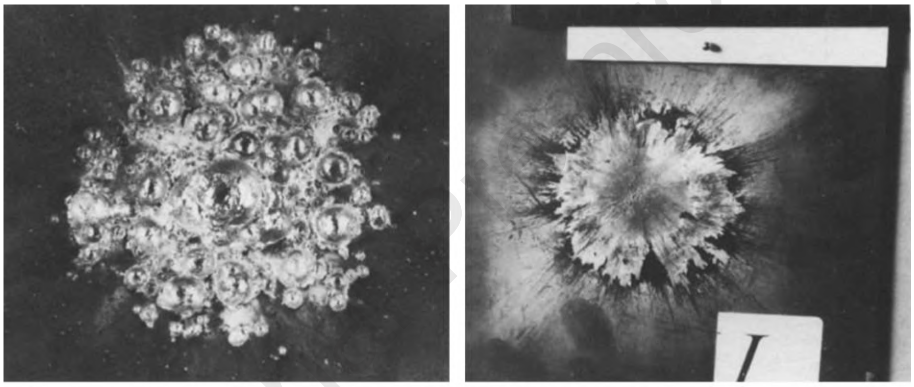

(a) (b)

Fig. 5. The debris and residue on copper witness plates induced by projectile impacting the single bumper and multi-bumper respectively [28]: (a) Impact single bumper; (b) Impact multi-bumper.

**2.3. Stuffed Whipple shield**

In order to provide effective protection for the international space station in a short overall spacing, the Stuffed Whipple shield (SW shield) was presented, and this shield includes an aluminum alloy bumper with considerable area density, a flexible intermediate layer combining fabrics with ultra high tensile strength, and a rear wall [33]. As shown in Fig. 6, the purpose of the outer aluminum bumper is to shatter the projectile into small pieces as much as possible, and the intermediate stuffed layer fabrics are used to intercept projectile fragments and aluminum alloy bumper fragments and further shatter large solid fragments. In addition, the intermediate stuffed layer can also cause the melting and gasification of solid fragments, and the intermediate stuffed layer itself does not produce hard fragments, which can lead to further reduction of rear wall damage. Generally, the spacing between the bumper and the intermediate stuffed layer needs to be greater than that between the intermediate stuffed layer and the rear wall to ensure that the debris cloud induced by the projectile impacting the bumper has enough space to expand, which can increase the area of the debris cloud impact the intermediate stuffed layer and improve the efficiency of the intermediate stuffed layer in intercepting fragments. The Stuffed Whipple shield can effectively improve the protective capability of spacecraft within a limited overall spacing.

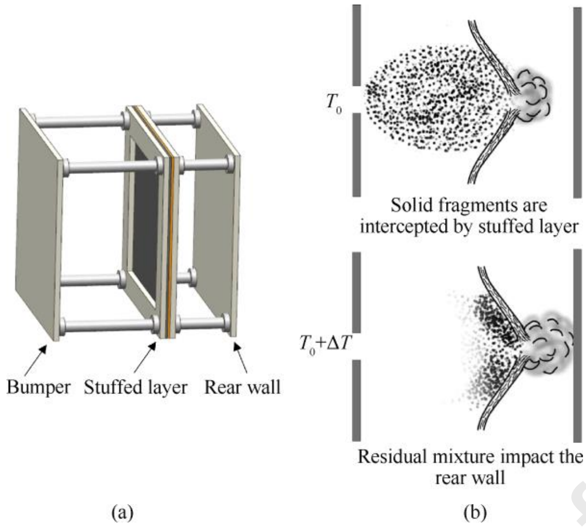


Fig. 6. The Stuffed Whipple shield and its protective mechanism: (a) Stuffed Whipple shield; (b) Protective mechanism of Stuffed Whipple shield.

## 3. Bumper materials and protective performance

### 3.1. Traditional metal materials

Initially, due to the excellent mechanical properties and low cost, metal materials were widely used in bumpers of Whipple shield, and the aluminum alloy materials were the most studied. The impact of the projectile on the metal bumper can produce high shock wave pressure, and metal materials have high crushing capacity for the projectile. Aluminum alloy plate commonly used as bumper materials include Al6061, Al2024 and AMG-6 [32. 34, 35]. The advantage of aluminum alloy is that it has high wave impedance, strength and hardness, and high pressure can be induced by impact. The disadvantage is that the density is higher than that of composite materials such as fiber fabrics, and the bumper is thinner under the limitation of limited areal density. Thinner bumper is easier to cause the shock wave in the projectile to be caught up and unloaded by the tensile wave reflected from the back of the bumper, which can reduce the duration of the shock wave inside the projectile, resulting in incomplete fragmentation of the projectile. There is a fragments concentration area at the head of the debris cloud induced by the impact of the projectile on the aluminum alloy bumper, which is easy to cause perforation of the rear wall. The initial melting threshold velocity of aluminum alloy is 4.9 km/s and the complete melting threshold velocity is 6.2 km/s, and the initial gasification threshold velocity of aluminum alloy is 9.4 km/s [36, 37]. Therefore, the projectile must impact the aluminum alloy bumper at a high velocity before melting and gasification of bumper can occur.

Schonberg [38] presented a corrugated aluminum alloy bumper enhanced shield, and the impact resistance of corrugated aluminum alloy bumper enhanced shield was studied. The results appears that a significant increase in protection against perforation by hypervelocity projectiles can be achieved if the traditional monolithic aluminum alloy bumper in a Whipple shield is replaced with a aluminum alloy corrugated bumper of equal or near-equal weight [39, 40]. Because of flat front plate of corrugated bumper, if the corrugated bumper is impacted obliquely by a hypervelocity projectile, a significant amount of damaging ricochet debris will be created. By removing the front plate and optimizing the rise angle α, creation of ricochet fragments can be reduced which can destroy external spacecraft subsystems, as shown in Figs. 7(a) and 7(b). The wave profiles of bumper can affect the direction of fragment spread, which in turn affects the damage of the rear wall, and designing reasonable waves is essential and cannot be ignored, as shown in Fig. 7(c) [41].

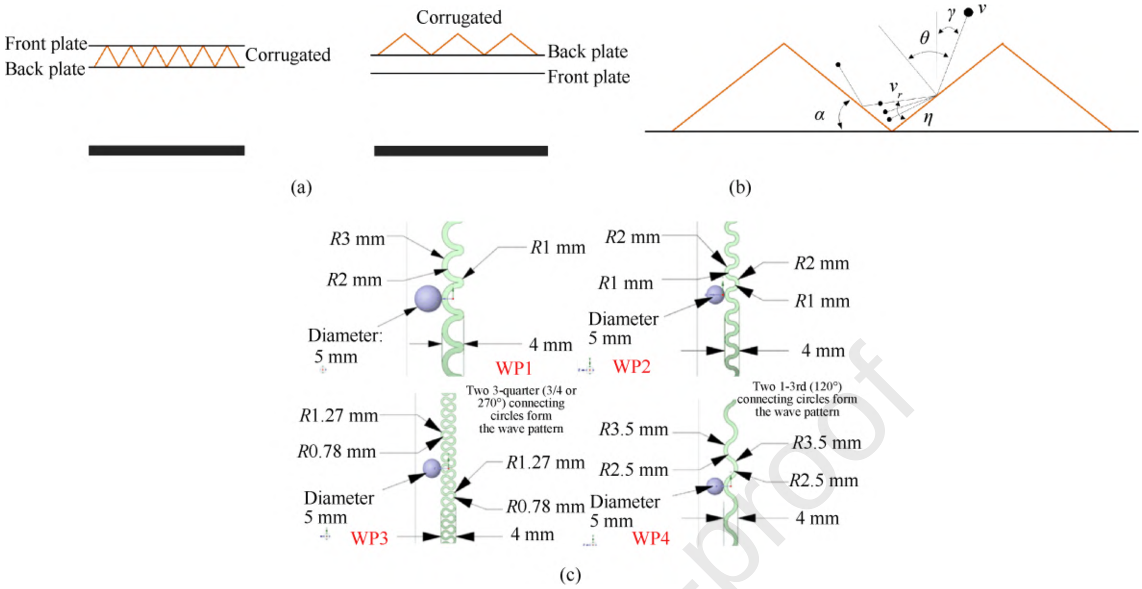


Fig. 7. The corrugated bumper enhanced shield and its optimization: (a) The corrugated aluminum alloy bumper before optimization; (b) The optimized corrugated aluminum alloy bumper; (c) The corrugated bumper with different wave profiles [41].

The damage and failure of titanium alloy and steel under hypervelocity impact were studied [42–47], and the methodology for orbital debris hypervelocity impact damage mitigation in the context of spacecraft design was discussed by studying the characteristics of debris cloud [48–51]. From the research results, the protective performance of titanium alloy is lower than that of aluminum alloy with the same weight, even though its strength is very high. Due to the large density of titanium alloy, its thickness is small under the same weight, so it cannot be used as a multi-layer bumper, and this also limits the improvement of its shielding performance. The strength of metals under hypervelocity impact was generally considered negligible, but the anisotropy of the strength of magnesium alloys still exhibited in impacts of 3.0 km/s, this caused the anisotropy in the debris cloud formation [52, 53].

For the traditional metal plate bumper, such as aluminum alloy, titanium alloy and steel plate, their hypervelocity impact resistance depends on the pressure induced by impact to shatter the projectile, and the projectile and metal bumper can produce a large number of fragments, which is favorable to reduce the rear wall damage. The rear wall is easily penetrated by the fragments concentration area at the head of the debris cloud induced by the impact of the projectile on the traditional metal plate bumper. In addition, in the velocity range of 3–7 km/s, the fragmentation caused by projectile impact on the bumper can disperse the energy density on the rear plate caused by the impact, improving the protective performance of the Whipple shield. However, as the impact velocity increases, the projectile and bumper materials will melt and vaporize, and the protective performance of the shield will also decrease with the increase of energy density on the rear plate. Traditional metal bumper themselves can also produce metal fragments during impact, which limit the further improvement of its shielding performance. Due to the low cost of traditional metal, it is widely used in the earlier Whipple shield, but the application proportion of the traditional metal plate in the bumper of some enhanced shields, such as Stuffed Whipple shield and multi-bumper shield, is reduced. Most of the traditional metal plates are only used as the first layer bumper of shield due to the requirements of the external structure of spacecraft.

**3.2. Kinetic energy absorbing materials**

Sandwich panels have been widely used in aerospace, automotive and national defense industries because of their superior properties such as high strength, high stiffness, lightweight, low cost, excellent energy absorption and impact resistance [54–58]. As shown in Fig. 8, sandwich panel consist of the front faceplate, the back faceplate and the core. There are two most widely used types: honeycomb sandwich panels and foam sandwich panels. Aluminum honeycomb is superior to foam honeycomb in specific energy absorption, which is due to the gradual folding of cell walls during crushing [59], and Aluminum honeycomb is also superior to Aluminum foam in compressive strength. In order to reduce the weight and meet the strength requirements of spacecraft, honeycomb sandwich panel was usually used as the load-bearing structure. Especially for spacecraft such as satellites, the weight or volume restrictions often prevent the inclusion of a dedicated shield for protection against the impact of orbital debris. In this case, the shield is generally provided by the primary structure commonly constructed of honeycomb core sandwich panel. The impact on the front faceplate of the sandwich panel can cause the fragmentation of the projectile, and the projectile fragments repeatedly impacts the multi-cellular wall of the honeycomb or foam core, causing the multi-cellular structure to distort, deform and tear, so as to absorb the kinetic energy of the debris cloud and stop the debris cloud particles. Multiple impacts of projectile fragments on multi-cellular structures will also cause melting and gasification the projectile and bumper materials.

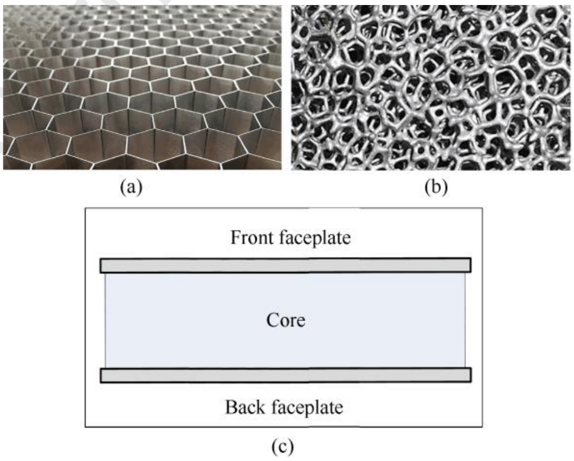


Fig. 8. Honeycomb aluminum, foam aluminum and sandwich panel: (a) Honeycomb aluminum; (b) Foam aluminum; (c) Sandwich panel.

**3.2.1. Honeycomb sandwich panel**

However, in contrast to the excellent energy absorption performance under the low velocity impact, the protective capability of honeycomb aluminum sandwich panel under the hypervelocity impact is rather poor, although their high specific strength and stiffness are ideal for structural requirements. After impacting the honeycomb aluminum sandwich panel, the cell walls of honeycomb restrict the radial expansion of debris cloud. The radial velocity of fragments in the debris cloud is gradually consumed by penetrating the cell wall, and fragments pass through the honeycomb core cell with the remaining axial velocity along the cell core. This is called the channel effect, as shown in Figs. 9(a) and 9(b). The hypervelocity impact experimental results of Whipple shield with honeycomb aluminum sandwich panel as bumper show that the debris cloud concentrated in a significantly smaller area, resulting the rear wall to bear more concentrated impact load and prone to perforation, as shown Figs. 9(d), 9(e) and 9(f). Based on the effective rear wall thickness, Taylor [60] quantified the decrease in quantified the performance degradation of Whipple shield, and the results showed that presence of honeycomb aluminum core resulted in a 50% decrease in Whipple Shield performance. By comparing the impact limit, Ryan [61] studied the influence of impact angle on the shielding performance degradation induced by the presence of honeycomb aluminum core, the performance degradation decreases with the increase of impact angle. The protective effect of the honeycomb core was quantified by Sennett and Lathrop [62], and they concluding that the thickness of the faceplate is more than twice the honeycomb cell size $D_{HC}$, the shielding capability will not increase with the increase of shielding thickness, as shown in Fig. 9(a). In order to reduce the channel effect of honeycomb aluminum on debris cloud, as shown in Fig. 9(c), Ke [63] designed a multi "Y-shaped" honeycomb aluminum core structure, the experimental results show that the "Y-shaped" core has reliable stability as the bracing structure, and it can effectively reduce the channel effect on the debris cloud. Warren [64] presented a honeycomb aluminum sandwich panel shield filled with a shear thickening fluid (STF), and the STF displayed a marked rise in viscosity with increasing shear rate above a critical shear rate. The experiments show that incorporation of STF into honeycomb aluminum core has the potential to dramatically improve the hypervelocity penetration resistance in a large velocity range. Kang [65] investigated the variation of the critical projectile diameter of honeycomb sandwich panel due to the channeling effect using smoothed particle hydrodynamics. It is revealed that the size of honeycomb core is the main parameter that has the greatest influence on the channel, and the critical projectile diameter varies with the size of the honeycomb core. Ryan and Christiansen [66] investigated the honeycomb sandwich panel with Nomex honeycomb, 3D aluminum honeycomb, and baseline aluminum materials as cores respectively through hypervelocity impact experiment, and the 3D aluminum honeycomb has excellent shielding performance because harmful channeling cells are eliminated by using the honeycomb composed of aluminum foils rotated at +45°/-45°. Schonberg [67] established a system of empirical equations to predict the number of perforations, debris cloud trajectory and spread angle induced by hypervelocity impact on honeycomb sandwich panel. Various ballistic limit equations of honeycomb sandwich panel were given through experimental and numerical simulation results [66–70], and the ballistic limit equations were improved by considering the channel effect and the relative dimensions between the projectile diameter and the honeycomb geometry [71, 72].

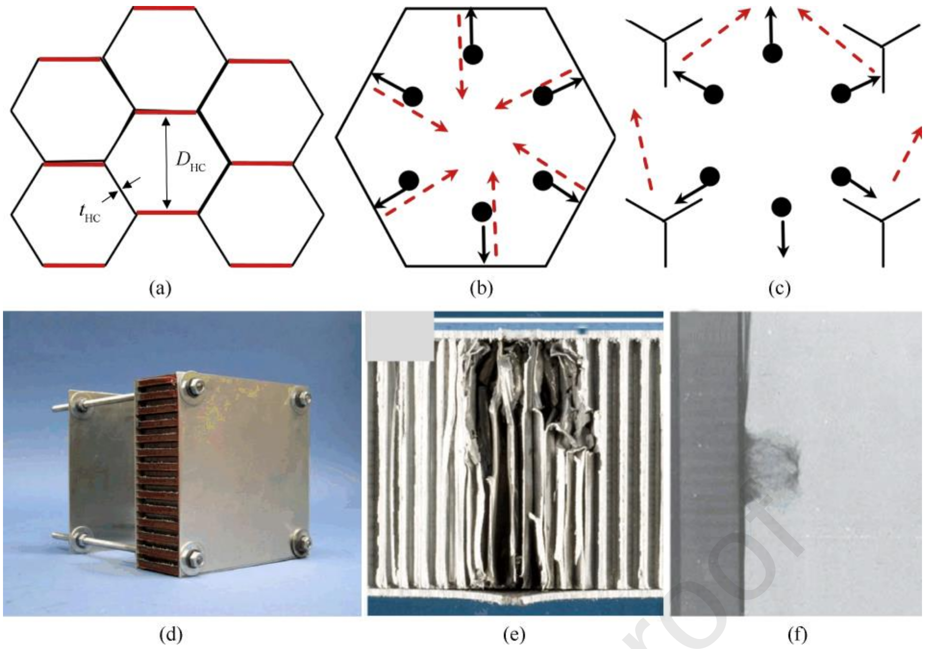


Fig. 9. The plane sketch of honeycomb aluminum congregating debris cloud and the damage of honeycomb aluminum sandwich panel under hypervelocity impact: (a) The plane sketch of honeycomb aluminum [60]; (b) The channel effect of honeycomb aluminum congregating debris cloud [63]; (c) The multi "Y-shaped" honeycomb aluminum core reduces the channel effect [63]; (d) The honeycomb aluminum sandwich panel shield [66]; (e) The damage of honeycomb aluminum sandwich panel under hypervelocity impact; (f) The debris cloud induced impacting on honeycomb aluminum sandwich panel [66].

#### 3.2.2. Foam sandwich panel

Compared with honeycomb core, the foam core has no channel effect under the hypervelocity impact, so it has better shielding performance. The bumper material of spacecraft shield usually adopts lightweight materials to meet the requirements of cost saving, and the foam sandwich panel is a suitable bumper material. A great deal of studied has been done on the low-velocity impact response of the foam sandwich panel [73–77], and there are relatively few systematic and detailed studies on hypervelocity impact of foam sandwich panel. Metallic foam, consisting of an metallic matrix with numerous bubbles, exhibits remarkable performance, for instance, low density, high specific strength, sound insulation and energy absorption [78–80]. Metallic foam is a functional material widely used in aerospace, automotive, architecture because of their unique combinations of mechanical properties [81–83]. As shown in Figs. 10(a) and 10(b), there are two competing metallic foams: open cell metallic foam and closed cell metallic foam. Although closed cell foam can retain some residual atmospheres in the cells, which may help to increase resistance to fragment penetration due to the existence of gas drag, and open cell foam is considered a more promising technology [84]. Open cell foam is usually lower in weight, and provides higher uniformity than low density closed cell foam. Ryan and Christiansen [66] have studied the influence of core characteristics (PPI: pores per linear inch, relative density and thickness) and the thickness of the faceplate on the shielding performance of the Al6061 foam core sandwich panel, as shown in Figs. 10(c), 10(d) and 10(e). The results show that the performance of foam core sandwich panels is expected to increase with increasing relative density; however, the rate of performance increase is considerably less than would be gained through adding weight to the panel faceplates; The performance of the foam core panels increased with increasing thickness, even minimal increase in the thickness of the back faceplate can substantial improve the protective capability, and the thickness of the front faceplate has little effect on the failure limit. Ryan and Christiansen [85–87] investigated the performance of metallic, ceramic, and amorphous foam sandwich panels as components of the shielding configurations according to the experimental results of projectiles hypervelocity impact on double-foam bumper shield. As shown in Fig. 11, the shielding capability of the various foam materials were ranked by the statistical analysis of the rear wall failure modes, and the result as follow (from best-to-worst): titanium > stainless steel > copper > aluminum > reticulated vitreous carbon (RVC)> silicon carbide > chromized nickel/chromium > nickel. Destefanis and Schaefer [89, 90] evaluated the alternative configurations with open-cell aluminum foam sandwich panel as bumper for the International Space Station (ISS) Columbus module shielding, and the authors concluded that the foam configuration was vulnerable to impact of large projectiles with diameter larger than 1 cm at low velocities (≤3 km/s), as the aluminum foam sandwich panel was unable to induce projectile fragmentation effectively. The damages and failure impact limits of foam aluminum sandwich panel shield were given by Yasensky and Christiansen [91]. Klavzar [92] studied the ballistic performance of hybrid metal foam sandwich panels under hypervelocity impact, and the protective performance of composite foam can be further optimized by reducing the thickness of the coating and using high-performance aluminum alloy as the base of the hybrid foam. Pasini [93] compared shielding performance of open cell aluminum foam sandwich panel shield and quadruple-layer aluminum alloy bumper shield, and the effect of projectile size on the damage process and dynamic response of foam core was studied.

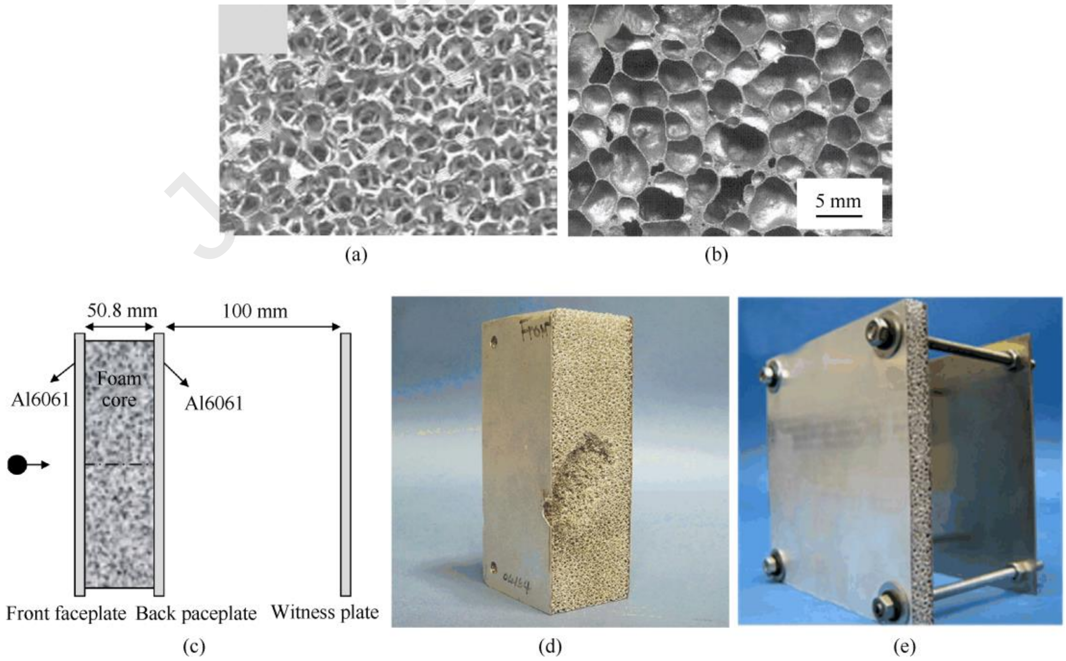


Fig. 10. The open-cell foam, close-cell foam, aluminum foam sandwich panel and aluminum foam enhanced Whipple shield [88]: (a) Open-cell foam; (b) Close-cell foam; (c) The structure of Al6061 foam core sandwich panel shield; (d) Aluminum foam sandwich panel; (e) Al6061 foam enhanced Whipple shield.

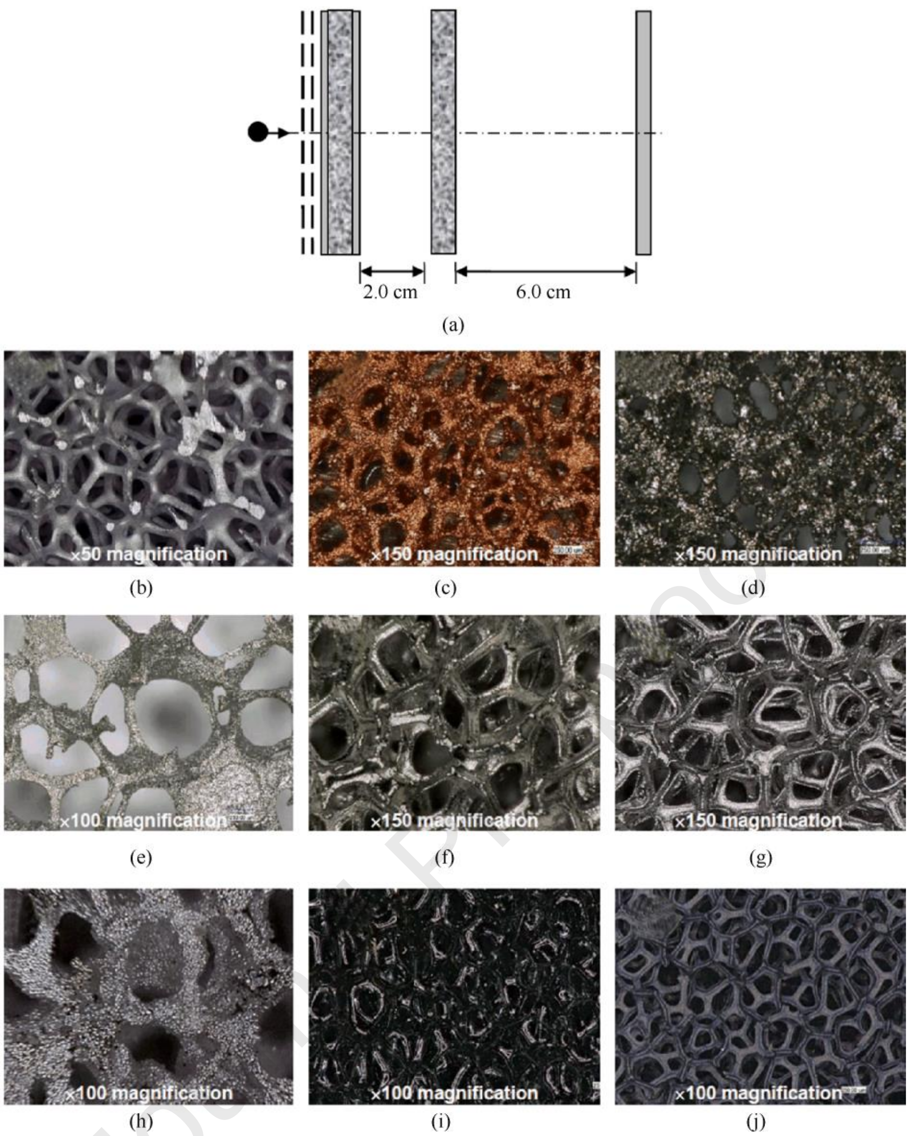


Fig. 11. The various foam materials for bumpers of shields: (a) The double-foam bumper shield [89]; (b) Aluminum foam [90]; (c) Copper foam [90]; (d) Titanium foam [90]; (e) Stainless steel foam [90]; (f) Nickel/chromium foam [90]; (g) Nickel foam [90]; (h) Ag foam [90]; (i) RVC foam [90]; (j) Silicon carbide foam [90].

For low velocity impact, to further improve their impact resistance, some researchers introduced the density gradient of graded foam as a core in the sandwich panel, finding that the negative density gradient of core assuredly improves the energy absorption capability of the panel [94–96]. As shown in Fig. 12, the shielding performance of the sandwich panel with density gradient foam core and single pore density foam core were compared by Ryan and Christiansen [66]. The results show that the sandwich panel with density gradient foam core 40/20/5 PPI was similar to the single pore density sandwich panel (40 PPI), and shielding performance of the sandwich panel with density gradient foam core 5/20/40 PPI configuration lower than the 40/20/5 PPI configuration.

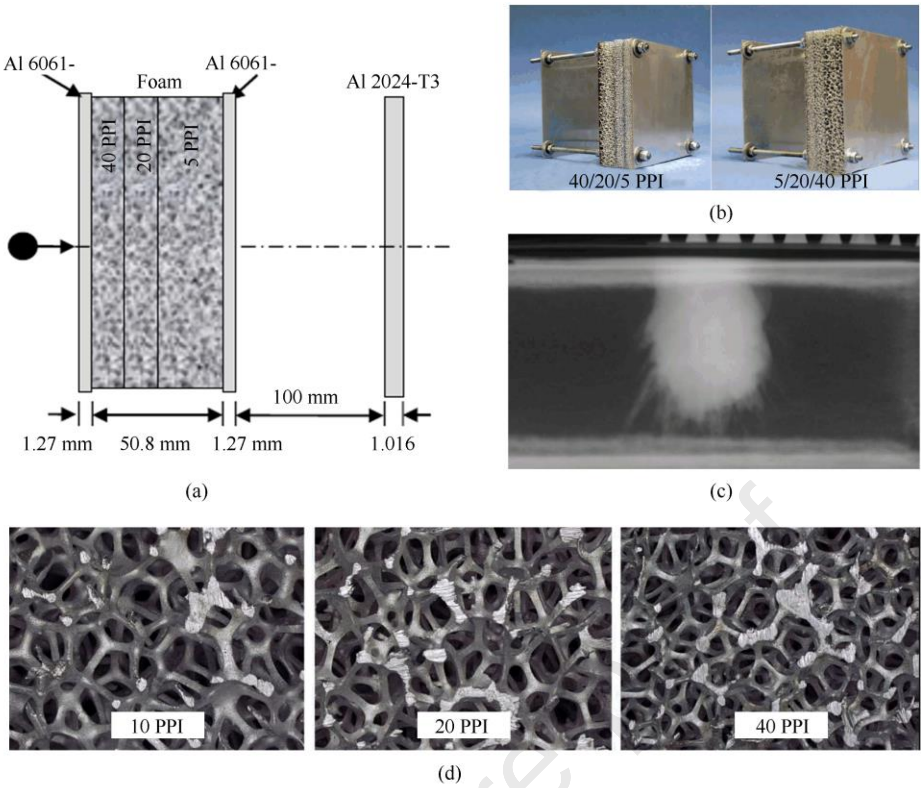


Fig. 12. The shield structure of sandwich panel with density gradient foam core and the different pore density Al6061 foam [66]: (a) The shield structure of sandwich panel with density gradient foam core; (b) The variable pore density Al6061 foam shield; (c) X-ray of typical damage features in thick porous target; (d) Foam core structure, 20 magnification.

As shown in Fig. 13, comparing the shielding performance of single honeycomb aluminum sandwich panel and single foam aluminum sandwich panel [66], the results show that due to the absence of channel effect, the shielding performance of ordinary foam aluminum sandwich panel shield is clearly superior to that of honeycomb aluminum sandwich panel shield with the same total areal density at both normal and oblique incidence, and is comparable to Whipple shield. Comparing the shielding performance of dual honeycomb aluminum sandwich panels and dual foam aluminum sandwich panels [98], the dual foam aluminum sandwich panel shield was found to provide a 15% improvement in critical projectile diameter at low velocity (3 km/s) and a 3% increase at high velocity (7 km/s) at normal incidence, and the improvement increase with the impact angle increase. There was clear evidence of projectile melting below 3.29 km/s for the dual foam aluminum sandwich panel shield, and the melting threshold was significantly reduced. Although sandwich panels have the advantage of high strength mass ratio, light weight and high efficiency energy absorption, a large space will be occupied for sandwich panel as bumper. When vertically impacting the honeycomb sandwich panel, the “channel effect” can cause fragments accumulation, but under oblique impact, the cell wall will form multiple impact loads on the projectile. Therefore, the honeycomb sandwich panel performs better under oblique impact than under normal impact. Therefore, changing the honeycomb core structure is the main direction for optimizing the protective performance of the honeycomb sandwich panel. The foam core of the foam sandwich panel can better absorb the debris cloud, and its protective ability is better than that of honeycomb aluminum. The combination of honeycomb cores with different densities and the optimization of foam core structure are the development direction of improving the protective performance of foam sandwich panel. Under conditions of constant relative density, the protective performance of foam sandwich panels improves as the cell size of the open-cell foam decreases [97]. In addition, the perforation of the rear wall of dual sandwich panel shield also shows that the sandwich panel itself will still produce solid fragments [98], which is unfavorable to reduce the damage of the rear wall.

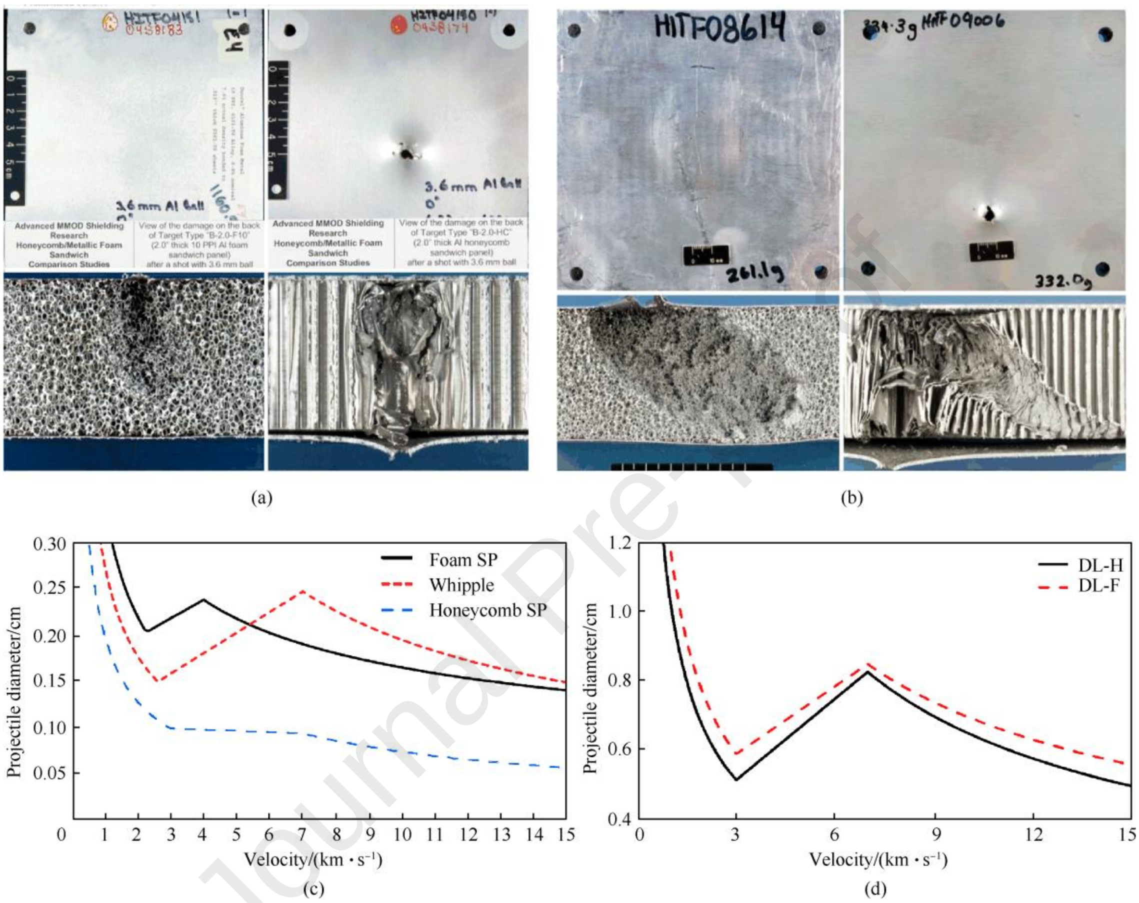


Fig. 13. Comparison of damage and ballistic limit curves of sandwich panels with honeycomb aluminum and foam aluminum as core respectively: (a) Damage of honeycomb aluminum and foam aluminum sandwich panels under normal impact [66]; (b) Damage of honeycomb aluminum and foam aluminum sandwich panels under oblique impact [66]; (c) Comparison of ballistic limit curves of single honeycomb sandwich panel shield, single foam aluminum sandwich panel shield, and Whipple shield with the same total areal density [98]; (d) Comparison of ballistic limit curves of dual honeycomb sandwich panel shield and dual foam aluminum sandwich panel shield with the same total areal density [98].

**3.2.3. Potential energy absorbing materials**

The lattice mechanical metamaterials are featured with extraordinary specific stiffness, specific strength, energy absorption, and demonstrate promising industrial applications potentials in aerospace, transport, and biomedical sections. A number of energy absorbers with different lattice structures such as lattice-walled structure [99], pyramid structure [100], lattice and bone structure [101], graded cell-wall structure [102]and rational gradient structure [103] have been proposed in recent years, as shown in Figs. 14(a), 14(b) and 14(d). Metamaterials achieve controllable deformation behavior and graded compression by designing geometric lattice structure for generating programmable energy absorption performances. To further improve energy absorption capacity, scientists and engineers have tried to learn from biological structures which, through years of evolution, have optimised their structure to improve the energy absorption efficiency under extreme mechanical conditions [104], as shown in Fig. 14(c). The better mechanical properties and energy absorption performances make it suitable for the application of protective devices. At present, there are few studies on the protection of lattice materials against hypervelocity impact [105], and most of them are applied to the energy absorption of low velocity impact. Using the metamaterials with excellent impact resistance cellular structures as the core material of sandwich panel can improve the hypervelocity impact protective performance of sandwich panel.

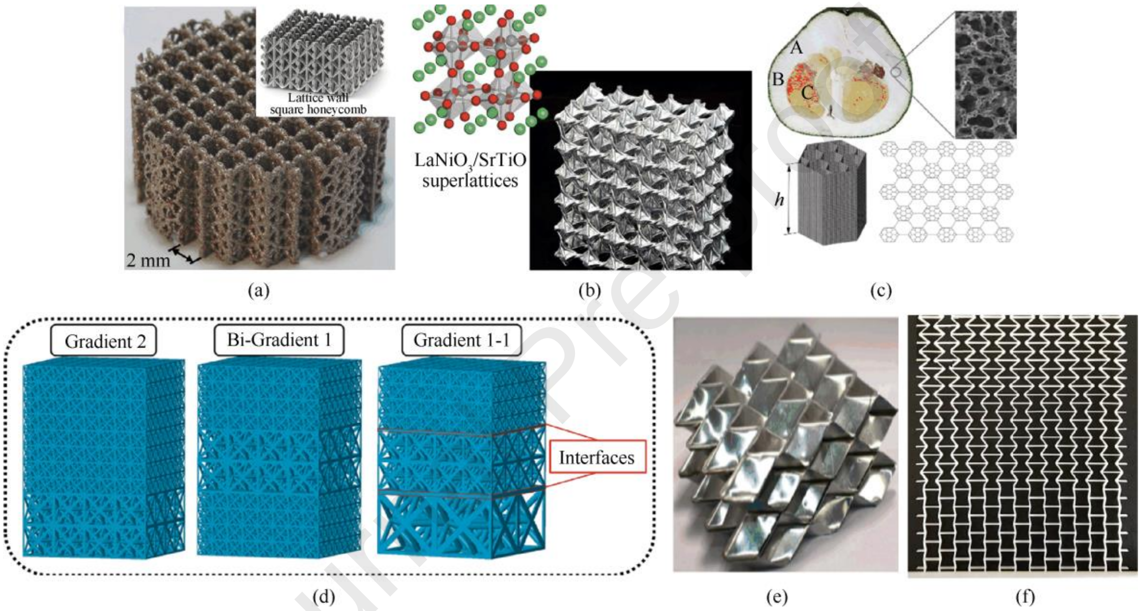


Fig. 14. Efficient energy absorbing metamaterials: (a) Lattice-walled metamaterial [99]; (b) Pyramid structure lattice metamaterial [100]; (c) Pomelo peel-inspired metamaterial [101]; (d) Rational gradient lattice metamaterial [102]; (e) Miura origami metamaterial [103]; (f) Graded cell-wall origami metamaterial [104].

Origami structures have received wide attention in the area of mechanical metamaterials due to the characteristics of large plastic deformation and high energy absorption [106], and it can be transformed into complex geometrical structures through coordinated folding. The force transmission of origami materials in out-of-plane compression and origami beams in bending can be achieved by adjusting fold parameters, which is favored in the design of protective structures [107]. The research shows that the origami core degradation of origami sandwich panel and friction play an important role in energy absorption under low velocity impact. The impact and explosion energy absorption of the optimized origami sandwich panel are better than that of aluminum honeycomb sandwich panel [108]. Lattice and origami metamaterials are potential energy absorbing materials for bumper of spacecraft shield, and research on hypervelocity impact characteristics of metamaterial bumper need be carried out to verify its energy absorption efficiency in hypervelocity impact. In addition, more hypervelocity impact testing on designed structures is needed.

Smirnov [109, 110] presented the thin walled gas-filled and fluid-filled shields. For the gas filling between the bumper and the rear wall, the deceleration effect of the gas on the debris cloud is not significant, but it can increase the impact area of the debris cloud on the rear wall, effectively dispersing the energy of the debris [111, 112]. In addition, gas can also heat the fragments in debris cloud, melting them into droplets. Droplets break down into small droplets under atmospheric action, and the energy of debris clouds is converted into gas internal energy. However, it should be noted that the shock wave overpressure formed when the atmospheric density is high may cause greater damage to the sealed container. For liquid filled shields, deceleration of fragment cloud takes place much faster in fluid than in gas, thus releasing energy more close to the front wall, which could cause its irreversible deformations and breakup. The findings showed that as the fragment slows down, its kinetic energy is converted into internal energy within the surrounding fluid, leading to the formation of diverging blast waves inside the containment. The density of the fluid affects deceleration and shockwave strength. Although filling with gas and liquid can improve the hypervelocity penetration resistance of spacecraft orbital debris shielding components over a broad range of impact velocities, however, the damage to the bumper and rear wall is closely related to the velocity and size of the projectile [113], especially the shock wave caused by the higher velocity and lager projectile can cause the breakup of the containment.

**3.3. Regulating and controlling shock wave propagation materials**

The change of internal material structure can optimize the interaction process between the projectile and the bumper to improve the impact resistance. This kind of materials can change the propagation path of shock wave in the projectile by changing materials physical properties, and increase the loading duration of shock wave in the projectile. The longer duration of the shock wave induced by impact can cause the longer duration tensile wave reflected from the back of the projectile, and the projectile will suffer a longer tensile effect. The projectile will be shattered into smaller fragments under the longer tensile effect. The projectile fragments in the debris cloud are evenly distributed to reduce the concentration of fragments in the head of debris cloud. In addition, increasing the duration of shock wave can increase the internal energy of the projectile, making the projectile more prone to melting and gasification.

Due to the high density of steel, it is not suitable for bumper materials with limited weight. Metal plate is a continuous material, and metal mesh is a discontinuous material. By removing excess bumper material, the mesh bumper is as capable of disrupting a projectile as a heavier continuous bumper. The mesh bumper is composed of overlapping wires in a square pattern. At the overlapping position of the wire, the thickness of the bumper is double the diameter of the wire, and the localized mesh areas with greater bumper thickness are created effectively [114]. These thick localized mesh areas can increase the duration of shock wave propagation in the projectile, which causes the projectile to be shattered into more small fragments. The damaging secondary external fragments induced by the metal mesh bumper are less. As shown in Fig. 15, the ratio $S/D$ of the wires diameter ‘’D’’ and spacing between the wires ‘’S’’ has an important influence on the perforated hole and the debris cloud. Decreasing the spacing and increasing the wires diameter can reduce perforation diameter, and decreasing the spacing and increasing the mesh density can increase the contact between the mesh and the debris cloud, which can improve the shielding performance [115]. Metal mesh bumper can reduce the velocity of center of mass of the debris cloud and increase the radial expansion velocity of debris cloud more effectively than metal continuous bumper [116], however, with the increase of thickness, debris cloud will be highly concentrated in the axial direction [117]. As is shown in Fig. 16, the single mesh bumper displays unfavorable mass dispersion, but the undesirable fragment clusters characterizing the debris clouds of single mesh penetrations may be eliminated readily by use of multiple meshes. Aluminum alloy can also be used as the materials of metal mesh bumper. Christiansen [118] first presented the mesh double-bumper shield. One of such concepts, the mesh double-bumper shield, is a highly efficient method to provide protection from meteoroid and orbital debris impacts. Hypervelocity impact testing of the mesh double-bumper shield have demonstrated weight savings of approximately 30% to 50% at light-gas gun velocities compared with conventional aluminum Whipple shield at normal impact angles. Even larger weight savings, approximately 70%, have been achieved at 45° oblique angles.

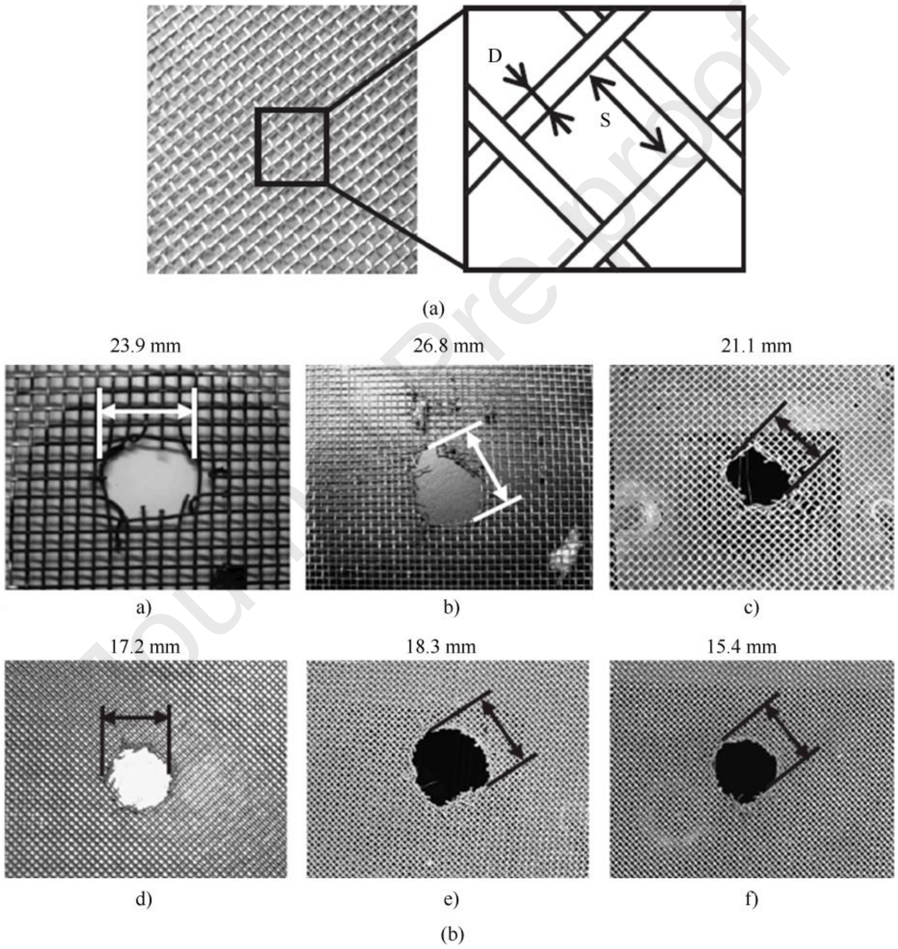


Fig. 15. The corrugated bumper enhanced shield and its optimization [115]: (a) Dimension of a mesh; (b) Perforated holes of mesh targets.

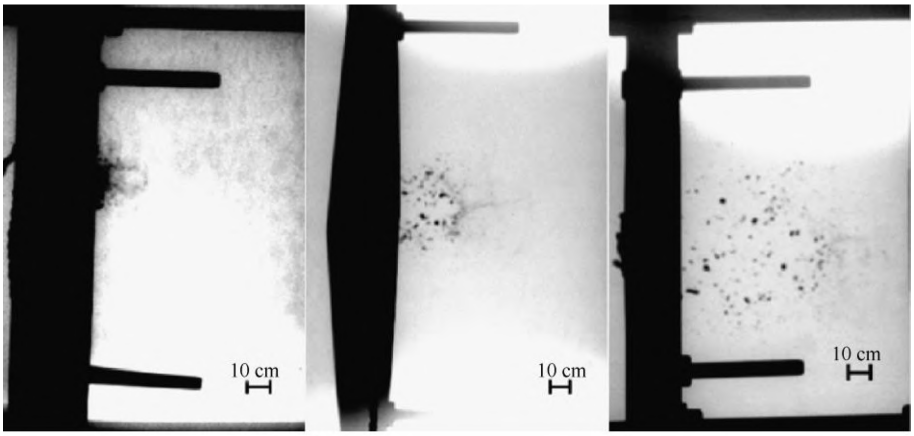


Fig. 16. The debris cloud induced by projectile impact the metal mesh bumper [117].

Inspired by fish scale armor [119–121], Kim [122] presented a flexible metal bumper composed of thin steel sheets through finite lamination, namely “dragon skin”, and it can provide an effective flexible bumper for space inflatable or expandable structures in space, as shown in Fig. 17. The thin steels with dense were material introduced to alleviate the decrease of the bumper performance induced by the accumulation of fragments owing to the dragon skin bumper shape effect. The overlapping of steel sheets can increase the duration of shock wave loading and form twice or even three times the projectile fragmentation effect. The supporting layer location and bumper shape effect can contribute significantly to the bumper performance. Due to the high density of steel, it can be inferred that the thickness of dragon skin is small under the finite area density limit, and the steel dragon skin itself will produce fragments under impact, which are its weaknesses in application to protection.

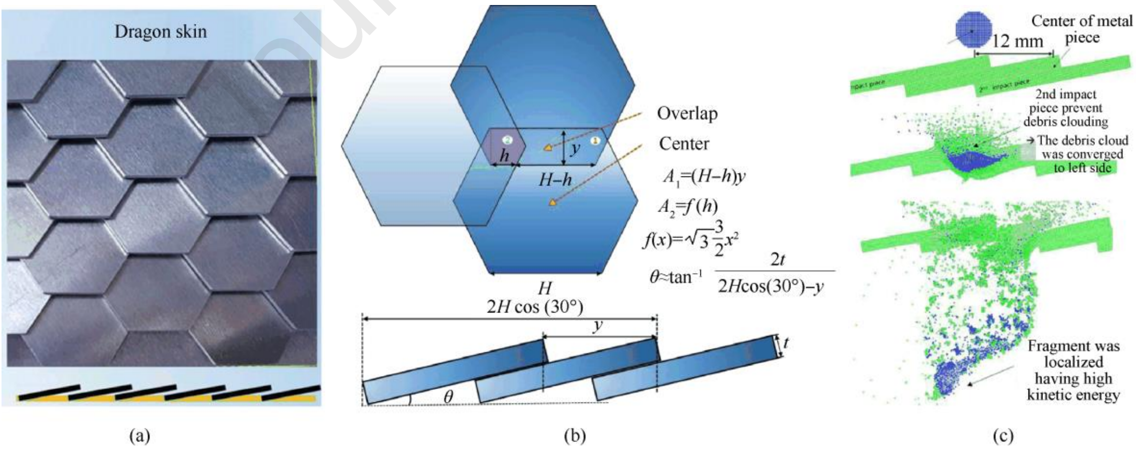


Fig. 17. “Dragon skin” flexible metal bumper composed of thin steel sheet [122]: (a) “Dragon skin” flexible metal bumper; (b) Arrangement of thin steel sheets constituting flexible metal bumper; (c) Numerical simulation of debris cloud induced by hypervelocity impact on flexible metal bumper.

Impedance-graded materials are a kind of heterogeneous materials with continuous or quasi continuous changes in structure and composition, resulting in the properties gradually change according to the change of structure and composition are obtained. The material with continuous impedance gradient change can significantly improve the wave impedance matching effect of heterointerfaces, and impedance-graded materials were often used to reduce and absorb the energy of explosion wave, acoustic wave and electromagnetic wave [123–127]. Riney [128] studied the hypervelocity impact resistance of a laminated metal plate. It is considered that the shielding performance depends on the areal density of bumper, and the increase of impact pressure is only subordinate. By studying the characteristics of debris cloud induced by hypervelocity impact on W/Ti and Ti/W bumpers, Stilp [129] believed that the change of shock wave propagation law caused by impedance gradient is the main factor to change the impact resistance. As shown in Fig. 18, Zhang and Gong [131–134] had carried out a large number of experimental and simulation studies on Ti/Al and Ti/Al/Mg impedance-graded materials, the results show that the shock impedance mismatch of the impedance-graded materials bumper can change the propagation of shockwave. Wen and Chen [135] considered that the multiple reflection and transmission of shock wave at the heterointerfaces in the bumper cause the increase of shock wave duration in the projectile, which is helpful for shattering the projectile and increasing the expansion angle of the debris cloud to make the fragments distribution more uniform in debris cloud, and this improve performance of the Ti/Al and Ti/Al/Mg shield. Zheng and Zhang [136] studied the phase transition of impedance gradient materials under hypervelocity impact, and impedance-graded bumper can make the debris cloud more prone to melting and gasification. Bumper materials with low melting and gasification threshold velocity are helpful to improve the shielding performance. For impedance-grade materials, the disadvantage is that it is difficult to manufacture, especially continuous impedance-gradient materials, and there are a large number of fragments induced by impedance-grade materials itself.

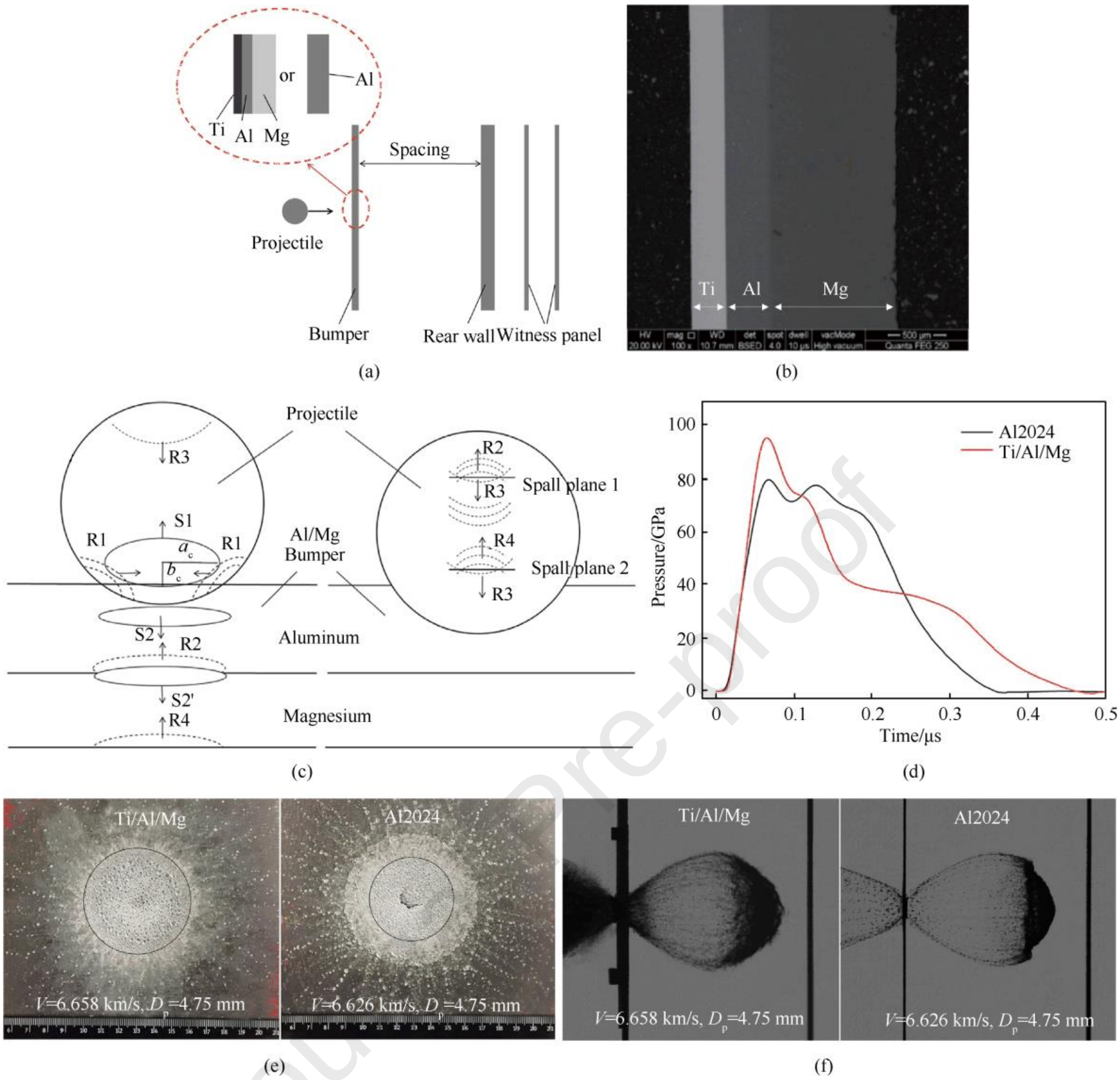


Fig. 18. The hypervelocity impact characteristics of Ti/Al/Mg impedance-graded composite enhanced Whipple shield: (a) Ti/Al/Mg impedance-graded composite enhanced Whipple shield [130]; (b) SEM diagram of Ti/Al/Mg impedance-graded bumper [133]; (c) The shock wave propagation induced by projectile impact on impedance-graded bumper [131]; (d) Comparison of the shock wave pressure induced by projectile impact on impedance-graded bumper and Al2024 bumper respectively [132]; (e) Comparison of the rear wall damage induced by projectile impact on impedance-graded bumper and Al2024 bumper respectively [134]; (f) Comparison of the debris cloud induced by projectile impact on impedance-graded bumper and Al2024 bumper respectively [134].

### 3.4. High hardness materials

The impact of projectile on high hardness material can produce higher shock wave pressure, and the stronger compressive stress and tensile stress can shatter the projectile more effectively. The debris cloud induced by the projectile impacting on the hardness materials has a high expansion velocity, and the size of the fragments in the debris cloud is small. High hardness materials generally have high brittleness and are prone to fracture and fragmentation under hypervelocity impact, which will also consume a lot of kinetic energy of the projectile.

### 3.4.1. Amorphous alloy materials

Due to unique physical and mechanic properties, amorphous alloys have greater advantages compared with the traditional aluminum alloy. The strength of amorphous alloys is extremely high, usually higher than 1 GPa, even approaches the theoretical limit [137–139]. For Fe-based amorphous alloys, the report shows that its strength is 3–5 GPa [140]. Although the density of $Fe_{77}Si_{19}B_4$ amorphous alloy 7.2 g/cm$^3$ is greater than 2.78 g/cm$^3$ of Al2024, the 3GPa strength of $Fe_{77}Si_{19}B_4$ amorphous alloy is much greater than 340 MPa of Al2024, the strength to mass ratio of $Fe_{77}Si_{19}B_4$ amorphous alloy is three times that of Al2024. Huang and Dai [141] studied the hypervelocity impact characteristics of Whipple shield with $Fe_{77}Si_{19}B_4$ amorphous alloy reinforced bumper, and discussed the shock wave propagation in the projectile and bumper, as show in Figs. 19(a) and 19(b). It is found that the amorphous alloy reinforced bumper can lead to higher shock pressures and higher temperature rise in the projectile, and the protective capability of Whipple shield was improved. Hofmann and Hamill [142, 143] studied high velocity impact testing of the ZrTiCuNiBe and TiZrNbCuBe amorphous alloy bumper. The results showed that the materials had good hardness and toughness, which can resist spalling caused by impact, and the amorphous alloy bumper has better performance in replacing the woven material filling layer of the Stuffed Whipple shield, as shown in Figs. 19(c) and 19(d). Zhong [144] studied the crack propagation and shear fracture of $(Ti_{37.31}Zr_{22.75}Be_{26.39}Al_{4.55}Cu_9)_{94}Co_6$ high-entropy bulk metallic glass (HE-BMGs) under dynamic mechanics, obtained constitutive model parameters, and verified the effectiveness of the model through perforation and debris cloud obtained from hypervelocity impact. Further comparative experiments are needed to prove the protective performance.

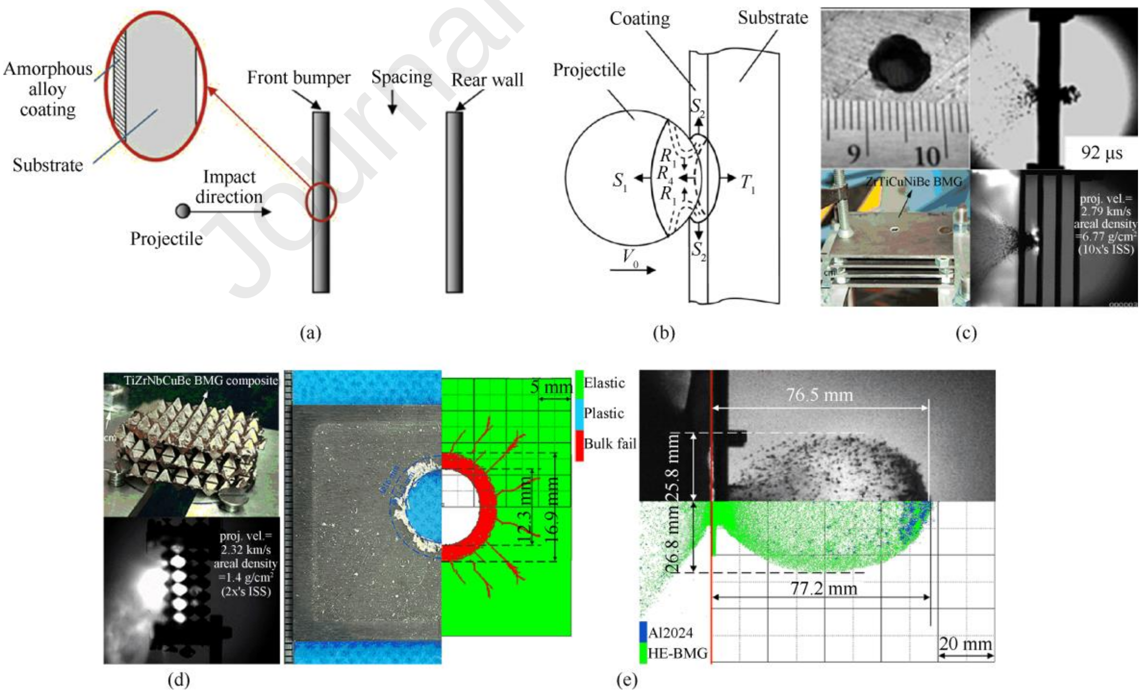


Fig. 19. Amorphous alloy spray reinforced bumper: (a) $Fe_{77}Si_{19}B_4$ amorphous alloy spray reinforced bumper [141]; (b) Shock wave propagation of projectile impacting amorphous alloy spray reinforced bumper [141]; (c) ZrTiCuNiBe amorphous alloy bumper [142]; (d) TiZrNbCuBe amorphous alloy bumper [143]; (e) $(Ti_{37.31}Zr_{22.75}Be_{26.39}Al_{4.55}Cu_9)_{94}Co_6$ HE-BMGs [144].

### 3.4.2. Ceramic-metal materials

Ceramics are nonmetallic inorganic materials, composed by metallic and nonmetallic elements connected by strongly interacting ionic and/or covalent bonds, as shown in Fig. 20. The ceramics have the potential for ultra-high hardness, resistance to catastrophic failure, high strength, light weight and low thermal expansion. Ceramics were usually used as protective structure materials for armored vehicle to enhance the capability of armor to resist penetration [145–150]. The research on ceramics mainly focused on the penetration resistance to long rod projectile.

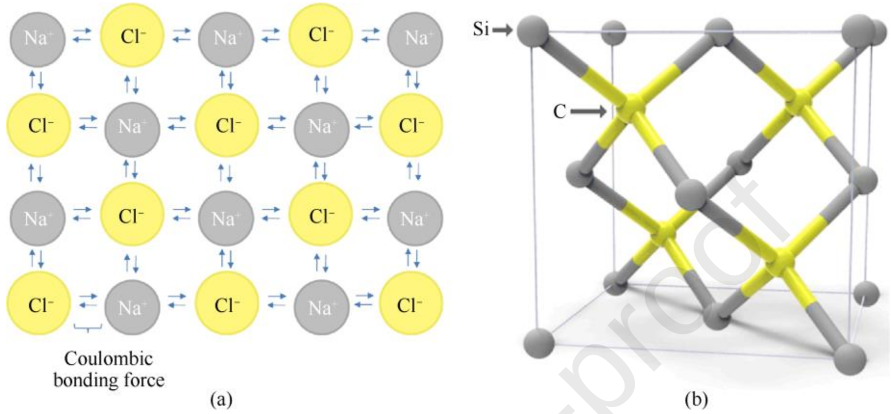


Fig. 20. Type of bonds in ceramics: (a) Ionic bond (NaCl); (b) Covalent bond (SiC).

Due to the ultra-high hardness, the long-rod projectile with a lower impact velocity can be forced to flow radially on the surface of ceramic plates for a period of time without significant penetration, and this process is called interface defeat [152–155], as shown in Fig. 21(a). The ceramic armor not only had the high efficiency protection ability to the projectile with low velocity (1.5–1.8 km/s), but also had the favorable penetration resistance to the projectile with hypervelocity [156, 157]. Ceramics are brittle materials, which will be seriously damaged induced by shattering and fracturing under the strong impact load, and low tensile strength and low toughness limit the application of ceramics in impact resistance. The failure area (failure wave) caused by compression fracture in the ceramic target is located in front of the interface between projectile and target during the impact progress, resulting in the decrease of target resistance. The failure wave velocity will increase with the increased of impact velocity, which leads to the decreasing of penetration resistance with the increasing of projectile velocity [158–160]. This is an unfavorable factor for the impact resistance of ceramic materials. In order to improve the fracture strength of ceramic, ductile metal was used as backing layer of the ceramic to form ceramic-metal composite with high hardness and high strength of ceramic properties and high tensile strength and high toughness of metal properties [161–163], as shown in Fig. 21(b). The backing ductile metal layer can delay the formation of ceramic fracture failure from the interface between ceramic layer and metal layer, and it will inhibit the fracture extent of ceramic under hypervelocity impact, which can improve the impact resistance of ceramic, as shown in Fig. 21(c). Because the ceramic layer will produce higher pressure on the projectile than Al2024 bumper, the projectile will be shattered and decelerated by the ceramic layer bound by the metal layer, and the metal backing layer keeps the fractured ceramic in its place and absorbs the residual energy of the projectile [164, 165], as shown in Fig. 21(d).

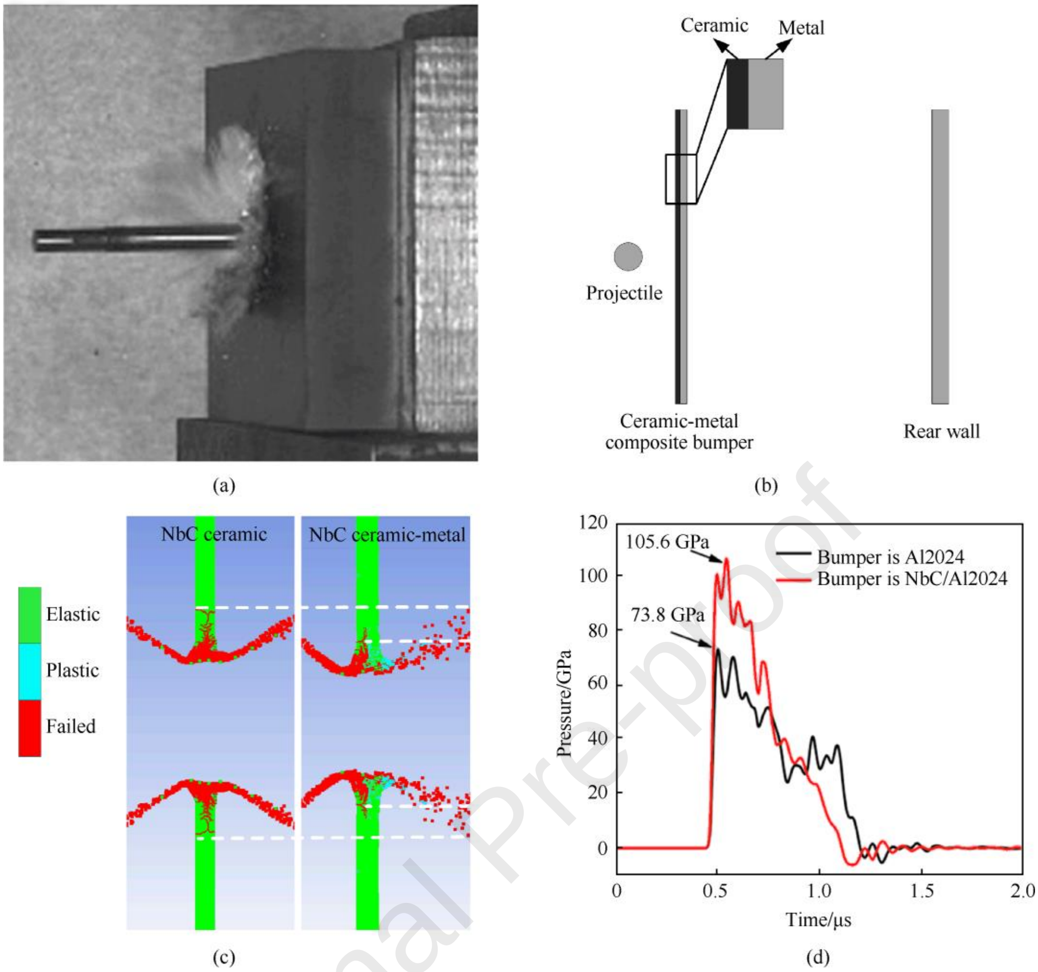


Fig. 21. Behavior Comparison of ceramic and ceramic-metal composite under the hypervelocity impact: (a) The Interface defeat induced by the penetration of long rod projectile into ceramic target [151]; (b) The Whipple shield with ceramic-metal composite as bumper [169]; (c) Comparison of bumper fracture induced by projectile hypervelocity impacting on ceramic and ceramic metal bumper respectively, 6 mm projectile, 7 km/s [169]; (d) Comparison of shock wave pressure inside the projectile induced by projectile hypervelocity impacting on Al2024 and ceramic metal bumper respectively, 6 mm projectile, 7 km/s [169].

Japan Aerospace Exploration Agency (JAXA) used silicon nitride ceramic as thruster material to resist the hypervelocity impact of micro meteoroids to the thruster of Venus probe [166]. In the hypervelocity impact experiments, there was no fatal fracture of silicon nitride ceramic components. The penetration limit equation was determined using crater depth results under the different impact conditions [167], and the fracture pattern of the silicon nitride subjected to hypervelocity impact can be predicted. Li et al. [168] studied the effect of temperature on hypervelocity impact resistance of SiC ceramic. Low temperature will lead to new micro-cracks in SiC ceramic, resulting in smoother fracture and reduced damage areal. Ren and Zhang et al. [169] investigated the hypervelocity impact resistance behaviors of NbC/Al2024 ceramic-metal composite. Compared with single NbC bumper and Al2024 bumper, NbC/Al2024 ceramic-metal bumper can increase the expansion velocity of debris cloud and reduce the head velocity of debris cloud. NbC ceramic layer can increase the shock wave pressure in the projectile, resulting in shattering the projectile into smaller fragments and the melting and gasification of more projectile materials, as shown in Fig. 22(a). The shielding performance of The $TiB_2$/Ni and $B_4C$/Al ceramic-metal Whipple shields were compared with that of aluminum alloy Whipple shield by Huang et al. [170, 171]. As shown in Figs. 22(b) and 22(c), the results show that the $TiB_2$/Ni and $B_4C$/Al ceramic-metal bumpers has better fragmentation effect on projectile, and can disperse debris cloud more effectively. The toughening effect of the metal of the ceramic-metal composite plays an important role in avoiding bumper failure induced by shock wave of hypervelocity impact. As shown in Fig. 22(d), Cherniaev et al. [172] developed SiC/Al6061 ceramic-metal bumper to enhance the Whipple shield, and they studied the debris cloud motion progress. They concluded that the optimal impedance matching realized by adjusting the mass fraction of ceramic layer can improve the shielding ability of ceramic-metal bumper. The SiC/Ti ceramic-metal composite was developed to resist the hypervelocity impact, and it showed excellent shielding performance [173].

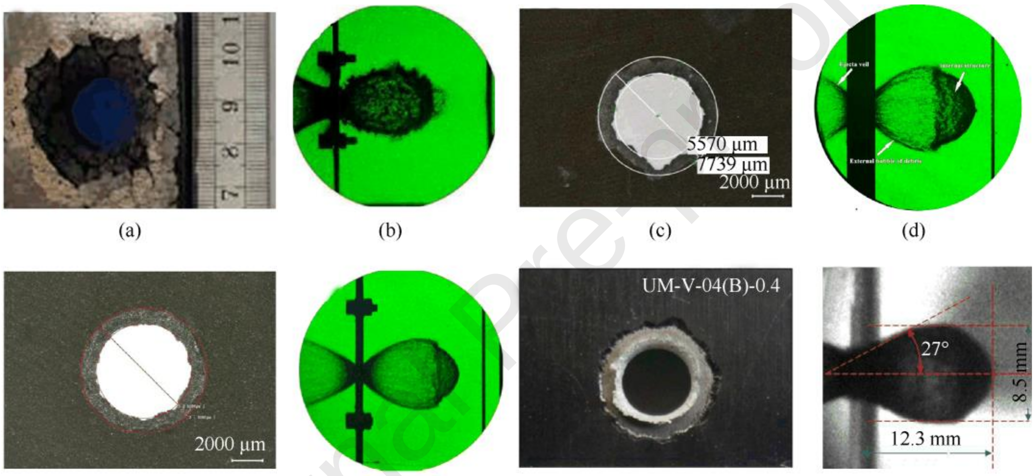


Fig. 22. Perforations and debris clouds of ceramic-metal bumper under hypervelocity impact: (a) NbC/Al2024 bumper, 4 mm projectile, 6.93 km/s [169]; (b) TiB/Ni bumper, 3 mm projectile, 7.22 km/s [170]; (c) $B_4C$/Al bumper, 3 mm projectile, 6.44 km/s [171]; (d) SiC/Al6061 bumper, 1 mm projectile, 7 km/s [172].

### 3.5. High tensile strength materials

High tensile strength materials can withstand high tensile stress without fracture, and have excellent interception effect to solid fragments. In particular, the tensile strength of low-density fiber fabrics are several times that of aluminum alloy. As an intermediate stuffed layer, it can effectively intercept the fragments produced by the projectile impacting the previous layer bumper. More importantly, the fiber fabrics itself do not produce hard solid fragments.

#### 3.5.1. Mesh reinforced aluminum matrix materials

Aluminum alloy is the optimal bumper material among metal materials. Its density and strength are desirable, but its protective capability needs to be further improved. In order to improve the hypervelocity impact resistance of aluminum alloy, the hypervelocity impact experiments using the SiC, $SiO_2$, borate whisker, graphite fiber, and glass fiber reinforced aluminum matrix composite metal as bumper were carried out [174–179]. However, the ballistic performance of these improved bumpers did not effectively improve the protection capability of Whipple shield. Mesh reinforced aluminum matrix composite metal enhance the mechanical properties by adding metal meshes wires to aluminum alloys, especially the tensile strength increases greatly. The addition of metal meshes hinders effective the penetration of hypervelocity projectile, and it also eliminates the adiabatic shear bands for aluminum alloy matrix, which can increase the failure stress of aluminum alloy. For example, the shear strength of Al6061 can be significantly improved by adding NiTi mesh [180], and $Al_9Si_3Cu$ alloy can obtain a high bending strength as 431 MPa by adding steel wire meshes [181]. These reports indicated that the improvement of strength and ductility as well as an excellent interfacial strength can be obtained by adding metal fibers.

Sun and Guo [183–185] developed a Ti–6Al–4V meshes reinforced aluminum alloy matrix composite bumper, and which damage behaviors impacted by hypervelocity aluminum projectiles were investigated, as shown Fig. 23(a). Results showed that Ti–6Al–4V meshes can disperse the applied load at the impact point effectively, and the number of dislocations density increases obviously leading to more energy consumption, as shown Figs. 23(b), 23(c) and 23(d). The Ti–6Al–4V meshes reinforced aluminum alloy matrix composite bumper exhibits better protection efficiency and energy absorption ability than aluminum alloy bumper. However, the research mainly focused on the micro analysis of the damage of the bumper. It is necessary to carry out ballistic impact experiments on the Whipple shield with the Ti–6Al–4V meshes reinforced aluminum alloy matrix composite as bumper to verify the protective capability. This material still does not effectively solve the problem of fragments generated by the bumper itself. In addition, the material has no advantage in lightweight as the foam sandwich panel and aluminum mesh.

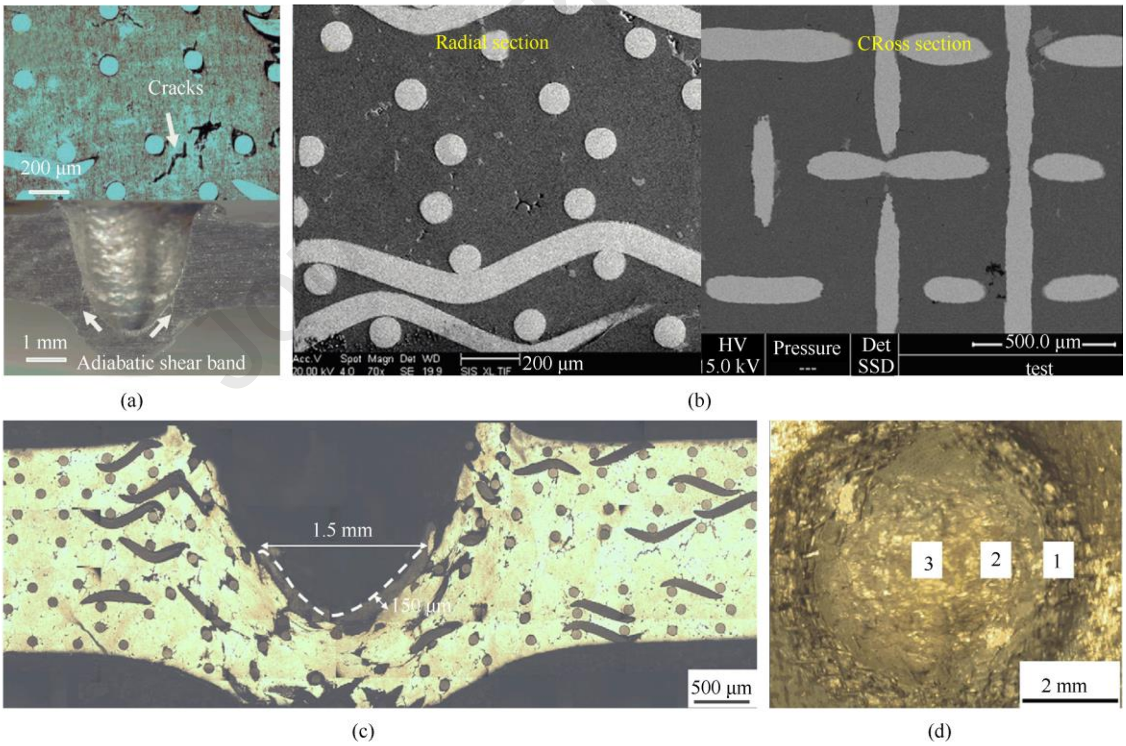


Fig. 23. Micro-damages in the vicinity of the crater for Ti–6Al–4V mesh reinforced Al–6Mg alloy matrix composite metal under the hypervelocity impact: (a) Cracks in region and shear bands in Al–6Mg alloy [182]; (b) SEM microstructure of radial section of Ti–6Al–4V mesh reinforced Al–6Mg alloy matrix composite metal after impact [183]; (c) SEM microstructure of the cross section of the region around the crater after impact [184]; (d) Ti–6Al–4V mesh reinforced Al–6Mg alloy matrix composite metal impacted by Al projectile with the diameter of 2 mm and the velocity of 3.79 km/s [185].

### 3.5.2. Fiber fabric

Fabrics based on high-performance fibers are among the advanced materials used in modern protective structure designs due to their light weight, tensile strength, toughness, and resistance to impact damage [186–190]. For example, Kevlar fiber [191–193] and ultra-high molecular weight polyethylene (UHMWPE) [194, 195] are widely used in helmet and body armor to resist the penetration of projectile. The advances in fiber properties have greatly improved the impact resistance of fiber materials, and protective structure can resist stronger impact with lighter weight compared with traditional metal materials. The strength and tensile modulus of Kevlar, Nextel, Carbon T300, Vectran, Basalt, UHMWPE are much higher than that of Al6061, with the density is smaller or equal to that of Al6061. This makes the fiber material have a higher ratio of strength and mass. Capturing a projectile by the fabric is essentially an energy conversion between the projectile and fabric through a combination of various energy absorption mechanisms, which include yarn decrimping, stretching, breakage, and pull-out.

Kevlar is a high molecular polymer fiber polymerized by p-phenylenediamine and p-benzoyl chloride, and Nextel is a ceramic fabric consisting of 62.5 wt% $Al_2O_3$, 24.5 wt% $SiO_2$ and 13 wt% from $B_2O_3$. Rudolph and Schafer [196] carried out hypervelocity impact tests on Kevlar and Nextel fabric bumpers, and analyzed the debris cloud and rear wall damage, as shown in Fig. 24. The shielding performance of Al5056, Kevlar and Nextel is compared by counting the radius of largest penetration and sum of all penetration areas of the rear wall. The debris clouds induced by impacting on Kevlar and Nextel bumper show the serrated front, and present the more efficient dispersion of projectile fragments than aluminum alloy.

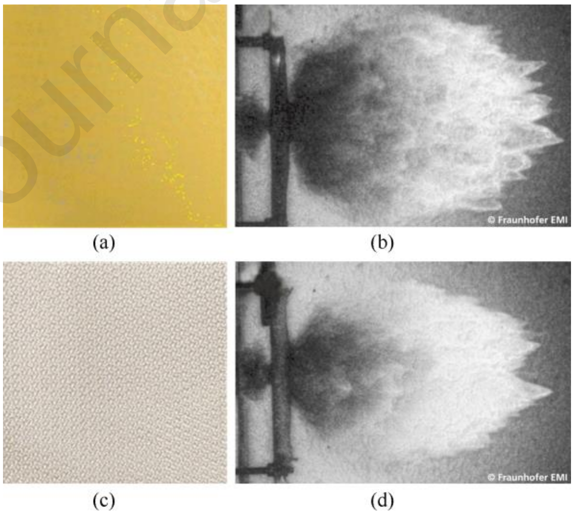


Fig. 24. Nextel and Kevlar fiber fabrics and their debris clouds [196]: (a) Kevlar fiber fabric; (b) Nextel fiber fabrics; (c) The debris cloud induced by hypervelocity impact on Kevlar fiber fabric; (d) The debris cloud induced by hypervelocity impact on Nextel fiber fabric.

The multi-bumper flexible shield was used to protect the Comet Nucleus Tour spacecraft from meteoroids hypervelocity impact when flying over three comets at a distance of 100 km. The multi-bumper flexible shield was composed of multi-layer Nextel bumper and rear wall, and the overall spacing was 20 cm, which saves 50% of the weight compared with Whipple shield with the same protective capacity [197], as shown in Figs. 25(a) and 25(b). However, since the overall spacing available for Space Station module protection is short (S=~11 cm and $S/d$<11), the multi-bumper shield are not as effective. In order to improve the protection capability of Space Station modules with the limited overall spacing, Johnson Space Center [33] develop a Nextel/Kevlar Stuffed Whipple shield, which includes a flexible blanket combining Nextel ceramic fabric and Kevlar fabric between the aluminum alloy bumper and rear wall of the Whipple shield. This shield includes an Al6061 bumper (2 mm thickness), a flexible intermediate layer combining Nextel ceramic fabric (6 layers) and Kevlar fabric (6 layers), an Al2219 rear wall (4.8 mm thickness), the overall areal density of the shield is 2.705 g/cm$^2$, and the overall spacing is 11.4 cm. This Nextel/Kevlar Stuffed Whipple shield can defeat the impact of projectile with maximum diameter of 1.45 cm at the velocity of 4–7 km/s. The Nextel ceramic fabric can shatter projectiles into smaller pieces than aluminum alloy, and Kevlar can more effectively reduce the velocity of debris cloud than aluminum alloy. Furthermore, the particle size within the debris cloud induced by the Nextel/Kevlar fiber stuffed layer itself is smaller than that of the aluminum alloy bumper, which results in less damage to the rear wall compared with the larger fragments produced by impacting on aluminum bumpers. This Nextel/Kevlar Stuffed Whipple shield was widely applied in the International Space Station (ISS) [197], and the Figs. 25(c) and 25(d) show the typical shields protecting cylinder/conical areas of U.S. modules [198], ESA Columbus [199] and NASDA Japanese Experimental Module [200, 201] and their ballistic limit curves. ESA configuration has the highest protective capability, which is caused by different areal density of Nextel/Kevlar stuffing layer and larger overall spacing of ESA configuration (ESA configuration is 13 cm, NASA and NASDA configurations are 11.4 cm). These three configurations have excellent shielding performance, which can effectively protect the spacecraft from the damage induced by the impact of the projectile with diameter larger than 1 cm with the velocity of 4–7 km/s. Christiansen [32, 202] gave the ballistic limit curve of Nextel/Kevlar Stuffed Whipple shield. A liquid crystal polymer fiber Vectran was developed by Japan [203], and it has the same shielding capability as Kevlar, which was verified by hypervelocity impact experiments.

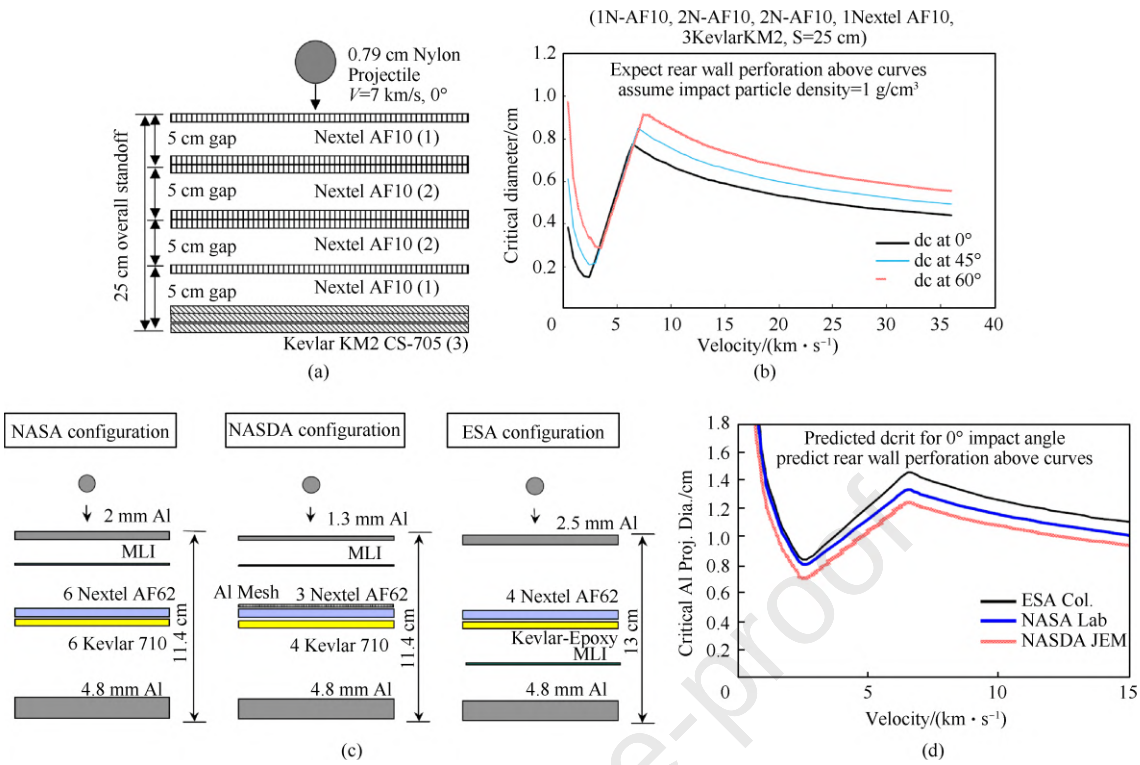


Fig. 25. Nextel/Kevlar multi-shock shield and ISS Nextel/Kevlar Stuffed Whipple shield [197]: (a) Nextel/Kevlar multi-shock shield; (b) The ballistic limit curve of Nextel/Kevlar multi-shock shield; (c) ISS Nextel/Kevlar Stuffed Whipple shield; (d) The ballistic limit curve of Nextel/Kevlar Stuffed Whipple shield.

Destefanis and Schafer et al. [204, 205] were funded by the European Space Agency (ESA) to improve and optimize the shield of the Columbus modulus of the ISS. The Columbus Stuffed Whipple shield is shown in Fig. 26 (a), and the stuffed layer made from Nextel fabric and Kevlar fabric impregnated with Epoxy resin. The total area density of The Nextel/Kevlar-Epoxy Stuffed Whipple shield is 3.2 g/cm$^2$ and the total spacing is 13 cm. It can provide protection against the impact of 14.5 cm diameter projectile with the velocity of 6.5 km/s. Another configuration was to convert the intermediate stuffing into aluminum foam and Kevlar 2D with the total area density and overall spacing are equal to the Nextel/Kevlar-Epoxy configuration, and the Al-foam Kevlar 2D configuration can show shielding performance comparable to that of Nextel/Kevlar-Epoxy configuration by comparing ballistic limit curve, as shown in Fig. 26(b). The results show that both Nextel/Kevlar-Epoxy configuration and Al-foam Kevlar 2D configuration can resist the impact of projectiles with the ≥ 1 cm diameter in the velocity range of 2–7 km/s. The Nextel and Kevlar fabric were applied to the Stuffed Whipple shield of Automated Transfer Vehicle (ATV) [206], the first layer bumper was the Beta fiber cloth, and the shielding performance of this shield is better than the Whipple shield without intermediate stuffing layer.

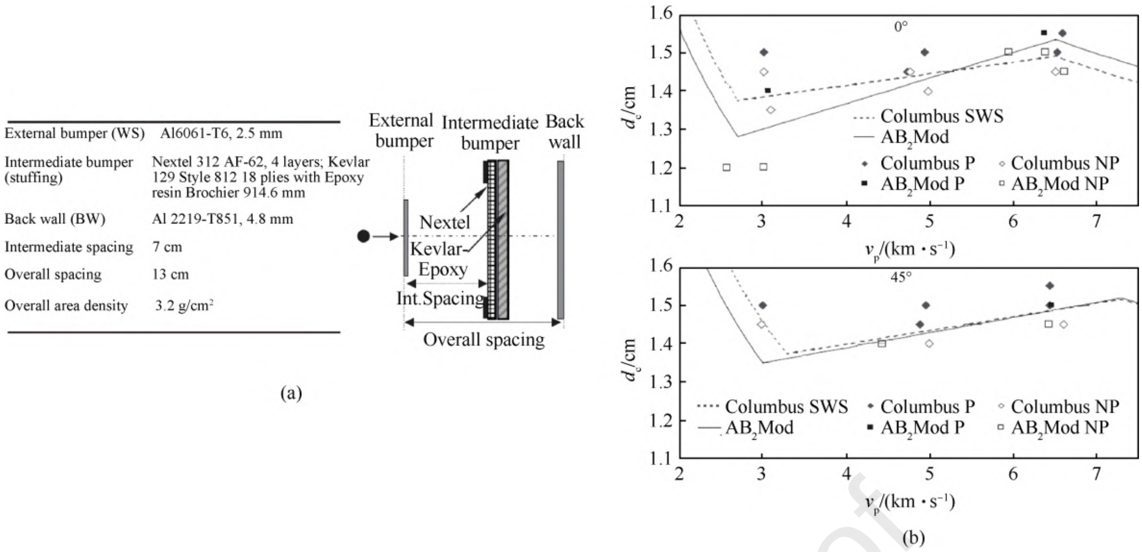


Fig. 26. The Stuffed Whipple shields for Columbus cabin and ballistic limit curves: (a) The Stuffed Whipple shield for Columbus cabin [204]; (b) The ballistic limit curves [205].

Basalt fiber is a continuous fiber drawn from natural basalt, and the application of basalt fiber is more and more widely in engineering due to its increased advantages in terms of physical properties and environmental cost [207–210]. Basalt fibers were usually used in combination with Kevlar fiber to obtain stronger properties [211, 212]. As shown in Fig. 27(a), the Beta cloth, Basalt and Kevlar fabrics was applied to the Whipple shield of Chinese Space Station [213, 214], and Beta cloth, Basalt and Kevlar fabrics as the bumper of shield. The Stuffed Whipple shield used Beta cloth, Basalt and Kevlar fabrics as the intermediate stuffing layer is comparable to both the ESA Columbus module debris shield and the NASA Stuffed Whipple shield, and a new ballistic limit equation (BLE) was derived from the available experimental data for the Stuffed Whipple shield, as shown in Fig. 27(b). Ke and Huang et al. [215, 216] studied the shielding performance of Stuffed Whipple shields with a variety of Aramid/Basalt fibers as intermediate stuffing layer, as shown in Figs. 27(c), 27(d) and 27(e). The influences of the intermediate stuffing layer positions on the shielding performance were relative with the fiber materials of intermediate stuffing layer. The adhesion degree between Basalt ceramic and Aramid fiber has a great influence on its shielding performance, and excessive adhesion will reduce the ability of the stuffing layer to absorb the kinetic energy of debris cloud.

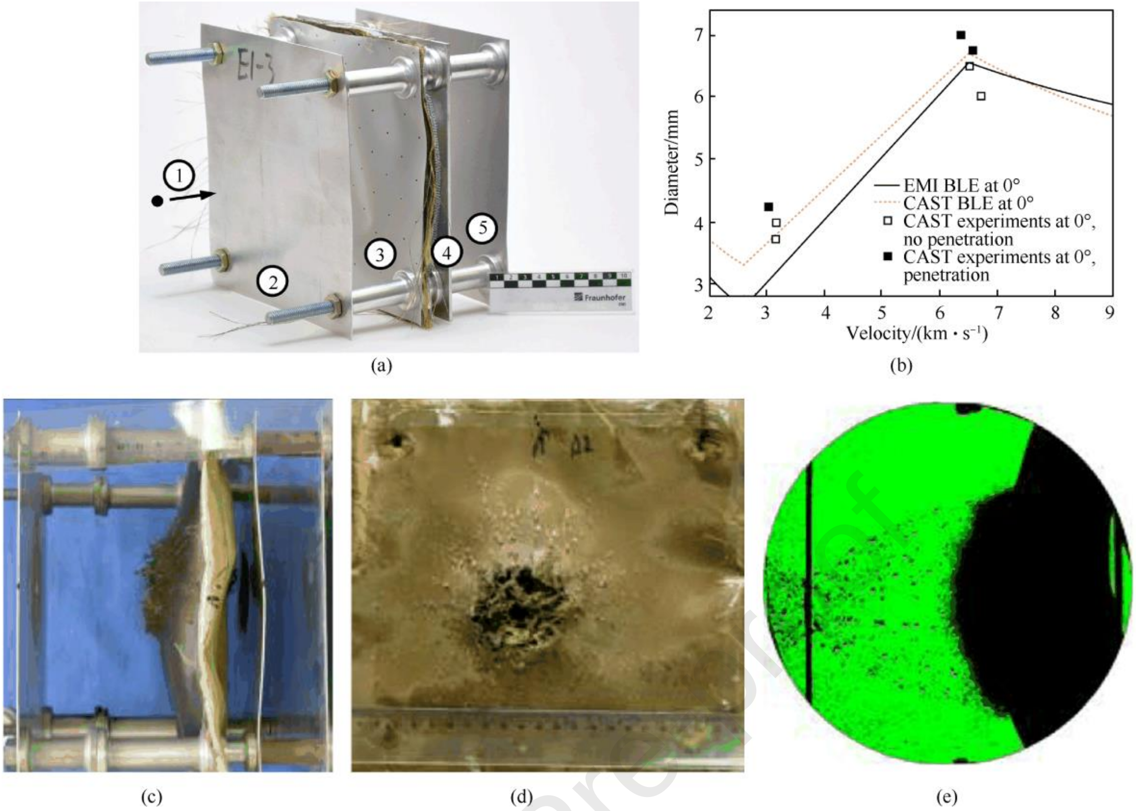


Fig. 27. Hypervelocity impact characteristics of the Stuffed Whipple shield with Basalt/Kevlar as intermediate stuffing layer: (a) The Chinese Space Station Stuffed Whipple shield with Beta/Basalt/Kevlar as intermediate stuffing layer [213]; (b) The ballistic limit curve of Chinese Space Station Stuffed Whipple shield [214]; (c) The Stuffed Whipple shield with Basalt/Kevlar as intermediate stuffing layer; (d) The damage of Basalt/Kevlar intermediate stuffing layer [215]; (e) The debris cloud impacting on the Basalt/Kevlar intermediate stuffing layer [216].

Carbon fibers have been used widely in aerospace and other industries due to their ultra-high modulus and tensile strength with the low densities [217–219]. In order to improve the thermal expansion of carbon fiber, interlayer properties, carbon fibers were compounded with other materials to form materials, such as carbon fiber reinforced polymer matrix materials and carbon fiber/PEEK materials [220–222]. They contain carbon fiber and other materials as reinforcement so that the properties of the materials can be better balanced by taking advantages of different reinforcing materials. Cherniaev and Garcia [223, 224] studied the behavior of carbon fiber fabricated by filament winding under the orbital debris hypervelocity impacts by experiments and simulations, as shown in Figs. 28(a), 28(b), and 28(c), and experimental results revealed that the following parameters: impact energy, pre-loading, and the degree of interweaving of filament bands have an obvious influence on the damage induced by orbital debris impacts. Xie and Xue [225–227] et al. found that the impact resistance of carbon matrix reinforced with carbon fibers materials increases after a single heating ramp from 25 ℃ to 1206 ℃, and the corresponding residual strength after the hypervelocity impacts increased by 47%. Matrix cracking and fiber breakages to spallation and delamination along the impact direction are the main damage modes. Lamontagne and Manuelpillai et al. [228, 229] carried a series of hypervelocity impacts on carbon fibre/PEEK materials, and the results show that the damage and debris cloud of carbon fibre/PEEK materials is independent of projectile density, rather dependent on diameter. Taylor et al. [230] determined the ballistic limit of a carbon fiber reinforced plastic faceplate with 1.6 mm thickness bonded to 45 mm aluminum honeycomb core by hypervelocity impact experiments. As shown in Fig. 28 (d), the nano-carbon fiber in epoxy matrix composite was used as the bumper and rear wall of Whipple shield for hypervelocity impact by Khatiwada et al. [231], the results show that nano-carbon fiber in epoxy matrix composite perform better as rear walls than the aluminum, but are lesser effective as bumper. As shown in Fig. 29(e), a self-healing carbon fiber reinforced polymer composite to be used mainly in space environment was successfully synthesized [232], and the autorepair composite was made of self-healing materials, which composed of microcapsules containing various combinations of a 5-ethylidene-2-norbornene and dicyclopentadiene monomers, reacted with ruthenium Grubbs catalyst, added into the carbon fiber reinforced polymer layer. This material can self-repair damage and has great potential application value. As shown in Fig. 28(f), through the hypervelocity impact experiments and simulations of carbon fiber overwrapped pressure vessels [233], it can be found that the fiber orientation determined that the circumferential amplitude of the initial stress wave was much greater than the axial amplitude. Due to the propagation of shock waves along the fiber direction, local interface shear occurs in adjacent layers in different directions, resulting in localized delamination.

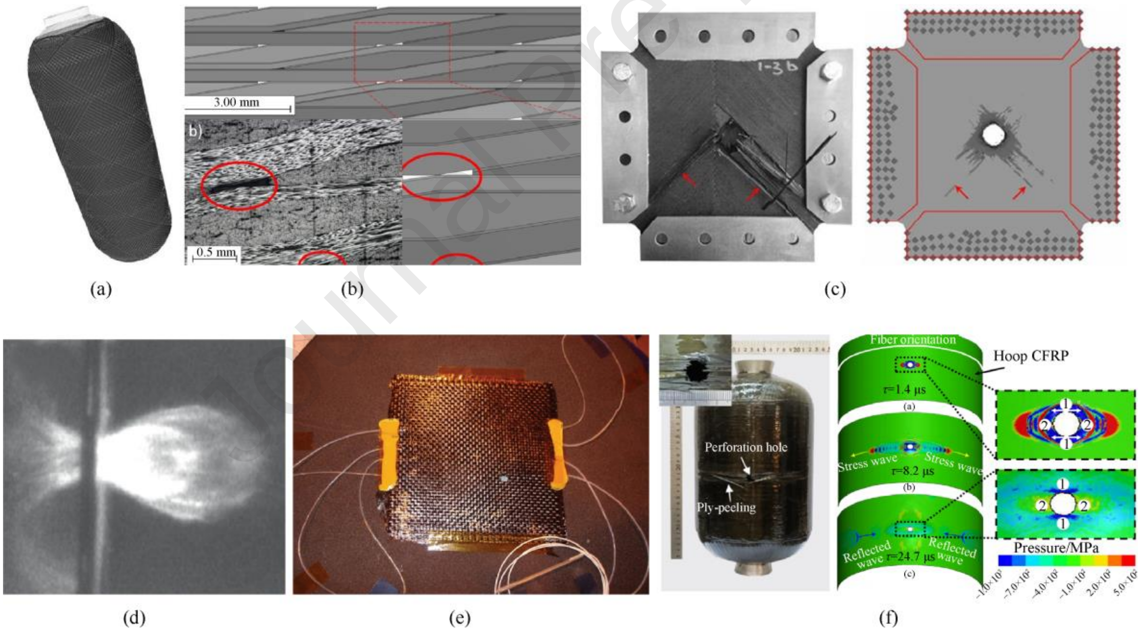


Fig. 28. Hypervelocity impact characteristics of carbon fiber materials: (a) Carbon fiber wound pressure vessel [223]; (b) The micro damage of carbon fiber under hypervelocity impact [223]; (c) Comparison of experimental results and numerical predictions for carbon fiber impact damage [224]; (d) The debris cloud induced by hypervelocity impact nano-carbon fiber composite [231]; (e) A self-healing carbon fiber reinforced polymer composite [232]; (f) Hypervelocity impact experiments and simulations of carbon fiber overwrapped pressure vessels [233].

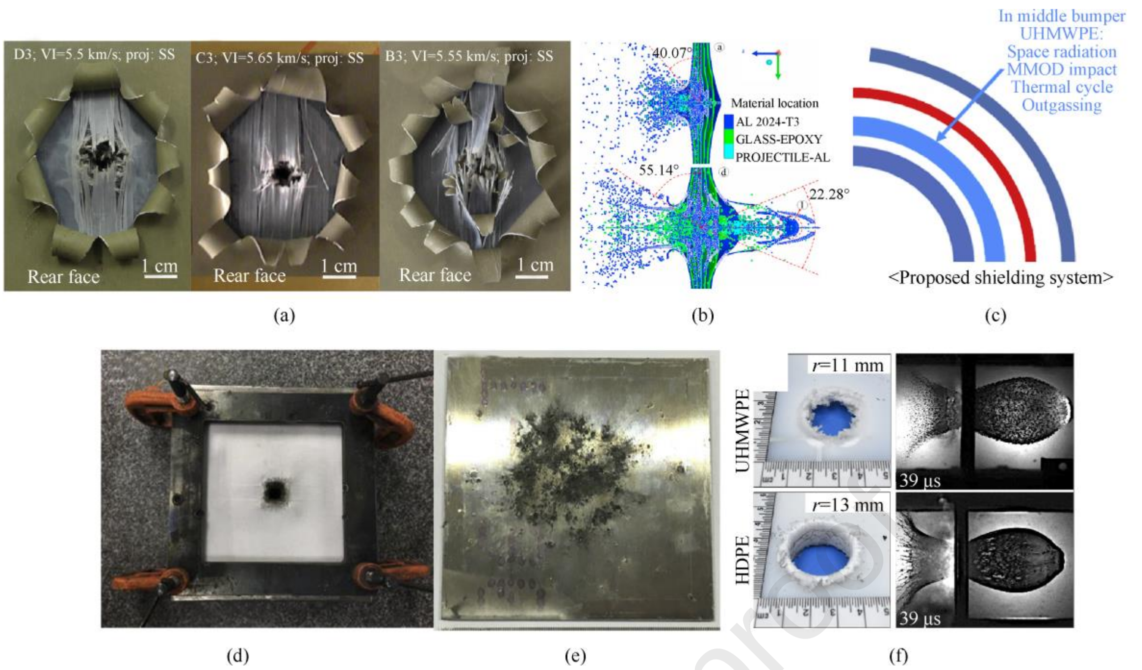


Fig. 29. Hypervelocity impact characteristics of glass fiber composite and UHMWPE fiber composite: (a) The damage of glass fiber reinforced aluminum bumper under hypervelocity impact [243]; (b) The simulation results of hypervelocity impacting on glass fiber reinforced aluminum bumper [244]; (c) UHMWPE fiber bumper shield; (d) Damage of UHMWPE fiber bumper [245]; (e) Damage of rear wall of Whipple shield with UHMWPE fiber as bumper [245]; (f) Comparison of hypervelocity impact results between UHMWPE and HDPE [247].

Although most reports only focused on the mechanical response of glass fiber composite [234–238] and high molecular weight polyethylene (UHMWPE) fiber composite [239–241] under ballistic impact, however glass fiber composite and UHMWPE fiber were also used as bumper materials to verify the shielding performance in a few reports [242–245]. The influence of projectile dimension and material on the limiting penetration thickness of fiberglass laminate target under hypervelocity impact was investigated [242], and the propagation of shock wave along the glass fiber will lead to the expansion of damage area. For the impact velocity of 3–7 km/s, the limiting penetration thickness of fiberglass plate is 1.5 times cavity depth of semi-infinite target. The response of glass fiber reinforced aluminum comprised variably thick aluminum layers and glass fiber reinforced epoxy composite laminate to hypervelocity impacts of orbital debris with velocities of higher than 7 km/s was studied by experiment and numerical simulation [243, 244], as shown in Figs. 29(a) and 29(b). The results show that the glass fiber composite laminate using multiple fiber orientations can disperse the shock front to reduce the shock wave pressure near the impact region. As shown in Figs. 29(c), 29(d) and 29(e), a Whipple shield design comprising of UHMWPE fiber were proposed to improve the shielding efficiency of conventional Whipple shields [245], and the shielding performance of UHMWPE Whipple shield is better than Kevlar Whipple shield, although UHMWPE fiber ballistic performance will be reduced at high temperatures. Stacked multi-layered glass fiber and aluminum laminate performance the better hypervelocity impact resistance than single glass fiber plate [246]. Due to the better toughness of high-density polyethylene (HDPE) compared to UHMWPE [247], which was less prone to local fracture and fragmentation, HDPE bumper can lose less mass under hypervelocity impact, resulting in a decrease in the momentum and kinetic energy of debris cloud, exhibiting a better protective performance.

Fiber material is the most successful bumper material developed and applied so far, especially Kevlar and Nextel fiber fabrics applied widely in ISS, and the advantages of light weight, tensile strength and toughness make it have excellent resistance to impact damage. More importantly, except for fracture filaments and small fabric fragments, it hardly produces hard fragments by itself, which can greatly reduce the impact damage of the bumper to the rear plate. It is worth noting that the energy absorption efficiency of the fiber bumper is affected by boundary condition of the fabric layers [248]. The disadvantage is that the preparation process of high performance fiber fabric is complex and the cost is high. The manufacturing of these fibers is limited to few industrial realities.

### 3.6. Energy releasing materials

The cardinal principle of selecting materials is that they can increase the impact pressure and extend the shock wave duration to shatter the projectile effectively. However, the transient of hypervelocity impact and the limited thickness of bumper will cause the shock wave in the projectile to be quickly caught up and unloaded by the tensile wave reflected from the bumper back face. The increase of shock wave pressure is often accompanied by the shortening of shock wave duration, which makes the improvement of shattering effect not obvious. Zhang and Wu et al. [249–251] presented a Whipple shield with PTFE/Al reactive materials as bumper, and the reactive material bumper will produce impact-induced detonation reaction under hypervelocity impact [252–254], as shown in Figs. 30(a) and 30(b). The combined effect of impact and detonation reaction can cause the projectile to be subjected to shock wave load twice, which greatly prolongs the duration of shock wave in projectile, as shown in Fig. 30(c). The reactive materials bumper can shatter the projectile into smaller, less massive and slower fragments due to the combined effect of impact and detonation reaction, and the reactive material bumper will not produce solid fragments because the reaction products are gas. The impact-induced reaction can increase the expansion velocity of debris cloud, reduce the mass center velocity of debris cloud [255], increase the material temperature in debris cloud, and increase the material temperature of the materials in debris cloud, as shown in Fig. 30(d). The shielding capability can be improved by increasing the energy density and reaction wave velocity of reactive materials [256]. Ren [257] presented a reactive material double-bumper shield, with a dual combined effect of impact-detonation that can better shatter projectile, and it can resist the impact of 1.05–1.47 cm projectile at a velocity of 3–7 km/s.

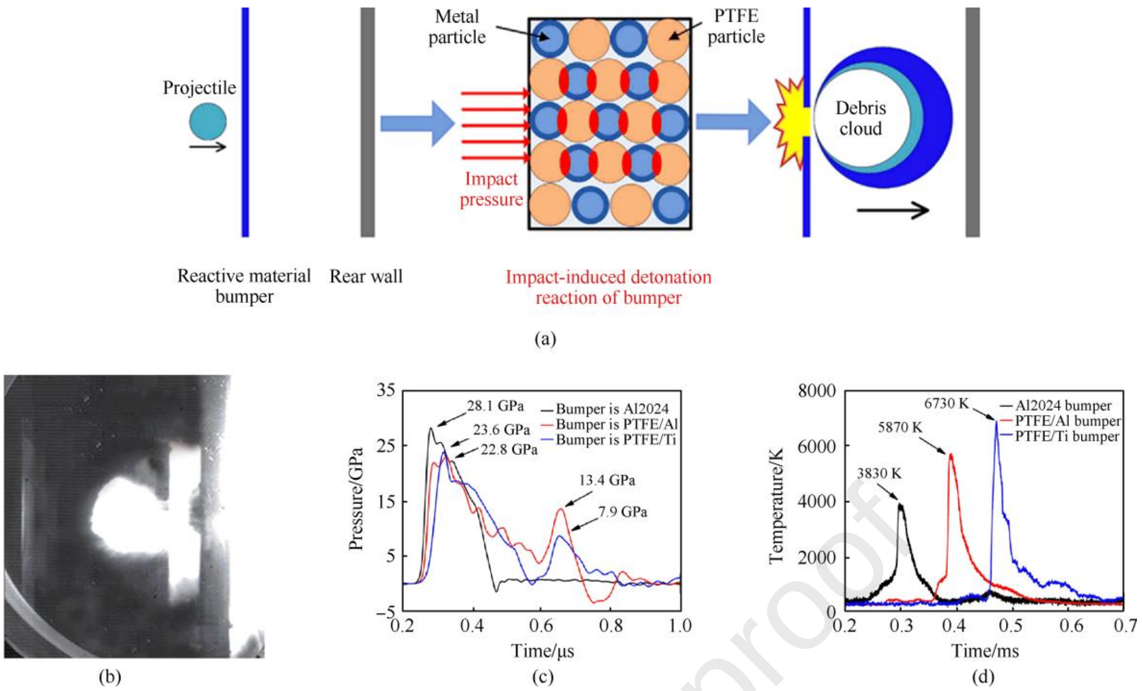


Fig. 30. Protective principle and hypervelocity impact characteristics of reactive material Whipple shield: (a) Protective principle of reactive material Whipple shield [256]; (b) The impact-induced reaction of reactive materials bumper under hypervelocity impact [249]; (c) The shock wave in the projectile induced by the combined effect of impact and detonation reaction [256]; (d) The reactive materials bumper can increase the temperature of the debris cloud [256].

The development of reactive materials provides an innovative idea. The combined effect of impact and detonation induced by the release of the internal chemical energy can greatly increase the duration of shock wave. The reactive materials can make the projectile fragmentation and decelerate more effectively, and the debris cloud disperses more effectively. In addition, the reaction products of the reactive materials are gas, which can effectively solve the problem of fragments generated by the bumper itself. The density of reactive material is lower than that of aluminum alloy. The disadvantage of reactive materials is the low strength, which makes it difficult for reactive material to be used as load bearing structure of spacecraft.

**3.7. Transparent materials**

Glass and transparent materials were used as optical devices for space station portholes and spacecraft solar panels [258], which were often subjected to hypervelocity impact, as shown in Fig. 31(a). The hypervelocity impact experiment of spacecraft impacting solar panels was carried out to study the influence of the damage caused by orbital debris impact on the electrical characteristics [260, 261]. Graham and Kearsley et al. [262] studied the impact of orbital debris and micrometeoroids on solar panel composed of a layer of silicone resin on the underlying silicon solar cell bonds the CMX glass layer and the top protective layer of borosilicate glass coated with a Mg+F layer, and residue material in impact craters was analyzed. The results show that some of the textural features observed in impact residues are dependent on the nature of the individual mineral components within the original impactor. The cracks of soda-lime (float) glass under the hypervelocity impact were studied to verify the effectiveness of the empirically determined power law spallation equation, which was used to predict the spallation diameters [263]. The damage characteristics of fused silica glass impacted by hypervelocity were studied by China Academy of Space Technology [264], and they suggested that 12 mm is the minimum thickness of the porthole windshield for a 400 km altitude orbit space station of 3 year's life time. NASA [265] tested the shielding performance of the fused silica window system of "Orion", next generation of US crewed spacecraft, as shown in Fig. 31(b), and the ballistic limit curve of fused silica glass was given to predict the perforation threshold. Yang et al. [266] developed a coupled thermo-mechanical model in the framework of thermodynamics with internal state variables to capture this extraordinary behavior of silica glass in hypervelocity impact, and they concluded that a highly efficient kinetic energy-absorption mechanism caused by the phase change emanating from high pressure characteristic to hypervelocity impact combined with irreversible densification of the material results in the high resistance to hypervelocity impact of silica-based glass. Hypervelocity impact experiments were performed on $SiO_2$ glass and polycarbonate plates to investigate their damage process by JAXA [267]. As shown in Fig. 31(c), it is found that $SiO_2$ glass damage is mainly composed of craters, internal damage area and cracks, the propagation velocity of surface fracture is almost constant, and the propagation velocity of internal damage area increase with decreasing target thickness. The propagation of stress wave in $SiO_2$ glass and polycarbonate was studied visually [268], as shown in Figs. 31(d) and 31(e). The interaction of the reflected longitudinal wave from free surface with shear wave causes the drastic nucleation of $SiO_2$ glass damage points, and the tensile waves reflected by the rear free surface and the both side free surfaces can cause the fracture of polycarbonate material.

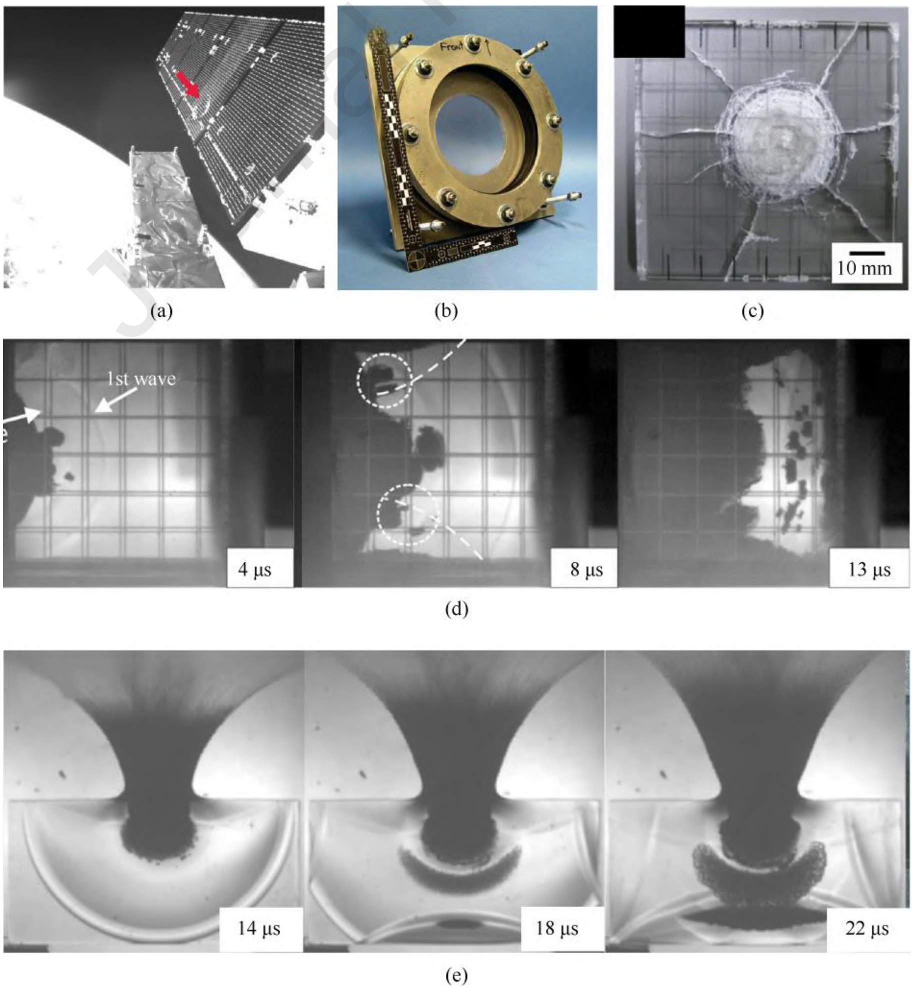

Fig. 31. Damage of glass and transparent materials induced by hypervelocity impact: (a) Solar panels damage induced by orbital debris impact [258]; (b) The fused silica window system of "Orion" crewed spacecraft [259]; (c) Damage of 5 mm thickness $SiO_2$ glass, 6.9 km/s [267]; (d) Shock wave shadowgraph images of $SiO_2$ glass impacted by a 3.2 mm aluminum sphere at 3.01 km/s [268]; (e) Shock wave shadowgraph images of polycarbonate impacted by a 4.7 mm polycarbonate sphere at 6 km/s [268].

### 3.8. Multifunctional materials

Nam and Kumar et al. [269] developed a stealth space hypervelocity impact shielding system containing electromagnetic wave absorption capability and impact shielding system, and the electrical modification of aramid fabric via a RF magnetron silver-sputtering coating technique was used to demonstrate excellent microwave absorption performance, as shown in Figs. 32(a) and 32(b). The silver coating has almost no effect the impact performance of the space stealth structure, and specific energy, type, and failure shape of the impact energy absorption of the proposed composite is similar to that of the original aramid composite. This silver coating material can realize multiple functions and has potential application value in military spacecraft with special characteristics. Polybenzimidazole (PBI) was developed as the film coating of carbon fiber materials to improve the hypervelocity impact shielding performance [270], and improve the shield system resistance to low earth orbit environment conditions like high vacuum, thermal cycling, atomic oxygen and ultraviolet radiation. Film coating material can bring other functions without affecting the shielding performance, and improve the multiple resistance of the shielding system to the space environment without obvious weight increase.

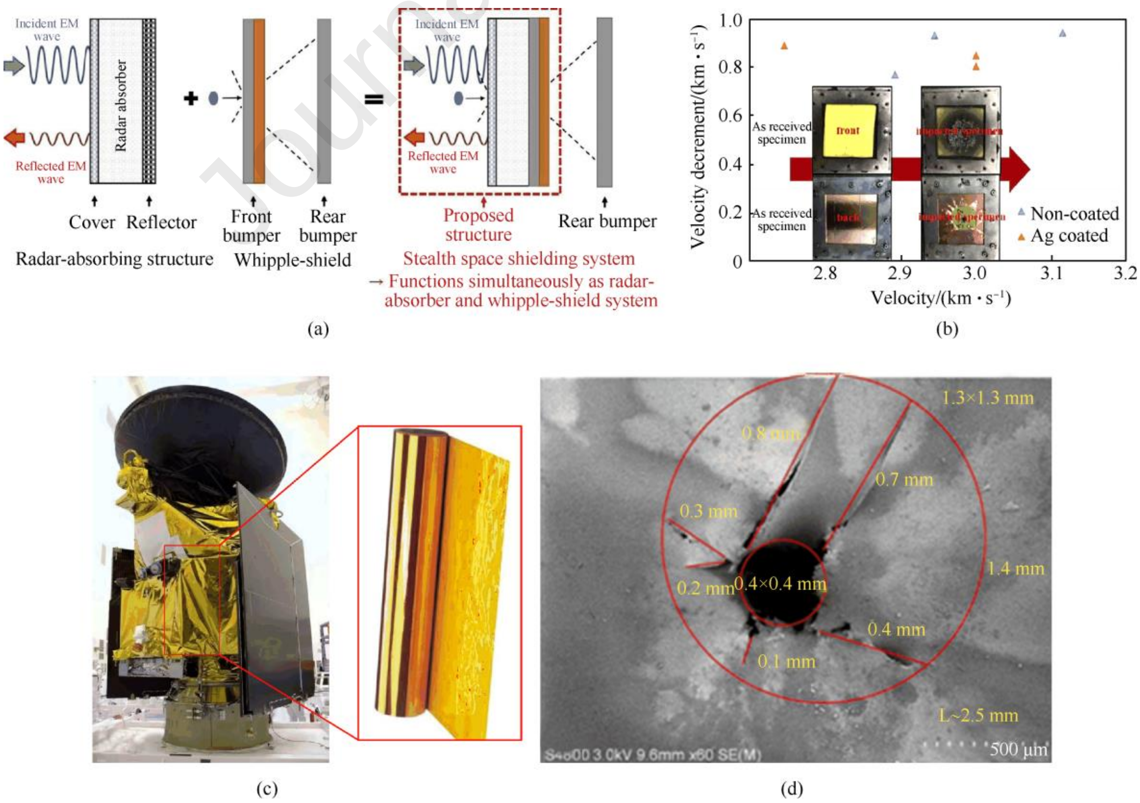


Fig. 32. Electromagnetic stealth material and polyimide film [269]: (a) Stealth space hypervelocity impact shielding system concept; (b) Deceleration ability of electromagnetic stealth materials to

projectile [269]; (c) Polyimide film as satellite thermal insulation materials [272]; (d) The damage of polyimide film under the hypervelocity impact [275].

Multilayer insulation (MLI) thermal blankets cover most areas of space station and many other spacecraft [271–273], the thermal blanket consists of multilayer aluminized, silverized or gilded polyimide film and multilayer mesh fabric separators to ensure that the spacecraft is within the allowable temperature range, as shown in Fig. 32(c). MLI was used as a component of shield system to test its influence on shielding performance. Canadian Space Agency adopted 1 to 2 layers Nextel enhanced MLI for RADARSAT satellite shield, which resulted that the risk of penetration dropped by a factor of 3 at the cost of a small increase in area density [274]. As shown in Fig. 32(d), though the impact tests, Liu and Zhang [275] observed the two failure modes of MLI: ductile penetration and brittle cracks damage, and the higher velocity and thinner film, the easier to produce brittle like cracks; length of the cracks increases with the decreasing film thickness and increasing impact velocity. The film thickness of MLI can change the morphology of debris clouds [276, 277]. Because MLI as a front bumper was less efficient in shattering the projectile compared to Al bumper of similar areal density, and MLI was often used as a stuffing layer [197]. Common impact signatures of MLI were ray patterns, melt, spallation, delamination, radial cracking, and blown-away coating, and the MLI and polyimide film's projectile size to impact hole diameter seems to have a dependence on film thickness, material type, or the effect between multi-layered [278].

Multifunctional materials are used as bumper material of spacecraft shield to meet some protection requirements, taking into account microwave absorption and thermal insulation functions. This can save weight, and the shielding performance can be strengthened with the saved weigh. However, because microwave absorbing materials and thermal insulation materials are not professional protective materials with high mechanical properties, they can only meet the lower protection requirements.

## 4. Numerical simulation of hypervelocity impact for advanced bumper materials

Numerical simulation can provide more data and details to better understand the impact process, and can also serve as a supplement to experiments to save research costs. Therefore, numerical simulation was widely used in the design and evaluation of space debris shield structure. Previously, the numerical simulation of traditional metal materials was relatively simple, the modeling methods and material parameters were relatively mature, and the numerical simulation results and experimental results had good consistency. With the emergence of more and more new materials, complex microstructures, diverse compositional materials, and unknown material parameters all pose new challenges to accurate numerical simulations.

As shown in Fig. 33, the development of new materials requires more advanced numerical simulation methods to improve computational accuracy and efficiency. Initially, the Finite Element Method (FEM) was applied to hypervelocity impact, such as the Lagrange algorithm [279, 280] and Euler algorithm [281, 282]. Lagrange has significant advantages in grid partitioning, computational feeiciency, and identifying fragment boundaries, but deleting the mesh to overcome large material deformation can result in significant discrepancies between the calculated and experimental results. The Euler algorithm can solve large deformation problems, but it needs to face problems such as material fracture and fragment boundary identification. CTH [283–285] is a code based on Euler algorithm for modeling large-deformation and strong shock problems in multiple dimensions and with multiple kinds of materials, and it is not able to treat non-eroding penetration/perforation problems very well. The ALE algorithm [286] combines Lagrange and Euler algorithms, but there was a problem of complex mixed grids.

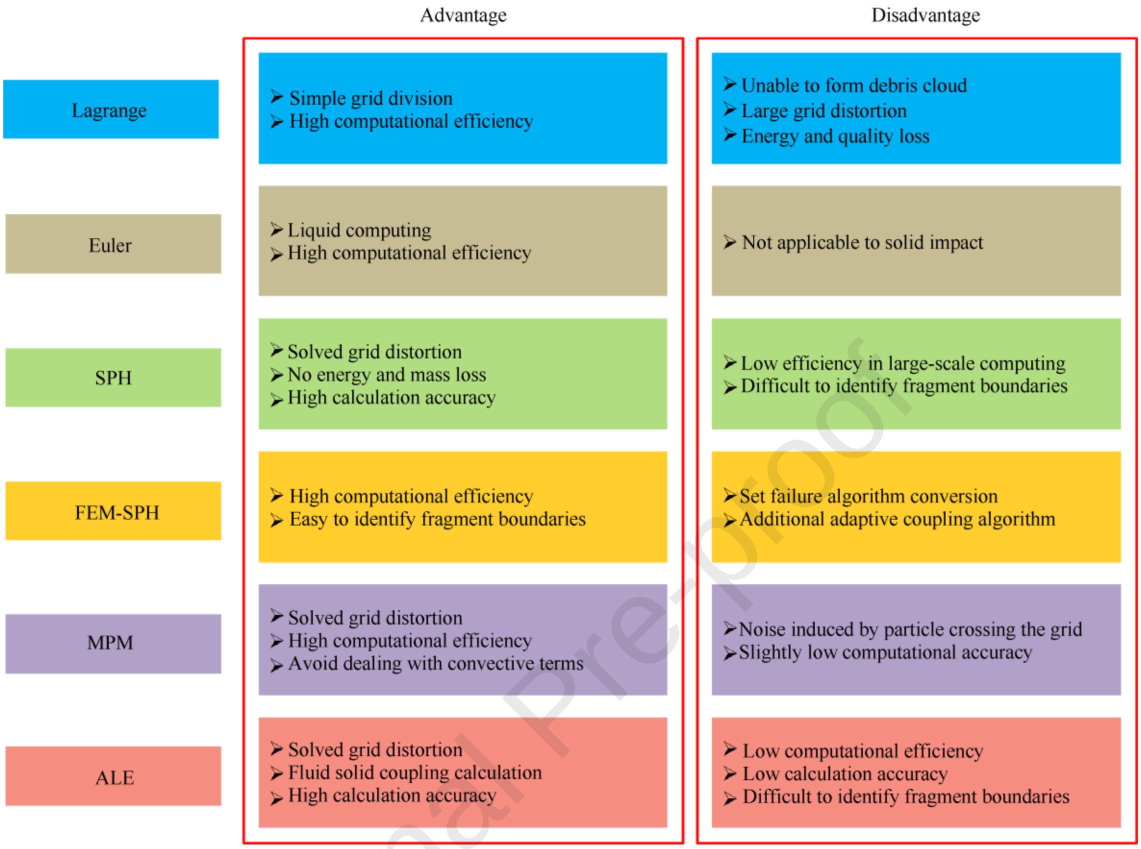


Fig. 33. Comparison of numerical simulation methods for hypervelocity impact.

In order to overcome the shortcomings of FEM, meshless method was widely used to solve the energy and mass loss problems caused by large deformations in hypervelocity impact. The early development of meshless method can be traced back to smoothed particle hydrodynamics (SPH) by Lucy [287], Gingold and Monaghan [288] for astrophysics modeling. The SPH algorithm, after multiple improvements, has been widely applied in research related to explosions and high velocity impacts. The SPH method solves the mesh distortion, but the large number of particles in the complex structure reduces the computational efficiency, especially facing the large scale differences between projectiles and targets. In addition, SPH also has the problem that the debris boundary is not easy to identify [289]. The material point method (MPM) is another particle kind meshless method proposed by Sulsky [290]. It uses particle discrete objects, is not limited by mesh distortion, and is easy to describe the fracture of materials [291]. Compared with Lagrange and Euler method, the MPM method is more advantageous when dealing with impact and penetration problems [292, 293].

The FEM-SPH adaptive coupling algorithm [294, 295] was proposed to solve the problems of material loss, large material deformation, and fragment boundary recognition, which replaces failed FEM elements with SPH particles to continue participating in calculations, and is currently being increasingly applied as a method. When materials have not failed, they are solved by the FEM, which provides suitable material models and equations of state for anisotropic materials. Failure materials, whose anisotropic properties can be ignored, are adequately represented by SPH particles [296–300]. Therefore, the FEM-SPH adaptive method is suitable for simulating anisotropic materials, but it is necessary to set appropriate loss criteria and additional adaptive transformation algorithms.

Many kinds of numerical simulation methods have been developed for sandwich panel hypervelocity impact, as shown in Fig. 34. The numerical simulation of hypervelocity impact of foam sandwich panels simulated by two methods of SPH and Lagrange was compared by Nitta [301], and Deconinck [72] converted the failed Lagrangian elements into SPH particles to ensure mass conservation and limit the step size drop at the contact interface. Chen [302] developed a new engineering model, and the honeycomb core was equaled to multi-parallel thin plates, which can represent the discontinuity of honeycomb core without complex boundary. The impact on honeycomb sandwich panel is essentially three-dimensional, especially for oblique incidence impacts that require three-dimensional modeling and analysis [65, 69]. However, it is reasonable to simplify the honeycomb sandwich panel to a two-dimensional model when only considering the normal impact, as the central fragment is mostly occurring phenomenon, leading to the damage of the back facesheet at normal incidence impact. Due to the computational cost and the concentration characteristics of debris clouds along the impact direction in normal collisions, two-dimensional axisymmetric simulation is sufficient to study the main physical phenomena [303]. Chen [304] used the adaptive algorithm coupled with FEM and SPH to calculate the hypervelocity impact of projectile on the honeycomb sandwich panel, converting the failed elements into particles, which can describe the movement of debris clouds and predict the damage of the honeycomb sandwich panel well.

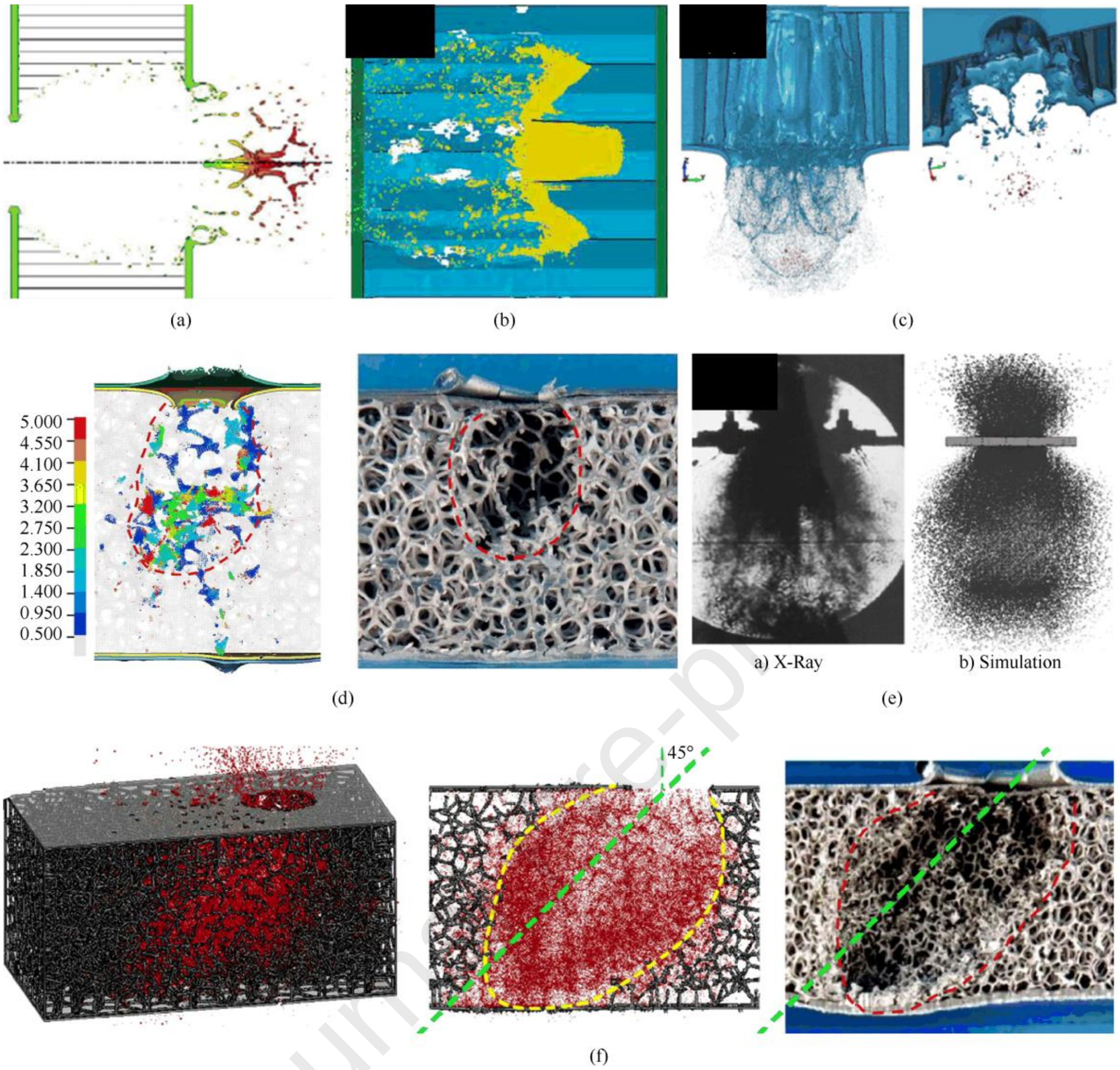


Fig. 34. The numerical simulation of hypervelocity impact sandwich panels: (a) Damage of honeycomb sandwich panel under normal impact [69]; (b) Debris cloud impacting honeycomb sandwich panel [72]; (c) Damage of foam sandwich panel under normal impact [304]; (d) Debris cloud impacting foam sandwich panel [311]; (e) Damage of foam sandwich panel under oblique impact [305]; (f) Finite element reconstruction (FER) simulation of impact of foam aluminum sandwich panel based on Voronoi technology [309, 310].

Zhang [305] proposed a Fractal Theory and Node-separation FEM to simulate the hypervelocity impact on foam sandwich panel. The Voronoi modeling technique is already used in the studies of crushing response simulations of the foam material. The beam element is used to model the ligaments in the open cell foam [306]; the shell element is used to model the walls in the close cell foam [307]; and the tetrahedron solid element is used in the foam model derived from the CT (Computed Tomography) scan [308]. However, all the three element types are not feasible in the hypervelocity impact simulation. Zhang [309, 310] coupled the Voronoi technique with the SPH method that is widely used for hypervelocity impact simulation. The voronoi tessellation method was used to model explicitly the cellular geometry, and the beam element was used to model the ligaments in the open cell foam. Then the cores of the cells are first generated by packing random spheres into the specified spatial domain, the weighted voronoi tessellation is then applied to make the cellular structure of the foam material, and hypervelocity impact simulation is conducted method combining the SPH and finite element reconstruction (FER) in LS-dyna. Cherniaev [311] obtained a realistic foam geometry model using X-ray computed tomography imaging, and conversed it to a meshless SPH model suitable for hypervelocity impact simulations. Ma [312, 313] produced the metallic foam using space-holding filler method, and three-dimensional SPH code for simulations of foams was developed.

As shown in Fig. 35, the delamination of fiber laminates, the 3D orthogonal woven microstructure micro model, and the non-circular fiber bundle interface are the difficulties in numerical simulation of fiber composite materials. The simulation of fiber composite materials was often calculated using SPH or FEM [314, 315], and treating each layer of material as a homogeneous material without considering the anisotropy of each phase material. The numerical simulation of fiber composite materials considering the preparation of three-dimensional material microscopic models has solved the problem of simplistic conventional models, greatly improving calculation accuracy. The application of SPH-FEM coupling algorithm has solved the problem of fiber bundle distortion and difficulty in identifying fragments in the calculation process of fiber materials [223, 316–319]. For numerical simulation model of fiber composite material, the model size needs to meet the actual needs of aerospace engineering and retain the main structural characteristics of the actual material, ignoring secondary factors, and minimizing the number of units and improving the quality of units as much as possible.

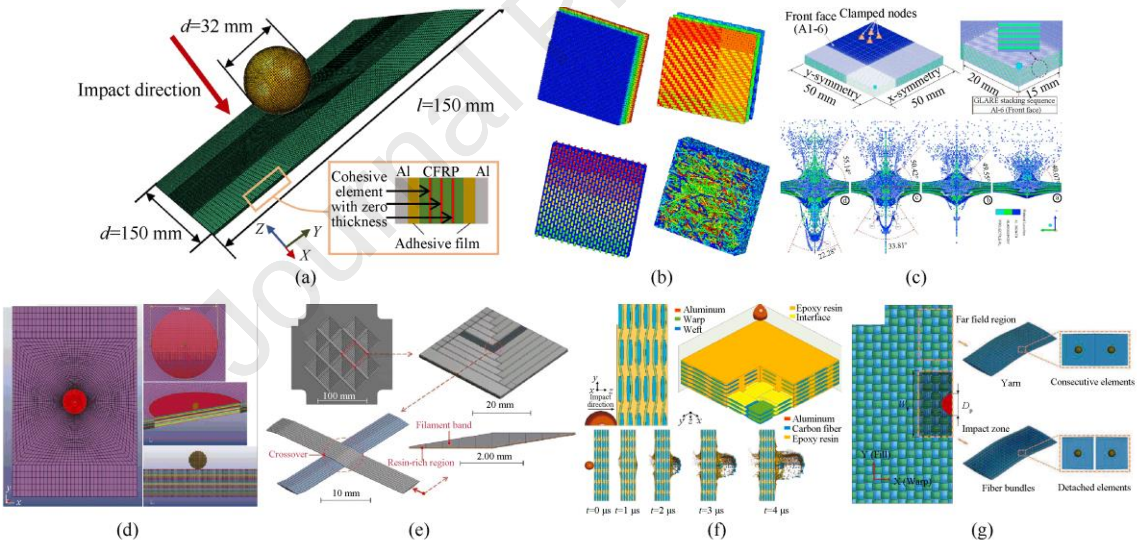


Fig. 35. The numerical simulation of fiber composite materials: (a) FEM Numerical simulation of carbon fiber reinforced aluminum alloy laminates [223]; (b) SPH Numerical simulation of carbon-fiber fabrics and epoxy composite [314]; (c) FEM-SPH numerical simulation of glass fiber reinforced aluminum fiber-metal laminates [315]; (d) FEM-SPH Numerical simulation of carbon fiber composite materials [316]; (e) FEM-SPH Numerical simulation of filament-wound carbon fiber composite [317]; (f) FEM-SPH Numerical simulation of carbon fiber-reinforced plastic laminate [318]; (g) FEM-SPH Numerical simulation of Kevlar fiber composite materials [319].

The numerical simulation of ceramic materials usually adopts FEM or SPH calculation [320–322]. The difficulty of simulation is to select the constitutive relationship and material parameters that determine the damage initiation, damage evolution, material strength degradation due to damage [163], crack initiation and crack propagation. Reasonable simulation of crack initiation, propagation, and branching requires a suitable numerical framework. Most of the determination of constitutive relationship parameters depends on the experimental results observed after impact, while ignoring the data during impact.

Material model of bumper for orbital debris protection is shown in Table 1. The selection of material models has a crucial influence on numerical simulation results, including strength models and equations of state (EOS).

Table 1

Material model of bumper for orbital debris protection.

| Reference | Material | Method | Strength model(s) | EOS(s) | Failure |
|---|---|---|---|---|---|
| Wen et al. [331] | Al2024 | SPH | SG model | Mie-Grüneisen, $\gamma_0$=2.0 | Grady spalling failure |
| Samet et al. [332] | Al2024 | FEM-SPH | JC model | Mie-Grüneisen,$\gamma_0$=1.97 | Maximum tensile stress failure |
| Iyer et al. [44] | Titanium | | JC model/SG model | EOS for Titanium | Grady spalling failure |
| Zhang et al. [132] | Ti/Al/Nylon Impedance graded | SPH | Al and Ti: SG model Nylon: Von-Mises model | Mie-Grüneisen, $\gamma_{0-\mathrm{Ti}}$ =1.23, $\gamma_{0-\mathrm{Al}}$ =2.0, $\gamma_{0-\mathrm{Nylon}}$=0.87. | Maximum tensile stress failure |
| Wen et al. [135] | Ti/Al/Steel Impedance graded | SPH | SG model | Mie-Grüneisen, $\gamma_{0-\mathrm{Al}}$ =2.0, $\gamma_{0-\mathrm{Mg}}$ =1.54, $\gamma_{0-\mathrm{Steel}}$=1.60. | Grady spalling failure |
| Chen et al. [304] | Al honeycomb sandwich: Al2024 facesheet, Al5056 honeycore | FEM-SPH | JC model | Mie-Grüneisen, $\gamma_{0-\mathrm{Al2024}}$ =2.0, $\gamma_{0-\mathrm{Al5056}}$=2.0. | Grady spalling failure |
| Liu et al. [335] | Al honeycomb sandwich: Al2024 facesheet, Al5052 honeycore | MPM | JC model | Mie-Grüneisen, $\gamma_{0-\mathrm{Al2024}}$ =2.0, $\gamma_{0-\mathrm{Al5052}}$=2.0. | Maximum tensile stress failure |
| Wang et al. [310] | Al6061 foam sandwich | SPH-FER | JC model | Mie-Grüneisen, $\gamma_0$=1.97 | Equivalent strain failure |
| Cherniaev et al. [311] | Al6061 foam sandwich | FEM-SPH | JC model | Mie-Grüneisen, $\gamma_0$=1.97 | / |
| Tang et al. [297] | Al6061 foam sandwich | FEM-SPH | JC model | Mie-Grüneisen, $\gamma_0$=1.97 | Maximum tensile stress failure |
| Zhong et al. [144] | $(Ti_{37.31}Zr_{22.75}Be_{26.39}Al_{4.55}Cu_9)_{94}Co_6$; HE-BMGs | SPH | JH-2 constitutive model | Polynomial EOS | JH-2 damage |
| Ren et al. [169] | NbC ceramic | SPH | JH-2 constitutive model | Polynomial EOS | JH-2 damage |
| Cherniaev et al. [172] | SiC ceramic | SPH | JH-1 constitutive model | Polynomial EOS | JH-1 damage |
| Ren et al. [256] | PTFE/Al | SPH | JC model | Lee–Tarver model, Reaction products JWL EOS, Unreacted PTFE/Al Mie-Grüneisen, $\gamma_0$=1.0 | Maximum tensile stress failure |
| Xu et al.[319] | Kevlar fiber | FEM-SPH | Orthotropic elastic model | Mie-Grüneisen, $\gamma_0$=0.7692 | Maximum strain-based failure |
| Yang et al. [333] | C/SiC fiber | SPH | Orthotropic elastic model | Nonlinear EOS | Orthotropic failure |
| He [318] | CFRP | FEM-SPH | Anisotropic material model MAT59 | Anisotropic material model MAT59 | EOS calculated by MAT59 automatically |

The commonly used strength models include ideal elastic-plastic model, Johnson-Cook (JC) model, and Steinberg-Guinan (SG) model [323–325]. The JC model is a description of the stress-strain relationship that considers the effects of strain hardening, strain rate hardening, and heat softening, and the JC model is widely considered suitable for low velocity impacts with low strain rates. Hauhurst and Livingstone's research [326] shows that the EOS is most critical in hypervelocity impact simulation, and the strength models have no significant effect on the development of phenomenon induced by hypervelocity impact. Therefore, the JC model still achieved good results in a large number of simulations of hypervelocity impacts. The SG model emphasizes the influence of pressure and temperature on the shear modulus and yield strength, and is more suitable for high strain rates than the JC model. For Fiber fabrics, the orthotropic models have to be used [327]. Fibers, such as Kevlar, Nextel, UHMWPE and other fibers, as the fundamental component in the fabric, are the anisotropic materials with linear elastic properties along the fiber axis and nonlinear inelastic properties in transverse direction. In anisotropic materials, the traditional independent approach for the solution of the strongly coupled EOS and strength models is complicated, as deviatoric strain leads to hydrostatic pressure and volumetric strain leads to deviatoric stress. The material model for fabric subjected to hypervelocity impact was developed based on a decoupled anisotropic constitutive relationship to considering shock response [319]. Johnson and Holmquist [328] proposed three models to predict spalling, formation of conoid, fragmentation and crack branching in the ceramic under dynamic load, namely Johnson-Holmquist I (JH1) and II (JH2) and the Johnson-Holmquist Bissel (JHB). The JH1 model used piecewise linear segments to describe the material strength and failure behavior, which suddenly change based on hydrostatic pressure and damage evolution. The JH2 model used continuous curves to represent dimensionless strength and damage, and sudden changes in strength and damage may represent a realistic description of the response of the brittle materials like ceramic. In the JHB model, the strength and damage are represented by analytic curves but changes in the material strength and damage with sudden jumps. Although the predicted results of JH1, JH2, and JHB ceramic material models are qualitatively similar, the JH1 and JHB provide results that are closer to the experimental results in terms of the spall plane in the flyer plate impact tests and the crack patterns and the conoid zone for the penetration problems [163]. For the description of the behavior of hypervelocity impact, such as debris cloud motion, bumper perforation, rear wall damage, both the predicted results of JH2 and JH1 have good consistency with the experimental results [144, 169, 172].

The EOS is a function that describes the relationship between pressure, density, and temperature of the material under the shock. Especially under strong load caused by hypervelocity impact, the impact pressure is much higher than the material strength, which lead to the weak strength effect in the initial stage of the impact, and the EOS plays the decisive role [326]. The strength effect gradually becomes apparent in the later stage of the impact. The Mie-Grüneisen EOS [281] can accurately describe the material dynamic behavior of solid metals under high temperature, high pressure, and high strain rate conditions. After modifying its parameters, it can also describe metals in liquid and gas phases. The Tillotson EOS [329] was constructed by combining the Thomas-Fermi model and the ideal gas model, and can describe the solid-gas transition. The compression and expansion states of materials, encompassing the solid, liquid, and gas phases, were depict by two complex forms, but ignores the melting and vaporization. The Gray

EOS [330] has a simpler analytical expression, and it can provide a broad description of the phase transition, including solid, liquid, and gas states, as well as the two-phase regions of melting and vaporization.

**5. Protective mechanism analysis and material selection principle**

Improving the shielding performance of spacecraft shield against hypervelocity impact of space debris is very important to aerospace safety. The further development of new bumper materials needs to resist the impact of centimeter-sized orbital debris to meet the safety requirements of manned space station. However, at present, only the Stuffed Whipple shield applied on the ISS can resist the impact of projectile with a diameter of 1–1.5 cm [33], and this is far from enough, due to the increase the penetration risk induced by rapid growth of the number of LEO small satellites. The improvement the shielding performance depends on the development of bumper materials with stronger characteristics. The change of material characteristics will lead to the change of physical phenomena in hypervelocity impact, including spall, fragmentation, internal energy increase, phase transition and debris cloud, and the internal physical essence is the energy exchange and the matter motion caused by the propagation and interaction of shock wave and tensile wave. The method of developing and improving materials is to change the propagation process and mode of stress wave, so as to change the energy redistribution and motion form between matters.

Tables 2–4 show the main physical properties of different materials. By studying and analyzing the development of bumper materials, it is summarized that the excellent impact resistance of the bumper materials depends on the following characteristics:

(a) Higher tensile strength, it can effectively increase resistance of projectile penetration and stop the projectile fragments;

(b) High modulus and high hardness, it can induce higher impact pressure, which can make the projectile effectively broken, melted and gasified;

(c) Low density, it can make bumper thickness as large as possible under the condition of limited area density, and shock wave in the projectile cannot be unloaded by the tensile wave reflected from the bumper back, resulting in a long duration of the shock wave;

(d) No large size and hard fragments were produced by itself, which can reduce the damage of the rear wall;

(e) Effectively dispersing debris cloud, it can disperse the debris cloud and reduce the load density at the impact center of the rear wall;

(f) Lower melting and gasifying temperature, bumper materials are more prone to melting and gasification.

(g) Low cost, this is a great advantage as a protective material for large spacecraft.

Table 2

Typical physical properties of metal materials.

| Material | Density/(g·cm$^{-3}$) | Tensile strength/MPa | Yield strength/MPa | Elastic modulus/GPa | Shear strength/MPa | Shear modulus/GPa | Note |
|---|---|---|---|---|---|---|---|
| Al2024 [334] | 2.78 | 483 | 345 | 73.1 | 285 | 28.6 | Advantages: low cost, low density, high toughness; Disadvantage: low strength and modulus; Al plate and Al mesh are recommended as the first bumper to shatter projectile. |
| Al6061 [334] | 2.75 | 310 | 276 | 68.9 | 270 | 27.6 | |
| Al2017 [334] | 2.8 | 427 | 276 | 72.4 | 280 | 26.7 | |
| Al5052 [335] | 2.68 | 426 | 265 | 73 | 250 | 26.9 | |
| SUS 304 [334] | 7.93 | 505 | 215 | 200 | 550 | 77 | Advantage: high tensile strength and modulus; Disadvantage: high density leads to the bumper being too thin under limited areal density conditions; It is not recommended as the bumper material. |
| Titanium [334] | 4.51 | 240 | 310 | 105 | 440 | 43.4 | The performance is between aluminum alloy and steel. Recommended as the first layer bumper to shatter projectile. |
| AZ31B Mg [52, 53] | 1.82 | 150 | 60 | 43 | 120 | 16.5 | Advantages: low density; Disadvantage: Low small strength and modulus; It is not recommended as the bumper material. |
| Ti/Al/Mg [131, 132] | / | / | / | / | / | / | The combination of three materials compensates for each other's shortcomings, allowing for better shattering, melting, and vaporing projectile, increasing the impact area of debris clouds on the rear wall; It is recommended as the first bumper to shatter projectile. |
| Al foam/ sandwich panel | / | / | / | / | / | / | Advantages: lightweight and high kinetic energy absorption efficiency; Disadvantage is that the volume is relatively large; It is recommended as the first or filling layer to shatter and absorb fragments. |

Table 3

Typical physical properties of ceramics and amorphous alloy.

| Material | Density/(g·cm$^{-3}$) | Elastic modulus/GPa | Shear modulus/GPa | Fracture toughness/(MPa·m$^{1/2}$) | Microhardness/GPa | Note |
|---|---|---|---|---|---|---|
| NbC [169, 336] | 4.8 | 345 | 164 | 2.5 | 23.5 | Advantages: high modulus, high hardnes, which can increase the impact pressure and better shatter the projectile; Disadvantages: slightly higher density, low the fracture toughness leading to easy to fracture failure; It is recommend using ductile metal Al as backing layer to form ceramic-metal as the first layer bumper to shatter and melt projectile. |
| $TiB_2$ [170] | 4.4 | 600 | / | 11.5 | 33 | Advantages: high modulus and high hardness, which can better shatter the projectile; Disadvantages: Although the fracture toughness is higher than most ceramics, it is much lower than that of metals, which make it easy to fracture failure; It is recommend using ductile metal Al as backing layer to form ceramic-metal as the first layer bumper to shatter and melt projectile. |
| $B_4C$ [171] | 2.5 | 448 | 220 | 4.81 | 50 | Advantages: high hardness, high modulus, and lower density; Disadvantages: low fracture toughness; It is recommended using ductile metal Al as backing layer to form ceramic-metal as the first layer bumper to shatter and melt projectile. |
| SiC [172] | 3.2 | 450 | 193.5 | 4.3 | 22 | Advantages: high hardness, high modulus.; Disadvantages: low fracture toughness; It is recommended using ductile metal Al as backing layer to form ceramic-metal as the first layer bumper to shatter and melt projectile. |
| $Al_2O_3$ [150, 336] | 3.8 | 400 | 120.3 | 3.5 | 20 | Advantages: high hardness, high modulus; Disadvantages: low fracture toughness, which make it easy to fracture failure; It is recommended |

| | | | | | | |
|---|---|---|---|---|---|---|
| | | | | | | using ductile metal Al as backing layer to form ceramic-metal as the first layer bumper to shatter and melt projectile. |
| $ZrO_2$ [336] | 6.0 | 200 | 90 | 12 | 13 | Advantages: high modulus and high hardness; Disadvantages: high density, although the fracture toughness is higher than other ceramics, it is much lower than that of metals, which make it easy to fracture failure. It is recommended as the surface coating for the first layer metal bumper to shatter and melt projectile. |
| $(Ti_{37.31}Zr_{22.75}Be_{26.39}Al_{4.55}Cu_9)_{94}Co_6$ HE-BMGs [144] | 5.27 | 108.7 | 40.5 | 50 | / | Advantages: high elastic modulus and shear modulus, high fracture toughness, which can ensure that the bumper will not break as a whole; Disadvantages: slightly high density; It is can be used as first layer bumper alone without adding a backing layer to shatter the projectile. |
| $Zr_{53}Cu_{30}Ni_9Al_8$ [337] | 6.45 | 883.1 | 30.5 | 122 | / | Advantages: high elastic modulus and shear modulus, high fracture toughness; Disadvantages: high density; It is recommended as the surface coating for the first layer metal bumper to shatter and melt projectile. |



Table 4

Typical physical properties of high strength fibers.

| Material | Density/(g·cm$^{-3}$) | Tensile strength/GPa | Tensile modulus/GPa | Fiber direction/Interlayer Shear modulus/GPa | Elongation at Break/% | Note |
|---|---|---|---|---|---|---|
| Kevlar [186] | 1.45 | 2.41–3.15 | 123 | 16.4/1.8 | 4.5 | Advantages: low density high tensile strength, modulus and elongation; Disadvantages: low shear modulus, making it prone to shear failure and perforation when used as the first layer bumper; It is recommended as the filling layer for SW shield or the last few |

| | | | | | | |
|---|---|---|---|---|---|---|
| | | | | | | layers for the MB shield to decelerate, intercept and further shatter fragments. |
| Nextel 610 [186, 338] | 2.7 | 1.7 | 257 | 25.8/14.4 | 3 | Advantages: higher elastic modulus and shear modulus than Kevlar, low density; It is generally placed in front of Kevlar when used as filling layer of SW shield to shatter and decelerate the fragments first. |
| CFRP [187] | 1.76 | 3.60 | 230–240 | 10/8.96 | 1.3 | Advantages: low density, high tensile strength and modulus; Disadvantages: low shear modulus; It is recommended as the filling layer for SW shield or the last few layers for the MB shield to decelerate, intercept and further shatter fragments. |
| Vectran/Epoxy [191, 339] | 1.41 | 3.61 | 83 | 1.41/0.82 | 4.26 | Advantages: low density, high tensile strength. Disadvantages: low shear modulus, low tensile modulus than other fiber, making it prone to significant deformation; It is recommended as the filling layer for SW shield with strong shatter ability material as the first layer of bumper. |
| Basalt fiber [192, 340] | 2.6 | 3.00 | 110 | 1.85/1.5 | 3.15 | Advantages: high tensile strength; Disadvantages: lower elastic modulus and shear modulus; It is recommended as the filling layer for SW shield to decelerate, intercept and further shatter fragments. |
| UHMWPE [194, 245] | 0.97 | 3.00 | 103 | 1.97/0.67 | 3.1 | Advantages: extremely low density, high tensile strength; Disadvantages: lower elastic modulus and shear modulus; It is recommended as the filling layer for SW shield to decelerate, intercept fragments. |
| Glass/Epoxy [243] | 1.8 | 1.4–2.5 | 30.8 | 8.1/3.89 | 1.14 | Advantages: low density and high tensile strength; Disadvantages: lower elastic modulus and shear modulus; It is recommended as the filling layer for SW shield to decelerate, intercept fragments. |

Because some of these properties will contradict each other, a material cannot have all of the above favorable properties. The shielding performance of the bumper ultimately depends on the results of the combined effect of the bumper material advantages and disadvantages. The current development trend is that a variety of materials make up for each other's disadvantages and will be combined to form the composite material and composite structure as the bumper. At present, the Stuffed Whipple shield and multi-bumper shield were proved to have high shielding performance, and bumper materials with different configurations can be selected according to the advantages and disadvantages of different materials. The material with the excellent ability to shatter projectile and disperse debris cloud is the primary choice for the first layer bumper, and it should also be considered that the first layer bumper material should have a higher strength as the load bearing structure of the outer surface of spacecraft. So, aluminum alloy plate, metal mesh, Ti/Al/Mg impedance-graded composite, mesh reinforced aluminum matrix composite and ceramic-metal composite are suitable for the first layer bumper of the spacecraft shield. The intermediate stuffing layer and the subsequent bumpers need to have an excellent ability to stop projectile fragments and absorb the kinetic energy of debris cloud, and the bumper itself cannot produce fragments to avoid increasing the damage of the rear wall. So, fiber fabric materials, foam sandwich panel and reactive materials are suitable for the intermediate stuffing layer and the subsequent bumpers of the spacecraft shield. The bumper of each layer may also be composed of composite materials formed from a variety of materials, and the protection scheme shall be determined according to the specific actual needs.

For the spacecraft with small overall spacing and weight for shield structure, Whipple shield has to be adopted. For the positions with low protection requirements, the bumper material of Whipple shield can be traditional metals. For the positions with high protection requirements, it is best to choose a material with strong projectile shattering ability, and that does not produce fragments by itself. This can ensure that the debris cloud expands sufficiently before impacting the rear wall of the spacecraft, and reduce its own damage to the rear wall.

The hypervelocity impact experiments and analysis of different structures with various material combinations need to be carried out, and the optimal material combination with the matching structure configuration can be selected. In general, the shield needs to be able to resist the impact of centimeter projectile on spacecraft, which can ensure the space operation safety of manned spacecraft and high valued satellites and deal with the threat of the explosive growth of centimeter space debris that may be caused by large-scale satellite constellation impact.

**6. Summary and future direction**

In this paper, a comprehensive overview of advances in the development of bumper materials for spacecraft shield applications was provided. In particular, we reviewed and discussed the protection mechanism and process of the bumper using different materials against hypervelocity impact. According to the properties of different materials, the advantages and disadvantages of each material used in shield were analyzed, and the principles and strategies of material selection were discussed.

Recommendations for the application of different types of materials in shields are as follows:

(a) Traditional metal materials, impedance-graded materials, metal mesh, amorphous alloy materials and ceramic-metal materials are suitable as the first layer bumper for all shields, which can better shatter the projectile;

(b) Fiber fabrics, reactive materials are suitable as the filling layer for Stuffed Whipple shield and last few layer bumpers of Multi-bumper shield, as these materials can intercept and further shatter fragments in the debris cloud without producing metal fragments themselves;

(c) Foam sandwich panel is suitable as the first layer bumper for shields and filling layer bumper for Stuffed Whipple shield, which depends on whether its core structure focuses on crushing effect or kinetic energy absorption efficiency;

(d) If mesh reinforced aluminum matrix materials can be further lightweight, it can be combined with fiber material as the filling layer of Stuffed Whipple shield, which must be located in front of the fiber fabric to reduce the threat of its own metal fragments to the rear wall.

The following opinions are suggested for future material development and research：

(a) At present, most material protection mechanisms are still traditional. Developing materials with novel protection mechanisms, rather than relying only on impact effect, breaks through the bottleneck of material protection ability;

(b) The current development trend is that a variety of materials make up for each other’s disadvantages and will be combined to form the composite material and composite structure as the bumper. All developed bumper materials with high shielding performance should be taken as the sample library, and several kinds shall be selected from the sample library according to their respective characteristics to form new composite in different combinations, and the shielding performance of the new composite should be verified based on hypervelocity impact tests results. The position, sequence and weight ratio of every bumper material in the shield structure should be consistent with its own advantages and characteristics;

(c) Using advanced technology, such as film coating technology and thin diaphragm thermal control technology, the resistance to low earth orbit environment conditions like high vacuum, thermal cycling, atomic oxygen, ultraviolet radiation, magnetic field and others can be integrated into the shielding system. Alternatively, high shielding performance materials with multi-functions can be developed to meet multiple functional requirements, and the shielding performance can be strengthened with the saved weigh;

(d) For new materials, the influence of structural characteristics, such as the number of bumper layers, spacing distribution and area density distribution, on the shielding performance of shield structure should be studied, and by optimizing the structure, the bumper materials can give full play to the advantage of impact resistance;

(e) The debris cloud models should be developed to analyze motion characteristics of debris clouds induced by different materials. According to the essence of shock wave propagation and interaction, the theoretical design method of bumper materials and shield structure should be established. It is necessary to accelerate the development of new numerical simulation technology, which can improve the efficiency of shielding system design;

(f) Satisfactory space environment resistance of materials is the premise of space application. However, at present, most new materials stay in the laboratory, and it is necessary to carry out engineering application research on the materials, so as to provide a solid foundation for application.

**Acknowledge**

This work was supported by National Natural Science Foundation of China (Grant Nos. 12202068, 12202087) and China National Space Administration Preliminary Research Project (Grant Nos. KJSP2023020201, KJSP2020010402).

**References**

[1] Klinkrad H. Large satellite constellations and related challenges for space debris mitigation. Journal of Space Safety Engineering 2017; 4(2):59-60.

[2] Petit A, Rossi A, Alessi EM. Assessment of the close approach frequency and collision probabilityfor satellites in different configurations of large constellations. Advance In Space Research 2021; 67:4177-4192.

[3] Foust J. SpaceX's space-Internet woes: Despite technical glitches, the company plans to launch the first of nearly 12,000 satellites in 2019. IEEE Spectrum 2019; 56(01):50-51.

[4] Smirnov NN, Kiselev AB, Smirnova MN, Nikitin VF. Space traffic hazards from orbital debris mitigation strategies. Acta Astronaut 2015; 109:144-152.

[5] Jane R, Marshall P, Michael ME, et al. The Science Performance of JWST as Characterized in Commissioning. Publications of the Astronomical Society of the Pacific 2023; 135:048001.

[6] Pearlman RZ. Soyuz spacecraft suffers 'fairly substantial' leak at space station, cancels spacewalk by Russian cosmonauts. Space News 2022.

[7] NASA. Orbital Debris Quarterly News. March 2023; Volume 27, Issue 1.

[8] Wen K, Chen XW, Lu YG. Research and development on hypervelocity impact protection using Whipple shield: An overview. Defence Technology 2020.

[9] Fang Y, Pan J, Luo Y, et al. Effects of deorbit evolution on space-based pulse laser irradiating centimeter-scale space debris in LEO. Acta Astronautica 2019; 165:184-190.

[10] Fang Y. Influence rules of ground-based laser active removing centimeter-sized orbital debris in LEO. Optik-International Journal for Light and Electron Optics 2018; 170:210-219.

[11] Gruntman M. Passive optical detection of submillimeter and millimeter sizespace debris in low Earth orbit. Acta Astronautica 2014; 105:156-170.

[12] Maiden CJ, Mcmillan AR. An investigation of the protection afforded a spacecraft by a thin shield. AIAA Journal 1964; 2(11):1992 -1998.

[13] Ang JA. Impact flash jet initiation phenomenology. International Journal of Impact Engineering 1990; 10(1):23-33.

[14] Piekutowski AJ. Characteristics of debris clouds produced by hypervelocity impact of aluminum spheres with thin aluminum plates. International Journal of Impact Engineering 1993; 14(1):573-586.

[15] Piekutowski AJ. Debris clouds generated by hypervelocity impact of cylindrical projectiles with thin aluminum plates. International Journal of Impact Engineering 1987; 5(1):509-518.

[16] Swift HF. "Hypervelocity Impact Mechanics" in Impact Dynamics, John Wiley & Sons, New York 1982.

[17] Schonberg WP, Mohamed E. Analytical hole diameter and crack length models for multi-wall systems under hypervelocity projectile impact. International Journal of Impact Engineering, 1999; 23(1):835-846.

[18] Lambert M, Schneider E. Shielding against space debris. A comparison between different

shields: The effect of materials on their performances. International Journal of Impact Engineering 1995, 17(4-6):477-485.

[19] Rogers JA, Bass NT, Wiest ML, et al. The pursuit of hypervelocities: A review of two-stage light gas gun aeroballistic ranges. International Journal of Impact Engineering 2024; 185:104861.

[20] Ren SY, Wu Q, Zhang PL, et al. Damage effects of aluminum alloy honeycomb sandwich panel double-layer structure induced by reactive projectile hypervelocity impact. Thin–Walled Structures 2024; 202:112076.

[21] Piekutowski AJ, Poormon KL. Meeting the challenges of hypervelocity impact testing at 10 km/s. International Journal of Impact Engineering 2023; 180:104665.

[22] Alesbrook LS, Burchell MJ, Cornwell LT, et al. Hypervelocity impact induced light flash experiments on single and dual layer Kapton targets to develop a time of flight space dust and debris detector. International Journal of Impact Engineering 2024; 187:104897.

[23] Hew YM, Close S. Hypervelocity impact flash expansion geometry under various spacecraft surface electrical conditions. International Journal of Impact Engineering 2021; 150:103792.

[24] Wang J, Gong LF, Long RR, et al. An expansion model of hypervelocity impact-generated plasma aided byspectral methods. International Journal of Impact Engineering 2024; 186:104896.

[25] Estacio B, Young SAQ, Lee N, et al. Experimental evidence of rapid target charging electromagnetic pulse from hypervelocity impact. International Journal of Impact Engineering 2023; 173:104473.

[26] Whipple FL. Meteorites and Space travels. The Astronmical Journal 1947; 1161:131.

[27] NASA Orbital Debris Program Office. Hypervelocity impact technology-shield development-basic concepts. https://hvit.jsc.nasa.gov/shield-development.

[28] Cour-palais BG, Crews JL. A Multi-Shock concept for spacecraft shielding. International Journal of Impact Engineering 1990;10:135-146.

[29] Cour-Palais BG, Piekutowski AJ. The multi-shock hypervelocity impact shield.1992.

[30] Dvorak BD. Multi-shock assembly for protecting a spacecraft surface from hypervelocity impactors: US, US6298765 B1. 2001.

[31] Zhang QM, Long RR, Huang FL, et al. A model for debris clouds produced by impact of hypervelocity projectiles on multiplate structures. Applied Physics Letters 2008, 93(21):215.

[32] Christiansen EL, Kerr JH. Ballistic limit equations for spacecraft shielding. International Journal of Impact Engineering 2001; 26:93-104.

[33] Christiansen EL, Crews JL, Williamsen JE, et al. Enhanced meteoroid and orbital debris shielding. International Journal of Impact Engineering 1995; 17:217-228.

[34] Piekutowski AJ, Poormon KL, Christiansen EL, et al. Performance of Whipple shields at impact velocities above 9 km/s. International Journal of Impact Engineering 2011; 38(6):495-503.

[35] Song Z, Pei X, J Yu, et al. Hypervelocity impact tests on a Whipple shield using a flyer plate in the velocity range from 4 km/s to 12 km/s. International Journal of Impact Engineering 2021; 156(11):103899.

[36] Bjork RL. The role of melting and vaporization in hypervelocity impact. Memo RM-3490-PR, 1965.

[37] Alfè D, Adlo LV, Price GD, et al. Melting curve of materials: theory versus experiments. Journal of Physics Condensed Matter 2004; 16(14):S973.

[38] Schonberg WP, Tullos RJ. Spacecraft wall design for increased protection against penetration by

orbital debris impacts. Aiaa Journal, 1990, 29(12):2207-2214.

[39] Olivieri L, Giacomuzzo C, Francesconi A, et al. Experimental characterization of multi-layer 3D-printed shields for microsatellites. Journal of Space Safety Engineering 2020, 7:125–136.

[40] Wadley H, Dharmasena KP, O'Masta MR, et al. Impact response of aluminum corrugated core sandwich panels. International Journal of Impact Engineering 2013; 62:114-128.

[41] Onder A. Projectile fragmentation and debris cloud formation behaviour of wavy plates in hypervelocity impact. International Journal of Impact Engineering 2024; 183,104788.

[42] Ratliff M, Christiansen EL, Bryant C. Single-wall equation for titanium shield, NESC Study of meteoroid protection for JWST cryogenic harnesses. May 2008.

[43] Arnold J, Christiansen EL, Davis A, et al. Handbook for Designing MMOD Protection. 2009.

[44] Iyer KA, Poormon KL, Deacon RM, et al. Hypervelocity impact response of Ti-6Al-4V and commercially pure titanium. Procedia Engineering 2013; 58:127-137.

[45] Li HT, Zhang YM, Yang DZ. Micro-damage of Ti–6Al–4V alloy under hypervelocity projectile impact. Materials Science & Engineering A 2000; 292:130-132.

[46] Belov GV, Golubev VK, Yutkina NA. Damage of a steel plate from hypervelocity impact. Combustion Explosion & Shock Waves 1997; 33:100-102.

[47] Shockey DA, Curran DR, Carli PD. Damage in steel plates from hypervelocity impact. I. Physical changes and effects of projectile material. Journal of Applied Physics 1975; 46:3766-3775.

[48] Iyer KA, Mehoke DS, Brown RC, et al. Use of hydrocode modeling to develop advanced MMOD shielding designs[C]// Aerospace Conference. IEEE, 2012.

[49] D Hote KD, Verma PN. Investigation of hole formation by steel sphere impacting on thin plate at hypervelocity. Thin-Walled Structures 2017; 126:38-47.

[50] D Hote KD, Verma PN. Investigation of Hole Size Formation by Steel Sphere Impacting on Thin Plate at Hypervelocity. Procedia Engineering 2017; 173:323-330.

[51] Verma PN, Dhote KD . Characterising primary fragment in debris cloud formed by hypervelocity impact of spherical stainless steel projectile on thin steel plate. International Journal of Impact Engineering 2018; 120:118-125.

[52] Kim YH, Knang MJ, Simpson G, et al. Anisotropic debris cloud formation after hypervelocity impact into rolled magnesium alloy plates. International Journal of Impact Engineering 2023; 182,104754.

[53] Zhang WG, Li K, Chi RQ, et al. Insights into microstructural evolution and deformation behaviors of a gradient textured AZ31B Mg alloy plate under hypervelocity impact. Journal of Materials Science & Technology 2021; 91:40-57.

[54] Zen S, Ava K, Gedikli H, et al. Low-energy impact response of composite sandwich panels with thermoplastic honeycomb and reentrant cores. Thin-Walled Structures 2020; 156:106989.

[55] Chen Z, Liu L, Gao S, et al. Dynamic response of sandwich beam with star-shaped reentrant honeycomb core subjected to local impulsive loading. Thin-Walled Structures 2021; 161:107420.

[56] Faidzi MK, Abdullah S, Abdullah MF, et al. Review of Current Trends for Metal-based Sandwich Panel: Failure Mechanisms and Their Contribution Factors. Engineering Failure Analysis 2021; 105302.

[57] Valean C, Sosdean C, Marsavina L, et al. Mechanical characterization of lightweight foam-based sandwich panels 2021; 45:4166-4170.

[58] Zhang J, Lu G, Zhang Y, et al. A study on ballistic performance of origami sandwich panels. International Journal of Impact Engineering 2021; 156:103925.

[59] Sun GY, Huo XT, Wang H, et al. On the structural parameters of honeycomb-core sandwich panels against low-velocity impact. Materials Part B Engineering 2021; 216:108881.

[60] Taylor EA, Glanville JP, Clegg RA, et al. Hypervelocity Impact On Spacecraft Honeycomb: Hydrocode Simulation And Damage Laws. International journal of impact engineering 2003; 29:691-702.

[61] Ryan S, Schaefer F, Destefanis R, et al. A ballistic limit equation for hypervelocity impacts on composite honeycomb sandwich panel satellite structures. Advances in Space Research 2008; 41:1152-1166.

[62] Lathrop BL, Sennett RE. Effects of hypervelocity impact on honeycomb structures. Journal of Spacecraft and Rockets 1968; 5:1496-1497.

[63] Ke FW, Jie H, Wen XZ, et al. Study of reducing the congregating effect of honeycomb structure on debris cloud. Acta Astronautica 2019; 170:145-153.

[64] Warren J, Cole M, Offenberger S, et al. Hypervelocity Impacts on Honeycomb Core Sandwich Panels Filled with Shear Thickening Fluid. International Journal of Impact Engineering 2013; 2:1352-1362.

[65] Kang P, Youn SK, Lim JH. Modification of the critical projectile diameter of honeycomb sandwich panel considering the channeling effect in hypervelocity impact. Aerospace Science and Technology 2013; 29:413-425.

[66] Ryan S, Christiansen EL. Hypervelocity impact performance of open cell foam core sandwich panel structures. NASA Johnson Space Center, Houston, NASA/TM-2015-218593, 2015.

[67] Schonberg W, Schaefer F, Putzar R. Hypervelocity impact response of honeycomb sandwich panels. Acta Astronautica 2010; 66:455-466.

[68] Ryan S, Schaefer F, Destefanis R, et al. A ballistic limit equation for hypervelocity impacts on composite honeycomb sandwich panel satellite structures. Advances in Space Research 2008; 41:1152-1166.

[69] Sibeaud JM , Thamie L, Puillet C. Hypervelocity impact on honeycomb target structures: Experiments and modeling. International Journal of Impact Engineering, 2008, 35:1799-1807.

[70] Xie WH, Meng SH, Ding L, et al. High-temperature high-velocity impact on honeycomb sandwich panels. Materials Part B. Engineering 2018; 138:1-11.

[71] Khodaei M, Farahani MS, Haghighi-Yazdi M. Numerical investigation of high velocity impact on foam-filled honeycomb structures including foam fracture model. Mechanics of Advanced materials and structures 2020; 4:1-13.

[72] Deconinck P, Abdulhamid H, Héreil PL, et al. Experimental and Numerical Study of Submillimeter-Sized Hypervelocity Impacts on Honeycomb Sandwich Structures. Procedia Engineering 2017; 204:452-459.

[73] Zhu YF, Sun YG. Low-velocity impact response of multilayer foam core sandwich panels with composite face sheets. International Journal of Mechanical Sciences 2021.

[74] Zhao Y, Yang Z, Yu T, et al. Mechanical properties and energy absorption capabilities of aluminium foam sandwich structure subjected to low-velocity impact[J]. Construction and Building Materials 2021; 273:121996.

[75] Huo X, Liu H, Luo QT, et al. On low-velocity impact response of foam-core sandwich panels.

International Journal of Mechanical Sciences 2020; 181:105681.

[76] Amith K. Low-velocity impact damage and energy absorption characteristics of stiffened syntactic foam core sandwich materials. Construction and Building Materials 2020; 246:118412.

[77] Zhang X, Xu F, Zang Y, et al. Experimental and numerical investigation on damage behavior of honeycomb sandwich panel subjected to low-velocity impact. Composite Structures 2020; 236:111882.

[78] An Y, Ma H, Zhang J, et al. Foaming Stabilization and Mechanical Properties of High-toughness Aluminum Foam Fabricated Using Non-thickening Foaming Technology. Journal of Materials Processing Technology 2021; 296:117212.

[79] Wan T, Liu Y, Zhou C, et al. Fabrication, properties, and applications of open-cell aluminum foams: A review. Journal of Materials Science and Technology 2021; 62:11-24.

[80] Maka B, Pjh B, Mai B, et al. Strain-rate dependency and impact dynamics of closed-cell aluminium foams. Materials Science and Engineering: A 2021; 818:141379.

[81] Kader MA, Islam MA, Saadatfar M, et al. Macro and micro collapse mechanisms of closed-cell aluminium foams during quasi-static compression. Materials & design 2017; 118:11-21.

[82] Saadatfar M, Mukherjee M, Madadi M, et al. Structure and deformation correlation of closed-cell aluminium foam subject to uniaxial compression - ScienceDirect. Acta Materialia 2012; 60:3604-3615.

[83] Lu G, Shen J, Hou W, et al. Dynamic indentation and penetration of aluminium foams. International Journal of Mechanical Sciences 2008; 50(5):932-9438.

[84] Schneider FE. Enhanced space debris shields for manned spacecraft. International Journal of Impact Engineering 2003; 29:215–226.

[85] Ryan S, Hedman R, Christiansen EL. Honeycomb vs. foam: Evaluating potential upgrades to ISS module shielding. Acta Astronautica 2010; 67:818-825.

[86] Ryan S, Christiansen EL. Hypervelocity Impact Testing of Advanced Materials and Structures for Micrometeoroid and Orbital Debris Shielding. NASA Johnson Space Center, Houston, NASA/TM-2010-XXXX, 2010.

[87] Ryan S, Christiansen EL. Hypervelocity impact testing of advanced materials and structures for micrometeoroid and orbital debris shielding. Acta Astronautica 2013; 83:216-231.

[88] Ryan S, Christiansen EL. Hypervelocity Impact Testing of Aluminum Foam Core Sandwich Panels. NASA Johnson Space Center, Houston, NASA/TM–2015–218593, 2015.

[89] Destefanis R, Enhanced Space Debris Shields for Manned Spacecraft Evaluation Report: Phase A and Phase B Tests, Alenia-Spazio, Turin, ESD-TN-Al-005, 2004.

[90] Schaefer FK, Behner T, Kurz C, Ryan S. Enhanced Debris Shields for Manned Spacecraft WP5000 Phase B Tests, Fraunhofer Ernst-Mach-Institute (EMI), Freiburg, Report No. I-37/04 (ESA Contract 15512/01/NL/CK), 2004.

[91] Yasensky J, Christiansen EL, Prior T. Hypervelocity Impact Evaluation of Metal Foam Core Sandwich Structures, GeoControl, Houston, NASA TP-2008-214776, 2008.

[92] Klavzar A, Chiroli M, Jung A, et al. Protective Performance of Hybrid Metal Foams as MMOD Shields. Procedia Engineering 2015; 103:294-301.

[93] Pasini D, Price MC, Burchell MJ, et al. Spacecraft Shielding: An Experimental Comparison Between Open Cell Aluminium Foam Core Sandwich Panel Structures and Whipple Shielding.

European Planetary Science Congress 2013. London, UK.

[94] Sun G, Wang E, Wang H, et al. Low-velocity impact behaviour of sandwich panels with homogeneous and stepwise graded foam cores. Materials & Design 2018; 160:1117-1136.

[95] Liu XR, Tian XG, Lu TJ, et al. Sandwich plates with functionally graded metallic foam cores subjected to air blast loading. International Journal of Mechanical Sciences 2014; 84:61-72.

[96] Zhou J, Guan ZW, Cantwell, WJ. The impact response of graded foam sandwich structures. Composite Structures 2013; 97:370-377.

[97] Chen Y, Tang QY, He QG. Review on hypervelocity impact of advanced space debris protection shields. Thin–Walled Structures 2024; 200:111874.

[98] Ryan S, Hedman T, Christiansen EL. Honeycomb vs. Foam: Evaluating a Potential Upgrade to ISS Module Shielding for Micrometeoroids and Orbital Debris. NASA Johnson Space Center, Houston, NASA/TM-2009-214793, 2009.

[99] Harris JA, Winter RE, Mcshane GJ. Impact response of additively manufactured metallic hybrid lattice materials. International Journal of Impact Engineering 2017; 104:177-191.

[100] Ha NS, Lu GX. A review of recent research on bio-inspired structures and materials for energy absorption applications. Materials Part B Engineering 2019; 181:107496.

[101] Wu X, Su YT, Shi J. In-plane impact resistance enhancement with a graded cell-wall angle design for auxetic metamaterials. Composite Structures 2020; 247:112451.

[102] Zhang P, Qi DX, Xue R, et al. Mechanical design and energy absorption performances of rational gradient lattice metamaterials. Composite Structures 2021; 277:114606.

[103] Wei YL, Yang QS, Liu X, et al. Multi-bionic mechanical metamaterials: A composite of FCC lattice and bone structures.

[104] Zhang W, Yin S, Yu TX, Xu J. Crushing resistance and energy absorption of pomelo peel inspired hierarchical honeycomb. International Journal of Impact Engineering 2019; 125: 163 72. International Journal of Mechanical Sciences 2022; 213:106857.

[105] Poole LL, Gonzales M, French MR, et al. Hypervelocity impact of PrintCast 316L/A356 materials. International journal of impact engineering 2020; 136:103407.

[106] Xiang XM , Lu GX, You Z. Energy absorption of origami inspired structures and materials. Thin-Walled Structures 2020; 157:107130.

[107] Li ZJ, Yang QS, Fang R, et al. Origami metamaterial with two-stage programmable compressive strength under quasi-static loading. International Journal of Mechanical Sciences 2020; 189:105987.

[108] Zhang JJ, Lu GX, Zhang Y, et al. A study on ballistic performance of origami sandwich panels. International Journal of Impact Engineering 2021; 156:103925.

[109] Smirnov NN, Kiselev AB, and Nikitin VF. Computational simulation of spacecraft honeycomb fluid-filled shield behavior in hypervelocity collision with space debris fragments. In Proceedings of the Sixth European Conference on Space Debris, p8, 2013.

[110] Smirnov MN, Kondratyev KA. Space debris fragments impact on multi-phase fluid filled containments. Acta Astronautica 2012; 79: 12-19.

[111] Smirnov MN, Kiselev AB, Kondratyev KA, et al. Impact of debris particles on space structures modeling. Acta Astronautica 2010; 67: 333-343.

[112] Smirnov NN, Kiselev AB, Zakharov PP. Numerical simulation of the hypervelocity impact of the ball and the spherical containment in three-material statement. Acta Astronautica 2020;

171: 215-224.

[113] Anand P, Nishant M, Aditya P, et al. Computational studies on hyper velocity impact of spherical projectiles on whipple shield with hybrid Newtonian fluid-filled core. Acta Astronautica 2024; 220:230–242.

[114] Hoerz F, Cintala M, See T, et al. Comparison of continuous and discontinuous collisional bumpers: Dimensionally scaled impact experiments into single wire meshes. NASA Technical Memorandum 104749, April, 1992.

[115] Hoerz F, Cintala MJ, Bernhard RP, et al. Impact experiments into multiple-mesh targets: Concept development of a lightweight collisional bumper. NASA Technical Memorandum 104764, March, 1993.

[116] Higashide M, Tanaka M, Akahoshi Y, et al. Hypervelocity impact tests against metallic meshes. International Journal of Impact Engineering 2006; 33(1/12):335-342.

[117] Hoerz F, Cintala MJ, Bernhard RP, et al. Multiple-mesh bumpers: A feasibility study. International Journal of Impact Engineering 1995; 17:431-442.

[118] Christiansen EL, Kerr JH. Mesh double-bumper shield: A low-weight alternative for spacecraft meteoroid and orbital debris protection. International Journal of Impact Engineering 1993; 14(1):169-180.

[119] Browning A, Ortiz C, Boyce MC. Mechanics of composite elasmoid fish scale assemblies and their bioinspired analogues. Journal of the Mechanical Behavior of Biomedical Materials 2013; 19:75 86.

[120] Barthelat F, Martini R. Stretch-and-release fabrication, testing and optimization of a flexible ceramic armor inspired from fish scales. Bioinspiration Biomim. 2016; 11:066001.

[121] Martini R, Balit Y, Barthelat F. A comparative study of bio-inspired protective scales using 3D printing and mechanical testing. Acta Biomater 2017;55: 36-72.

[122] Kim Y, Choi C, Kumar S, et al. Behavior of dragon skin flexible metal bumper under hypervelocity impact. International Journal of Impact Engineering 2019; 125:13-26.

[123] Hui D, Dutta PK. A new concept of shock mitigation by impedance-graded materials. Materials Part B Engineering 2011; 42:2181-2184.

[124] Fernando LNP, Mohotti D, Remennikov A, et al. Behaviour of explosively welded impedance-graded multi-metal composite plates under near-field blast loads - ScienceDirect. International Journal of Mechanical Sciences 2019; 163:105124.

[125] Kuwahara O, Wang N, Ueha S. Reconstruction of Acoustic Impedance Distribution of Functionally Gradient Materials by Using Reflection Impulse Response. Japanese Journal of Applied Physics Supplement 1992; 31:102-104.

[126] Zimmermann G, Schievenbusch A. Materials with an acoustic impedance gradient. Materials Science Forum 1999; 308:533-538.

[127] Pu L, Li S, Zhang Y, et al. Polyimide-based graphene composite foams with hierarchical impedance gradient for efficient electromagnetic absorption. Journal of Materials Chemistry C 2021; 9: 2086-2094.

[128] Riney TD. Chapter V-Numerical evaluation of hypervelocity impact phenomena. High-Velocity Impact Phenomena. Salt Lake City, UT, US: Academic Press, 1970:157 -212.

[129] Stilp AJ, Weber K. Debris clouds behind double-layer targets. International Journal of Impact Engineering 1997; 20:765 -778.

[130] Zhang PL, Cao Y, Chen C, et al. Ballistic limit of an impedance-graded-material enhanced Whipple shield. Explosion and Shock Waves 2021; 41:1-9.

[131] Zhang PL, Gong ZZ, Tian DB, et al. Comparison of shielding performance of Al/Mg impedance-graded-material-enhanced and aluminum Whipple shields. International Journal of Impact Engineering 2019; 126:101-108.

[132] Zhang PL, Xu KB, Li M, et al. Study of the shielding performance of a Whipple shield enhanced by Ti-Al-nylon impedance-graded materials. International Journal of Impact Engineering 2019; 124:23-30.

[133] Song GM, Li M, Wu Q, et al. Debris cloud characteristics of graded-impedance shields under hypervelocity impact. Explosion and shock wave 2021;41:1-15.

[134] Cao Y, Song GM, Wu Q, et al. Experimental Study of the temperature effects on the shielding performance of a Whipple shield enhanced by Ti-Al-Mg impedance-graded materials. Proceedings of the International Astronautical Congress, IAC. 2019; 10:156883.

[135] Wen K, Chen XW. Influence of the impedance gradient on the debris cloud produced by hypervelocity impact. International Journal of Impact Engineering 2022; 159: 104034.

[136] Zheng KQ, Zhang QM, Long RR, et al. Phase Transition Characteristics of Debris Cloud of Ti/Al/Mg Wave Impedance Gradient Material Subjected to Hypervelocity Impact. ACTA Armamentarii 2021; 42(4):774-780.

[137] Dai LH, Bai YL. Basic mechanical behaviors and mechanics of shear banding in BMGs. International Journal of Impact Engineering 2008; 35:704-716.

[138] Jiang MQ, Dai LH. On mechanical properties of metallic glass and its liquid vitrification characteristics. Advanced Materials Research 2008; 41-42:247-252.

[139] Jiang MQ, Ling Z, Meng JX, Dai LH. Energy dissipation in fracture of bulk metallic glasses via inherent competition between local softening and quasicleavage. Philosophical Magazine 2008; 88:407-426.

[140] Inoue A, Shen BL, Chang CT. Fe- and Co-based bulk glassy alloys with ultrahigh strength of over 4000 MPa. Intermetallics 2006; 14:936-944.

[141] Huang X, Ling Z, Liu ZD, et al. Amorphous alloy reinforced Whipple shield structure. International Journal of Impact Engineering 2012; 42:1-10.

[142] Hamill L, Roberts S, Davidson M, et al. Hypervelocity Impact Phenomenon in Bulk Metallic Glasses and Composites. Advanced Engineering Materials 2014; 16:85-93.

[143] Hofmann DC, Hamill L, Christiansen E, et al. Hypervelocity Impact Testing of a Metallic Glass-Stuffed Whipple Shield. Advanced Engineering Materials 2015; 17:1313-1322.

[144] Zhong XZ, Zhang QM, Ma MZ, et al. Dynamic mechanical response and constitutive model of $(Ti_{37.31}Zr_{22.75}Be_{26.39}Al_{4.55}Cu_{9})_{94}Co_{6}$ high-entropy bulk metallic glass. International Journal of Plasticity 2024; 179:104047.

[145] Tan ZH, Han X, Zhang W, et al. An investigation on failure mechanisms of ceramic/metal armour subjected to the impact of tungsten projectile. International Journal of Impact Engineering 2010; 37:1162-1169.

[146] Zaera R, Galvezs VS. Analytical modelling of normal and oblique ballistic impact on ceramic/metal lightweight armours. International Journal of Impact Engineering 1998; 25:819–829.

[147] Goncalves DP, Melo FCLD, Klein AN, et al. Analysis and investigation of ballistic impact on

ceramic/metal composite armour. International Journal of Machine Tools & Manufacture 2004; 44:307-316.

[148] Seifert W, Strassburger E, Dolak M, et al. Experimental study on the dependency of the ballistic performance of tiled ceramic/metal targets on inter tile gap width and projectile impact position[J]. International Journal of Impact Engineering 2018; 122:50-59.

[149] Garcia-Avila M, Portanova M, Rabiei A. Ballistic Performance of a Composite Metal Foam-ceramic Armor System. Procedia Materials ence 2014; 4(4):151-156.

[150] Serjouei A, Chi R, Zhang Z, et al. Experimental validation of BLV model on bi-layer ceramic-metal armor. International Journal of Impact Engineering 2015; 77:30-41.

[151] Behner T, Heine A, Wickert M. Dwell and penetration of tungsten heavy alloy long-rod penetrators impacting unconfined finite-thickness silicon carbide ceramic targets. International Journal of Impact Engineering 2016; 95:54-60.

[152] Sternberg J. Material properties determining the resistance of ceramics to high velocity penetration. Journal of Applied Physics 1989; 65:3417-3424.

[153] Shokrieh MM, Javadpour GH. Penetration analysis of a projectile in ceramic composite armor. Composite Structures 2008; 82:269-276.

[154] Madhu V, Ramanjaneyulu K, Bhat TB, et al. An experimental study of penetration resistance of ceramic armour subjected to projectile impact. International Journal of Impact Engineering 2005; 32:337-350.

[155] An X, Tian C, Sun Q, et al. Effects of material of metallic frame on the penetration resistances of ceramic-metal hybrid structures. Defence Technology 2020; 16:77-87.

[156] Hohler V, Stilp Aj, Weber K. Hypervelocity penetration of tungsten sinter-alloy rods into aluminum. International Journal of Impact Engineering 1995; 17:409-418.

[157] Han Y , Yuan M , Tang E , et al. Experimental study on flash radiation and damage characteristics of C/SiC materials induced by hypervelocity impact. International Journal of Impact Engineering 2021; 155:103902.

[158] Kozhushko AA, Orphal DL, Sinani AB, et al. Possible detection of failure wave velocity using hypervelocity penetration experiments. International Journal of Impact Engineering 1999; 23:467-475.

[159] Strassburger E, Senf H, Rothenhäusler, H. Fracture propagation during impact in three types of ceramics. Journal De Physique IV 1994; C8:653-658.

[160] Subramanian R, Bless SJ. Penetration of semi-infinite AD995 alumina targets by tungsten long rod penetrators from 1.5 to 3.5 km/s. International Journal of Impact Engineering 1995; 17:807-816.

[161] Manfredi D, Pavese M, Biamino S, et al. Microstructure and mechanical properties of co-continuous metal/ceramic materials obtained from Reactive Metal Penetration of commercial aluminium alloys into cordierite. Materials Part A Applied Science & Manufacturing 2010; 41(5):0-645.

[162] Kursa M, Kowalczyk GK, Petryk H. Multi-objective optimization of thermo-mechanical properties of metal-ceramic materials. Materials Part B Engineering 2014; 60:586-596.

[163] Islam MRI, Zheng JQ, Batra RC. Ballistic performance of ceramic and ceramic-metal composite plates with JH1, JH2 and JHB material models. International Journal of Impact Engineering 2020; 137:103469.

[164] Feli S, Asgari MR. Finite element simulation of ceramic/composite armor under ballistic impact. Materials Part B Engineering 2011; 42:771-780.

[165] Krishnan K, Sockalingam S, Bansal S, et al. Numerical simulation of ceramic composite armor subjected to ballistic impact. Materials Part B Engineering 2010; 41:583-593.

[166] Motoyashiki Y, Hasegawa S, Okudaira K, et al. Micrometeoroid impact on ceramic thin components for interplanetary probe. International Journal of Impact Engineering 2008; 35:1666-1671.

[167] Kawai N, Tsurui K, Shindo D, et al. Fracture behavior of silicon nitride ceramics subjected to hypervelocity impact. International Journal of Impact Engineering 2011; 38(7):542-545.

[168] Li T, Mo J, Yu X, et al. Mechanical behavior of C/SiC materials under hypervelocity impact at different temperatures: Micro-structures, damage and mechanisms. Materials Part A Applied Science & Manufacturing 2016; 88:19-26.

[169] Ren SY, Long RR, Zhang QM, et al. The hypervelocity impact resistance behaviors of NbC/Al2024 ceramic-metal materials. International Journal of Impact Engineering 2021; 148:103759.

[170] Huang XG, Yin C, Ru HQ, et al. Hypervelocity impact of TiB2-based materials as front bumpers for space shield applications. Materials & Design 2016; 97:473-482.

[171] Huang XG, Yin C, Ru HQ, et al. Hypervelocity impact damage behavior of B4C/Al composite for MMOD shielding application. Materials & Design 2019; 186:108323.

[172] Cherniaev A, Telichev I. Sacrificial Bumpers with High-Impedance Ceramic Coating for Orbital Debris Shielding: A Preliminary Experimental and Numerical Study. International Journal of Impact Engineering 2018; 119:45-56.

[173] Shojaei P, Trabia M, O'Toole B, et al. Enhancing hypervelocity impact resistance of titanium substrate using Ti/SiC Metal Matrix Nanocomposite coating. Materials Part B: Engineering 2020;194:108068.

[174] Shojaei P, Scazzosi R, Trabia M, et al. Material Model Characterization of a Ti/SiC Metal Matrix Nanocomposite Coating Subjected to Hypervelocity Impact. Procedia Structural Integrity 2020; 28:525-537.

[175] Silvestrov VV, Plastinin AV, Pai VV, et al. An Investigation of ceramic/Aluminum materials as shields for hypervelocity impacts. International Journal of Impact Engineering 1999; 23:859-867.

[176] Zhen L, Li GA, Zhou JS, et al. Micro-damage behaviors of Al–6Mg alloy impacted by projectiles with velocities of 1–3.2 km/s. Materials Science and Engineering: A 2005; 391:354-366.

[177] Robinson JH, Nolen AM. An investigation of metal matrix materials as shields for hypervelocity orbital debris impacts. International Journal of Impact Engineering 1995; 17:685-696.

[178] Li HT, Fei WD, Yang DZ. Damage of aluminum borate whisker reinforced 6061 aluminum composite under impact of hypervelocity projectiles. Materials Science & Engineering A 2002; 333:377-379.

[179] Hasan MZ. Experimental and analytical assessment of the hypervelocity impact damage of glass fiber reinforced aluminum. Defence Technology 2021; 11.

[180] Hehr A, Marcelo JD. Interfacial shear strength estimates of NiTi Al matrix materials

fabricated via ultrasonic additive manufacturing, Materials Part-B 2015; 77:199-208.

[181] Szczepanik S. Materials of aluminium alloy matrix reinforced by a steel mesh. Materials Today Proceedings 2015; 2:9-18.

[182] Zhu DZ, Chen GQ, Wu GH, et al. Hypervelocity impact damage to Ti–6Al–4V meshes reinforced Al–6Mg alloy matrix materials. Materials Science & Engineering A 2009; 500:43-46.

[183] Guo Q, Sun DL, Jiang LT , et al. Damage behavior of Ti–6Al–4V wire mesh reinforced 5A06 alloy matrix materials under high speed impact. Materials Science and Engineering: A 2012; 534:277-281.

[184] Guo Q, Sun DL , Han XL , et al. Damage behaviour of Al matrix composite reinforced with Ti–6Al–4V meshes under the hypervelocity impact[J]. Materials Science & Engineering A 2012; 535:136-143.

[185] Zheng ZX, Zhu DZ, D X, et al. Hypervelocity impact damage and microstructure evolution of woven Ti6Al4V fabric reinforced aluminum matrix materials. Materials & Design 2016; 108:86-92.

[186] Sen Yang, Chalivendra VB, Yong KK . Fracture and impact characterization of novel auxetic Kevlar/Epoxy laminated materials. Composite Structures 2017; 168:120-129.

[187] Khodadadi A, Gholamhossein L, Bahramian AR. High velocity impact behavior of Kevlar/rubber and Kevlar/epoxy materials: A comparative study. Composite Structures 2019; 126:159-167.

[188] Masoud K, Reza EF, Ali S. Evaluation of repeated high velocity impact on polymer-based materials reinforced with basalt and Kevlar fibers. Materials Today Communications 2018; 17:76-81.

[189] Awais H, Nawab Y, Anjang A, et al. Effect of fabric architecture on the shear and impact properties of natural fibre reinforced materials. Materials Part B: Engineering 2020; 195:108069.

[190] Basak R, Dey S, Gohil PP, et al. Property alterations for fiber matrix materials using numerous surface treatments: A review. Materials Today 2021; 45: 7156-7161.

[191] Stopforth R, Adali S, et al. Experimental study of bullet-proofing capabilities of Kevlar, of different weights and number of layers, with 9mm projectiles. Defence Technology 2019; 15:186-192.

[192] Bhattacharjee D, Kumar A, Biswas I. Energy absorption and dynamic defor-mation of backing material for ballistic evaluation of body armour. Defence Science Journal 2013; 63:462-466.

[193] Lee YS, Wetzel ED, Wagner NJ. The ballistic impact characteristics of Kevlar® woven fabrics impregnated with a colloidal shear thickening fluid. Journal of Materials Science 2003; 38:2825-2833.

[194] Zhao ZN, Han B, Zhang R, et al. Enhancement of UHMWPE encapsulation on the ballistic performance of bi-layer mosaic armors. Materials Part B: Engineering 2021; 221:109023.

[195] Wang HG, Weerasinghe D, Mohotti D, et al. On the Impact Response of UHMWPE Woven Fabrics: Experiments and Simulations. International Journal of Mechanical Sciences 2021; 24:106574.

[196] Rudolph M, Schaefer F, Destefanis R, et al. Fragmentation of hypervelocity aluminum projectiles on fabrics. Acta astronautica 2012; 76: 42-50.

[197] Christiansen EL. Meteoroid/debris shielding[R]. NASA TP-2003-210788.

[198] Schonberg W, Bean A, Darzi K. Hypervelocity impact physics. NASA contractor report 4343, 1991.

[199] Lambert M. Shielding against orbital debris: a comparison between different shields. ESA-ESTEC EWP no. 1740, The Netherlands, 1994.

[200] Shiraki K, Terada F, Harada M. Space station JEM design implementation and testing for orbital debris protection. International Journal of Impact Engineering 1997; 20:723-732.

[201] Noda N, Shiraki K, Harada M. Final design for JEM MM/OD protection system. IAF-01-I.5.07, Toulouse, France, 2001.

[202] Christiansen EL. Design and performance equations for advanced meteoroid and debris shields. International Journal of Impact Engineering 1993; 14:145-156.

[203] Tanakaa M, Moritakaa Y, Akahoshi, Y. Development of a lightweight space debris shield using high strength fibers. International Journal of Impact Engineering 2001; 26:761-772.

[204] Destefanis R, Schafer , Lambert M, et al. Selecting enhanced space debris shields for manned spacecraft. International Journal of Impact Engineering 2006; 29:215-226.

[205] Destefanis R, Schafer F, Lambert M, et al. Enhanced space debris shields for manned spacecraft. International Journal of Impact Engineering 2003; 29:215-226.

[206] Destefanis R, Lambert M, Schafer F, Drolshagen G, Francesconi D. Debris shielding development for the ATV integrated cargo carrier. In: Proceedings of the fourth European conference on space debris, Darmstadt, Germany, 2005 (ESA SP-587, August 2005).

[207] Prasad VV, Talupula S. A Review on Reinforcement of Basalt and Aramid (Kevlar 129) fibers. Materials Today Proceedings 2018; 5:5993-5998.

[208] Bandaru AK, Ahmad S, Bhatnagar N, et al. Ballistic performance of hybrid thermoplastic composite armors reinforced with Kevlar and basalt fabrics. Materials, Part A. Applied science and manufacturing 2017; 97:151-165.

[209] Bandaru AK, Patel S, Sachan Y, et al. Mechanical behavior of Kevlar/basalt reinforced polypropylene materials. Materials Part A 2016; 90:642-652.

[210] Fu HD, Feng XY, Liu JX, et al. An investigation on anti-impact and penetration performance of basalt fiber materials with different weave and lay-up modes. Defence Technology 2019; 16: 787-801.

[211] Ramesh V, Anand P. Evaluation of mechanical properties on Kevlar/Basalt fiber reinforced hybrid materials. Materials Today: Proceedings 2020; 39:1494-1496.

[212] Bandaru AK , Chouhan H, Bhatnagar N. High strain rate compression testing of intra-ply and inter-ply hybrid thermoplastic materials reinforced with Kevlar/basalt fibers. Polymer Testing 2020; 84:106407.

[213] Putzar R, Zheng SG, An J, et al. A Stuffed Whipple shield for the Chinese space station. International Journal of Impact Engineering 2019; 132:103304.

[214] Yan J, Zheng SG, Han ZY, et al. A filled Whipple protective structure based on basalt fiber fabric and its manufacturing method. Patent CN105659753b. 2014.

[215] Ke FW, Huang J, Wen XZ, et al. Test study on the performance of shielding configuration with stuffed layer under hypervelocity impact. Acta Astronautica 2016; 127:553-560.

[216] Ke FW, Huang J, Wen XZ, et al. The influences of aramid fibre and its compound with ceramic on shielding performance of stuffed layer. Acta Astronautica 2018; 151:928-941.

[217] Samuel J, Ramadoss R, Gunasekaran KN, et al. Studies on mechanical properties and characterization of carbon fiber reinforced hybrid composite for aero space application[J]. Materials Today: Proceedings 2021.

[218] Hegde S, Shenoy BS, Chethan KN. Review on carbon fiber reinforced polymer (CFRP) and their mechanical performance. Materials Today: Proceedings 2019;19:658-662.

[219] Yuan WK, Li YL, Zhao J. Mechanical properties of a novel Tri-directional carbon-flax-aramid fiber reinforced composite. Materials Science and Technology 2021; 213:108923.

[220] Hmeidat NS, Elkins DS, Peter HR, et al. Processing and mechanical characterization of short carbon fiber-reinforced epoxy materials for material extrusion additive manufacturing. Materials Part B: Engineering 2021; 223:109122.

[221] Zhou XA , Belianinov A, Naskar AK. Analyzing Carbon Fiber Structures Observed by Helium Ion Microscopy and their Mechanical Properties. Carbon Trends 2021; 4:100055.

[222] Rinawa AM, Chauhan P, Suresh D, et al. A review on mechanical properties of natural fiber reinforced polymer (NFRP) materials. Materials Today: Proceedings 2021.

[223] Cherniaev A, Telichev I, et al. Experimental and numerical study of hypervelocity impact damage in composite materials fabricated by filament winding. International Journal of Impact Engineering 2016; 98:19-33.

[224] Garcia MA, Davis BA, Miller JE. Development of a Numerical Model of Hypervelocity Impact into a Pressurized Composite Overwrapped Pressure Vessel. 2017.

[225] Xie WH, Meng SH, Ding L, et al. High velocity impact tests on high temperature carbon-carbon materials. Materials Part B Engineering 2016; 98:30-38.

[226] Xue LZ, Li KZ , Jia Y, et al. Hypervelocity impact behavior and residual flexural strength of C/C materials. Vacuum 2017; 144:101-106.

[227] Xue LZ, Li KZ, Jia Y, et al. Effects of hypervelocity impact on thermal expansion behavior of 2.5D carbon/carbon materials from 850 °C to 2500 °C. Composite Structures 2017; 178:210-216.

[228] Lamontagne CG, Manuelpillai GN, Kerr JH. Projectile density, impact angle and energy effects on hypervelocity impact damage to carbon fibre/peek materials. International Journal of Impact Engineering 2001; 26:381-398.

[229] Lamontagne CG, Manuelpillai GN, Taylor EA, et al. Normal and oblique hypervelocity impacts on carbon fibre/peek materials. International Journal of Impact Engineering 1999; 23:519-532.

[230] Taylor EA, Herbert MK, Vaughan BAM, et al. Hypervelocity impact on carbon fibre reinforced plastic/aluminium honeycomb: Comparison with whipple bumper shields. International Journal of Impact Engineering 1999; 23:883-893.

[231] Khatiwada S, Armada CA, Barrera EV. Hypervelocity Impact Experiments on Epoxy/Ultra-high Molecular Weight Polyethylene Fiber Materials Reinforced with Single-walled Carbon Nanotubes. Procedia Engineering 2013; 58:4-10.

[232] Assa B, Tagziria K, Haddad A, et al. The Self-Healing Capability of Carbon Fibre Composite Structures Subjected to Hypervelocity Impacts Simulating Orbital Space Debris. Isrn Nanomaterials 2012; 351205.

[233] Duan YP, Chi RQ, Pang BJ, et al. Experimental and numerical study of hypervelocity impact

damage on composite overwrapped pressure vessels. Defence Technology. https://doi.org/10.1016/j.dt.2023.01.009.

[234] Wang W, Zhao Y, Chen S, et al. Low-velocity impact behaviors of glass fiber-reinforced polymer laminates embedded with shape memory alloy. Composite Structures 2021; 272:114194.

[235] Nassir NA, Gharkan MR. Impact response of composite laminates based on epoxy and glass fibre. Materials Today: Proceedings 2021; 42:1901-1907.

[236] Domun N, Kaboglu C, Paton KR, et al. Ballistic impact behaviour of glass fibre reinforced polymer composite with 1D/2D nanomodified epoxy matrices. Materials Part B Engineering 2019; 167:497-506.

[237] Sevkat E, Liaw B, Delale F, et al. A combined experimental and numerical approach to study ballistic impact response of S2-glass fiber/toughened epoxy composite beams. Materials Science & Technology 2009; 69:965-982.

[238] Kumar D, Shankar PA, Lalith KK. Failure investigation on high velocity impact deformation of Boron Carbide reinforced fiber metal laminates of Titanium / Glass fiber reinforced polymer. Defence Technology 2021;

[239] Hu PC, Cheng YS, Zhang P, et al. A metal/UHMWPE/SiC multi-layered composite armor against ballistic impact of flat-nosed projectile. Ceramics International 2021; 47:22497-22513.

[240] Omsta MR, Compton BG, Gamble EA, et al. Ballistic impact response of an UHMWPE fiber reinforced laminate encasing of an aluminum-alumina hybrid panel. International Journal of Impact Engineering 2015; 86:131-144.

[241] Mo G, Ma Q, Jin Y, et al. Delamination process in cross-ply UHMWPE laminates under ballistic penetration. Defence Technology 2021; 17:278-286.

[242] Gorshkov NN, Plastinin AV, Sil'Vestrov VV. Puncture of a fiberglass laminate during hypervelocity impact. Combustion Explosion & Shock Waves 1992; 28:426-430.

[243] Hasan MZ. Micrometeoroid impact-induced damage of GLAss fiber REinforced aluminum fiber-metal laminates. Acta Astronautica 2019; 170:172-187.

[244] Hasan MZ. Experimental and analytical assessment of the hypervelocity impact damage of GLAss fiber REinforced aluminum. Defence Technology 2021.

[245] Cha JH, Kim YH, Kumar S, et al. Ultra-High-Molecular-Weight Polyethylene as a Hypervelocity Impact Shielding Material for Space Structures. Acta Astronautica 2019; 168:182-190.

[246] Qu KF, Wu CQ, Liu J, et al. Ballistic performance of multi-layered aluminium and UHMWPE fibre laminate targets subjected to hypervelocity impact by tungsten alloy ball. Composite Structures 2020; 253:112785.

[247] Rogers JA, Mote A, Mead PT, et al. Hypervelocity impact response of monolithic UHMWPE and HDPE plates. International Journal of Impact Engineering 2022; 161:104081.

[248] Kumar SKS, Kim YH, Cha JH, et al. Hybrid interspaced and free-boundary aramid fabric back bumper for hypervelocity impact shielding system. International Journal of Impact Engineering 2023; 171:104377.

[249] Wu Q, Zhang QM, Long RR, et al. Potential space debris shield structure using impact-initiated energetic materials composed of polytetrafluoroethylene and aluminum. Applied Physics Letters 2016; 108:135-83.

[250] Wu Q, Zhang QM, Long RR, et al. Perforation Characteristics of Energetic Material Shield Induced by Hypervelocity Impact of Spherical Projectile. Acta Armamentarii 2017; 38:2126-2133.

[251] Wu Q, Zhang QM, Gong ZZ, et al. Experimental investigation into performances of an active Whipple shield against hypervelocity impact. Explosion and Shock Wsves 2021; 41:1-9.

[252] Lee RJ, Jr WM, Carney JR, et al. Reactive materials studies. American Institute of Physics 2006; 169-74.

[253] Mock WJ, Holt WH. Impact initiation of rods of pressed polytetrafluoroethylene (ptfe) and aluminum powders 2006;845:1097-1100.

[254] Guo J, Zhang QM, Zhang LS, et al. Reaction behavior of polytetrafluoroethylene/Al granular materials subjected to planar shock wave. Propellants Explos Pyrotech 2016; 42:230-230.

[255] Ren SY, Zhang QM, Wu Q, et al. A debris cloud model for hypervelocity impact of the spherical projectile on reactive material bumper composed of polytetrafluoroethylene and aluminum. International Journal of Impact Engineering 2019; 130:124-137.

[256] Ren SY, Zhang QM, Wu Q, et al. Influence of impact-induced reaction characteristics of reactive materials on hypervelocity impact resistance. Materials & Design 2020; 192:108722.

[257] Ren SY, Zhang QM, Wu Q, et al. A reactive material double-bumper shield for centimeter sized projectile.International Journal of Impact Engineering 2021; 158:104028.

[258] NASA Orbital Debris Program Office. Risk from Orbital Debris[C]. RAS Specialist Discussion Meeting on Space Dust and Debris in the Vicinity of the Earth London, UK, 2018.

[259] Paul K G, Igenbergs EB, Berthoud L. Hypervelocity impacts on solar cells-observations, experiments, and empirical scaling laws. International Journal of Impact Engineering 1997; 20:627-638.

[260] Liou JC. NASA Orbital Debris Program Office Overview. NASA Orbital Debris Program Office. The ReDSHIFT Final Conference Florence, Italy, 13-14 March 2019.

[261] Harano T, Machida Y, Fukushige S, et al. Preliminary study on sustained arc due to plasma excited by hypervelocity impact of space debris on the solar array coupon. International Journal of Impact Engineering 2006; 33:326-334.

[262] Graham GA, Kearsley AT, Grady MM. Natural and simulated hypervelocity impacts into solar cells. International Journal of Impact Engineering 1999; 23:319-330.

[263] Taylor EA, Mcdonnell J. Hypervelocity impact on soda lime glass: Damage equations for impactors in the 400–2000 m range. Advances in Space Research, 1997, 20:1457-1460.

[264] Pang HW, Gong ZZ, Zhang WB. Hypervelocity impact damage of fused silica glass and M/OD impact risk assessment of spacecraft windshield[J]. Spacecraft Environment Engineering 2007; 3:135:139.

[265] Miller JE, Bohl WE, Christiansen EL, et al. HVI Ballistic Limit Characterization of Fused Silica Thermal Panes. Procedia Engineering 2015; 103:413-420.

[266] Yang J, Fish J. Coupled thermodynamically consistent thermo-mechanical model of silica glass subjected to hypervelocity impact. Computer Methods in Applied Mechanics and Engineering 2020; 368:113153.

[267] Kawai N, Tsurui K, Moriguchi K, et al. Damage Evolution in $SiO_2$ Glass Subjected to Hypervelocity Impact. Procedia Engineering 2013; 58:702-708.

[268] Kawai N, Zama S, Takemoto W, et al. Stress Wave and Damage Propagation in Transparent

Materials Subjected to Hypervelocity Impact. Procedia Engineering 2015; 103:287-293.

[269] Nam YW, Kumar S, Akhil V, et al. Multi-functional aramid/epoxy composite for stealth space hypervelocity impact shielding system. Composite Structures 2018; 193:113-120.

[270] Kumar SKS, Jurado-Manriquez EA, Kim YH, et al. Polybenzimidazole (PBI) film coating for improved hypervelocity impact energy absorption for space applications. Composite Structures 2018; 188:72-77.

[271] Kanda M, Matsumoto K, Yamaguchi S. Heat transfer through multi-layer insulation (MLI). Physica C Superconductivity 2020; 1353799.

[272] Kang CS. Multilayer Insulation for Spacecraft Applications. Cospar Colloquia 1999; 10:175-179.

[273] Theodore DS, Birur GC, et al. NASA thermal control technologies for robotic spacecraft. Applied Thermal Engineering 2003; 23:1055-1065.

[274] Terrillon F, Warren HR, Yelle MJ, Orbital Debris Shielding Design of the RADARSAT Spacecraft, IAF-91-283, 1991.

[275] Liu T, Zeng ZX, Zhang XH, et al. Performance of polyimide film under hypervelocity impact of micro flyer: Numerical and analytical modeling. Acta Astronautica 2019; 160:138-146.

[276] Liu T, Zeng ZX, Zhang XH, et al. Performance of polyimide film under hypervelocity impact of micro flyer: Experiments and simulations[J]. Acta Astronautica 2019; 159:452-470.

[277] Liu T, Qiu XM, Zhang XH , et al. Experimental investigation on the hypervelocity impact damage behavior of polyimide film. International Journal of Impact Engineering 2020; 141:103538.

[278] Murray MA, Meador PDA, CowardinHM. Analysis of hypervelocity-impacted thin films for space applications. International Journal of Impact Engineering 2023; 180:104709.

[279] Zhang XT, Li XG, Liu T, et al. Element fracture technique for hypervelocity impact simulation. Advances In Space Research 2015; 55:2293-2304.

[280] Thompson S, Lauson H. Improvements in the CHART D radiationhydrodynamic code II: a revised program. Albuquerque, N Mex (USA): Sandia Labs. 1974.

[281] Holian KS, Burkett MW. Sensitivity of hypervelocity impact simulations to Eq. of state. International Journal of Impact Engineering 1987; 5:333-341.

[282] Horner JK. A comparison of ballistic limit with adaptive-mesh Eulerian hydrocode predictions of one- and two-plate aluminum shielding protection against millimeter-sized Fe-Ni space debris. International Journal of Impact Engineering 2008; 35:1602-1605.

[283] Scheffler DR. Modeling non-eroding perforation of an oblique aluminum target using the Eulerian CTH hydrocode. International Journal of Impact Engineering 2005; 32:461-472.

[284] Bouchey SNQ, Hollenshead JT. Mesoscale modeling of hypervelocity impacts using the CTH shock physics code. International Journal of Impact Engineering 2020; 137:103462.

[285] McGlaun JM, Thompson S, Elrick M. CTH: a three-dimensional shock wave physics code. International Journal of Impact Engineering 1990; 10:351-360.

[286] Addessio FL, Baumgardner JR, Dukowicz JK, Johnson NL, Kashiwa BA, Rauenzahn RM, Zemach C. CAVEAT: a computer code for fluid dynamics problems with large distortion and internal slip. Revision 1. NM (United States): Los Alamos National Lab. 1992.

[287] Lucy LB. A numerical approach to the testing of the fission hypothesis. Astronomical Journal 1977; 82:1013-1024.

[288] Gingold RA, Monaghan JJ. Smoothed particle hydrodynamics: Theory and application to non-spherical stars. Oxford University Press, Oxford, UK 1977;375-389.

[289] Chen JS, Hillman M, Chi SW. Meshfree methods: progress made after 20 years. Journal Of Engineering Mechanics 2017; 143: 04017001.

[290] Sulsky D, Chen Z, Schreyer HL. A particle method for history-dependent materials. Computer Methods in Applied Mechanics and Engineering 1994; 118:179-96.

[291] Chen F, Chen R, Jiang BH. The adaptive finite element material point method for simulation of projectiles penetrating into ballistic gelatin at high velocities. Engineering Analysis with Boundary Elements 2020; 117:143-156.

[292] Chen ZP, Qiu XM, Zhang X, et al. Improved coupling of finite element method with material point method based on a particle-to-surface contact algorithm. Computer Methods in Applied Mechanics and Engineering 2015;293:1-19.

[293] Sinaie S, Ngo TD, Kashani A, et al. Simulation of cellular structures under large deformations using the material point method. International Journal of Impact Engineering 2019; 134:103385.

[294] Xue B, Peng YX, Ren SF, et al. Investigation of impact resistance performance of pyramid lattice sandwich structure based on SPH-FEM. Composite Structures, 2021; 261:113561.

[295] Wu CY, He QG, Chen XW, et al. Debris cloud structure and hazardous fragments distribution under hypervelocity yaw impact. Defence Technology 2023; 27:169-183.

[296] Samet C, Zahra SK. Numerical investigation of hypervelocity impact simulation with FEM/SPH formulation for space structures. International Journal of Impact Engineering 2024; 187:104926.

[297] Tang QY, He QG, Chen XW. Numerical simulation study on mesoscopic metallic foam core sandwich panels under hypervelocity impact. Thin–Walled Structures 2024; 195:111440.

[298] Fowler K, Teixeira-Dias F. Optimisation of hybrid composite shields for hypervelocity Micro-Meteoroid and Orbital Debris (MMOD) impact. Advances in Space Research 2024; 73:6194-6208.

[299] Deng YJ, Ren YF, Liu X, et al. Protection performance of aluminum matrix ceramic ball composite materials plate for hypervelocity impact based on FE-SPH adaptive method. Composite Structures 2024; 338:118103.

[300] Chen LT, He QG, Chen XW. Numerical study on the phase-transition characteristics of debris cloud under hypervelocity impacts. International Journal of Impact Engineering 2024; 187:104922.

[301] Nitta K, Higashide M, Kitazawa Y, et al. Response of a Aluminum Honeycomb Subjected to Hypervelocity Impacts. Procedia Engineering 2013; 58:709-714.

[302] Chen H, Francesconi A, Liu S, et al. Effect of honeycomb core under hypervelocity impact: numerical simulation and engineering model. Procedia Engineering 2017; 204:83-91.

[303] Giacomuzzo C, Pavarin D, Francesconi A, et al. SPH evaluation of out-of plane peak force transmitted during a hypervelocity impact. International Journal of Impact Engineering 2008; 35: 1534-1540.

[304] Chen Y, He QG, Chen XW. Numerical study on debris cloud and channeling effect of honeycomb sandwich shields under hypervelocity impact. Thin-Walled structures 2023; 191:111052.

[305] Zhang XT, Jia GH, Huang H, et al. Numerical Investigation of Aluminum Foam Shield Based on Fractal Theory and Node-separation FEM. Chinese Journal of Aeronautics 2011; 24:734-740.

[306] Wejrzanowski T, Skibinski J, Szumbarski J, et al., Structure of foams modeled by Laguerre Voronoi tessellations, Comput. Mater. Sci. 67 (2013) 216 221.

[307] Z. Li, J. Zhang, J. Fan, et al., On crushing response of the three-dimensional closed-cell foam based on Voronoi model, Mech. Mater. 68 (2014) 85 94.

[308] Sun Y, Li QM, Lowe T, et al., Investigation of strain-rate effect on the com-pressive behaviour of closed-cell aluminium foam by 3d image-based mod-elling, Mater. Des. 89 (2016) 215 224.

[309] Zhang XT, Wang RQ, Liu J, et al. A numerical method for the ballistic performance prediction of the sandwiched open cell aluminum foam under hypervelocity impact. Aerospace Science and Technology 2018; 75:254-260.

[310] Wang RQ, Zhang XT, Lu CY, et al. Numerical studies on ballistic limit and cellular dispersion of aluminium foam sandwich panel under hypervelocity impact Numerical studies on ballistic limit and cellular dispersion of aluminium foam sandwich panel under hypervelocity impact. Materials Today Communications 2022; 33:104330.

[311] Cherniaev A. Modeling of hypervelocity impact on open cell foam core sandwich panels. International Journal of Impact Engineering 2021; 155:103901.

[312] Ma ZT, Jia B, Pang BJ,et al. Behavior of Aluminum Foams under Hypervelocity Impact: Validation of Numerical Simulation. Advanced Engineering Materials 2007; 9:888-891.

[313] Jia B, Ma ZT, Pang BJ. Numerical simulation investigation in hypervelocity impact on shield structure containing aluminum foam. Chinese Journal of High Pressure Physics 2009; 23(6): 453-459.

[314] Zhu S, Peng WF, Shao YY, et al. Experimental and numerical study on the high-velocity hail impact performance of carbon fiber aluminum alloy laminates. International Journal of Impact Engineering 2023; 179:104664.

[315] Zhao S, Song Z, Espinosa HD. Modelling and Analyses of Fiber Fabric and Fabric-Reinforced Polymers under Hypervelocity Impact Using Smooth Particle Hydrodynamics[J]. International Journal of Impact Engineering 2020; 144:103586.

[316] Hasan MZ. Micrometeoroid impact-induced damage of GLAss fiber REinforced aluminum fiber-metal laminates. Acta Astronautica 2019; 172-187.

[317] Giannaros E, Kotzakolios A, Kostopoulos V, et al. Hypervelocity impact response of CFRP laminates using smoothed particle hydrodynamics method: Implementation and validation.International Journal of Impact Engineering 2018; 123:56-69.

[318] He QG, Chen XW. Simulation method of debris cloud from fiber-reinforced composite shield under hypervelocity impact. Acta Astronautica 2023; 204:402–417.

[319] Xu HD, Zhou J, Cao Xu, et al. Simulations of the interaction between fiber bundles/yarns and the energy absorption of the fabric under hypervelocity impact. International Journal of Impact Engineering 2023; 181:104733.

[320] Pan GC, LXX, Wang JS. Coupled FEM-SPH simulation of the protective properties for metal/ceramic composite armor. International Journal of Lightweight Materials and Manufacture 2023; 6:543-551.

[321] Xie Y, Wang T, Wang LM, et al. Numerical investigation of ballistic performance of SiC/TC4/UHMWPE composite armor against 7.62 mm AP projectile. Ceramics International 2022; 48:24079-24090.

[322] Deng YJ, Wang Y, Qu KF, et al. Ballistic performance of multi-layered B4C ceramic and UHMWPE fibre laminate targets subjected to hypervelocity impact by tungsten alloy ball. Structures 2022; 45:542-559.

[323] Cherniaev A, Telichev I. Numerical simulation of impact damage induced by orbital debris on shielded wall of composite overwrapped pressure vessel. Applied Composite Materials 2014; 21:861-884.

[324] Cherniaev A, Telichev I. Weight-efficiency of conventional shielding systems in protecting unmanned spacecraft from orbital debris. Journal of Spacecraft and Rockets 2017; 54:75-89.

[325] Pai A, Sharma A, Eby IM, et al. A numerical approach for response of whipple shields with coated and monolithic front bumper to hypervelocity impact by spherical projectiles. Acta Astronautica 2023; 202:433-441.

[326] Hayhurst CJ, Livingstone IH. Advanced numerical simulations for hypervelocity impacts-AUTODYN simulations Century Dynamics Ltd; 1998. Report R098.

[327] Pai A, Rodriguez-Millan M, Nishida M, et al. Numerical Analysis of Hyper Velocity Impact on quasi-isotropic carbon fiber reinforced polymer laminates. Acta Astronautica 2024; 217:323-332.

[328] Johnson G, Holmquist T. A computational constitutive model for brittle materials subjected to large strains, high strain rates and high pressures. Shock Wave High Strain-Rate PhenomMater 1992:1075–81.

[329] Wu MZ, Zhang QM, Zhong XZ, Ren SY. An improved multiphase equation of state for aluminum in hypervelocity impact. International Journal of Impact Engineering 2024; 192:105031.

[330] GRAY Royce EB. A three-phase equation of state for metals. USRL-51121 1971.

[331] Wen K, Chen XW. Influence of the impedance gradient on the debris cloud produced by hypervelocity impact, International Journal of Impact Engineering 2022; 159:104034.

[332] Samet C, Zahra SK. Numerical investigation of hypervelocity impact simulation with FEM/SPH formulation for space structures. International Journal of Impact Engineering 2024; 187:104926.

[333] Yang Y, Xu F, Gao XY, et al. Two failure modes of C/SiC composite under different impact loads. Composites Part B 2018; 136:158-167.

[334] Pai A, Divakaran R, Anand S, et al. Advances in the Whipple Shield Design and Development. Journal of Dynamic Behavior of Materials 2021.

[335] Liu P, Liu Y, Zhang X. Internal-structure-model based simulation research of shielding properties of honeycomb sandwich panel subjected to high-velocity impact. International Journal of Impact Engineering 2015; 77:120-133.

[336] Santos C, Maeda LD, Cairo CAA , et al. Mechanical properties of hot-pressed ZrO2–NbC ceramic composites.International Journal of Refractory Metals & Hard Materials 2008; 26:14-18.

[337] Chang YS, Hsu KT, Li JB, et al. Effect of cast process and microalloying on the fracture toughness of Zr-based bulk amorphous alloys. Journal of Alloys and Compounds 2014;

614:87-93.

[338] Renato SMA, Maroof AH, Walter ECP, et al. The use of bundles with higher filament count for cost reduction of high-strength oxide ceramic composites. Open Ceramics 2023; 15:100389.

[339] Abdullah SIBS, Iannucci L, Greenhalgh ES, et al. The delamination behaviour of Vectran/Epoxy composites having a novel Non-Crimp Fabric architecture. Composites Part B 2022; 228:109413.

[340] Xu EC, Chen J, Cui XF, et al. Low-velocity impact analysis and multi-objective optimization of hybrid carbon/basalt fibre reinforced composite laminate. Composite Structures 2024; 343:118305.

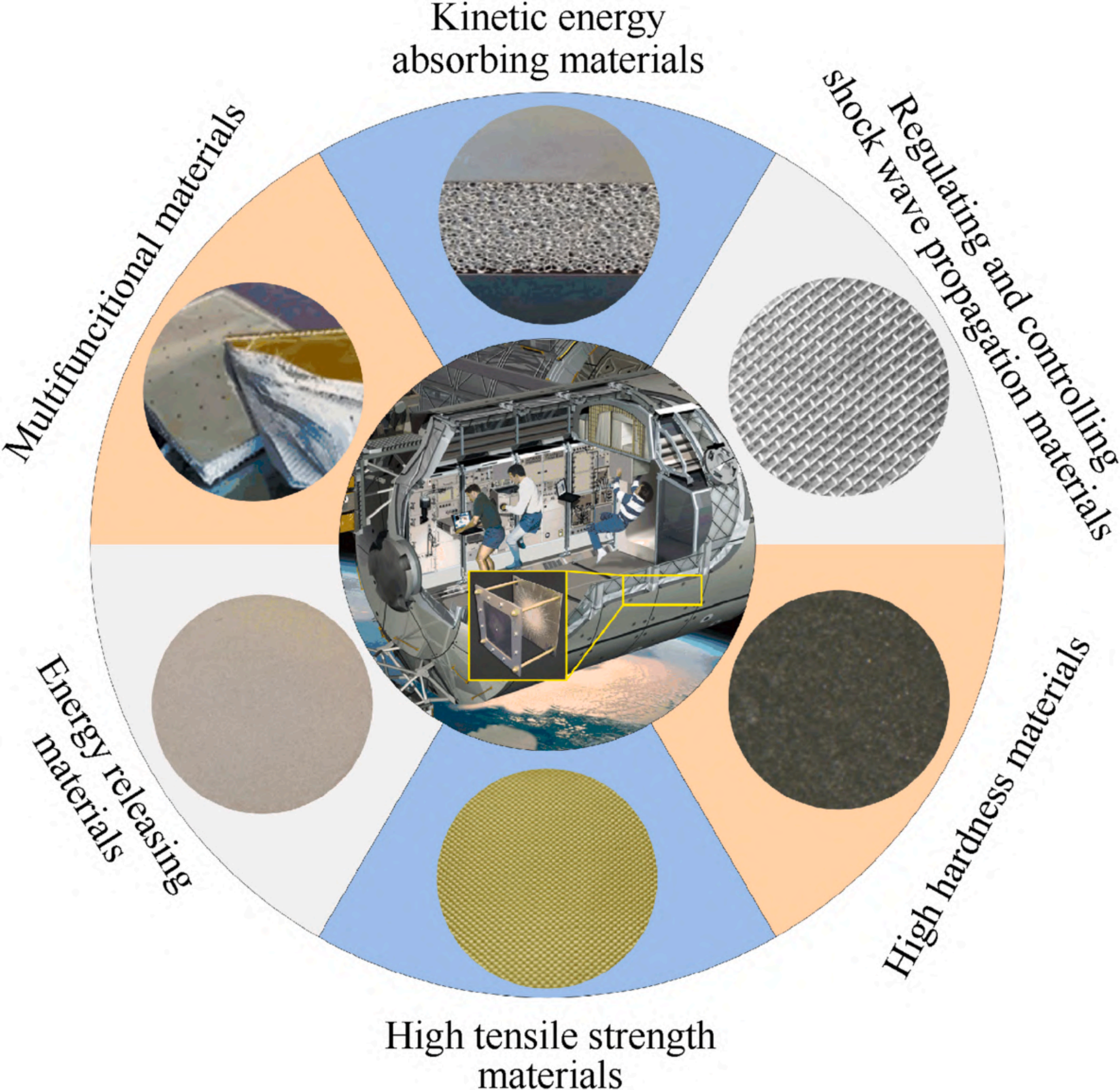
Kinetic energy absorbing materials
Regulating and controlling shock wave propagation materials
High hardness materials
High tensile strength materials
Energy releasing materials
Multifuncitional materials

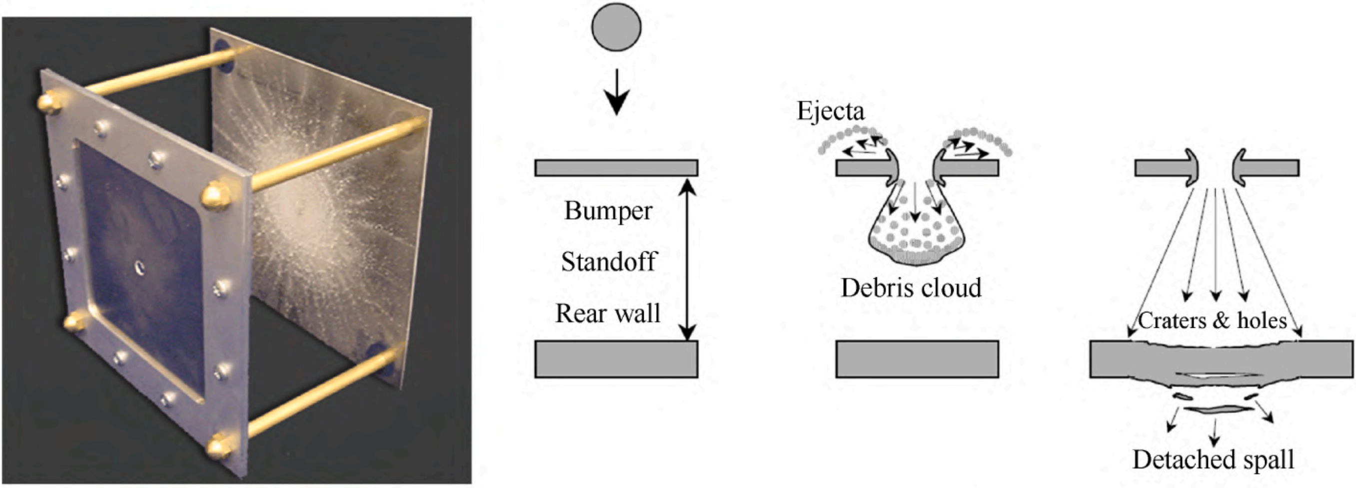

Bumper
Standoff
Rear wall
Ejecta
Debris cloud
Craters & holes
Detached spall


(a) (b)

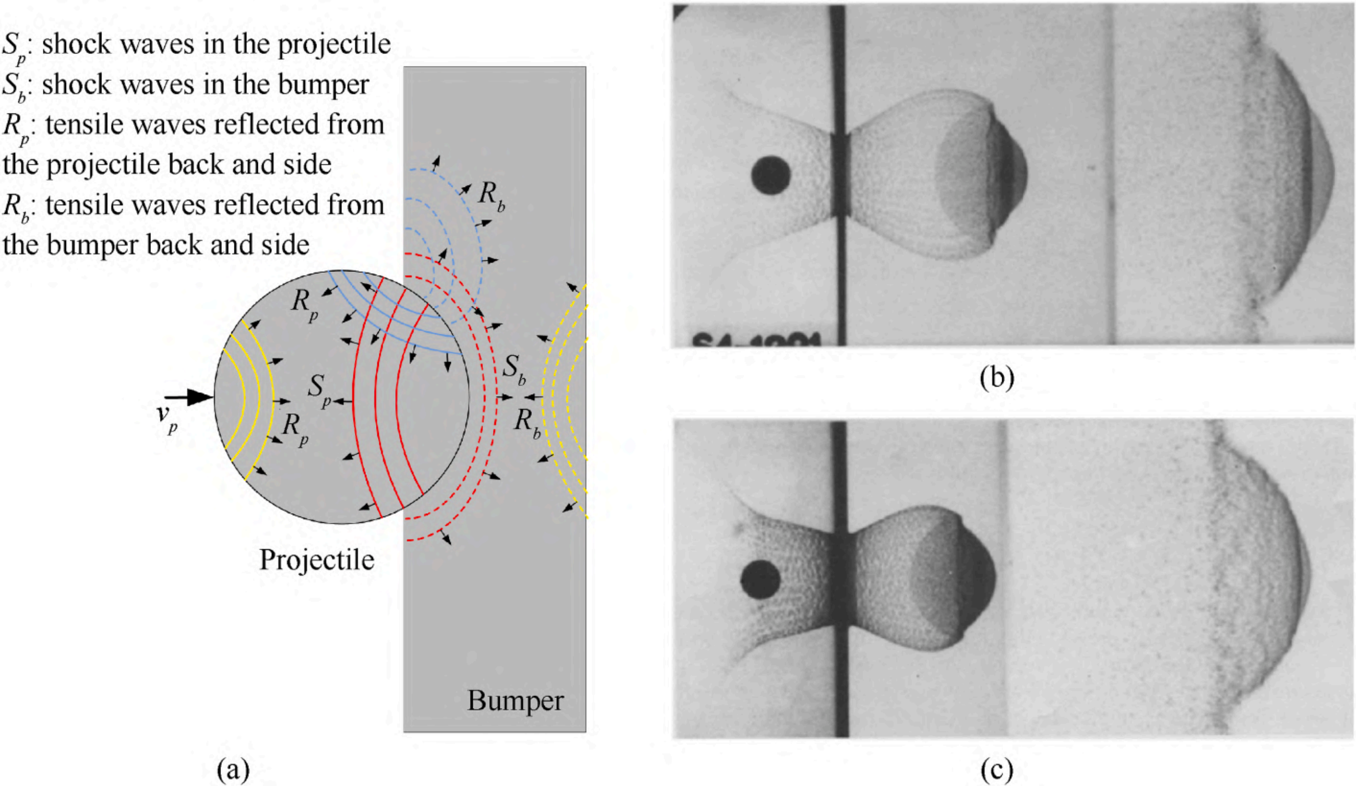
$S_p$: shock waves in the projectile
$S_b$: shock waves in the bumper
$R_p$: tensile waves reflected from the projectile back and side
$R_b$: tensile waves reflected from the bumper back and side
$R_b$
$R_p$
$S_p$
$S_b$
$R_b$
$R_p$
$v_p$
Projectile
Bumper
(a)
(b)
(c)

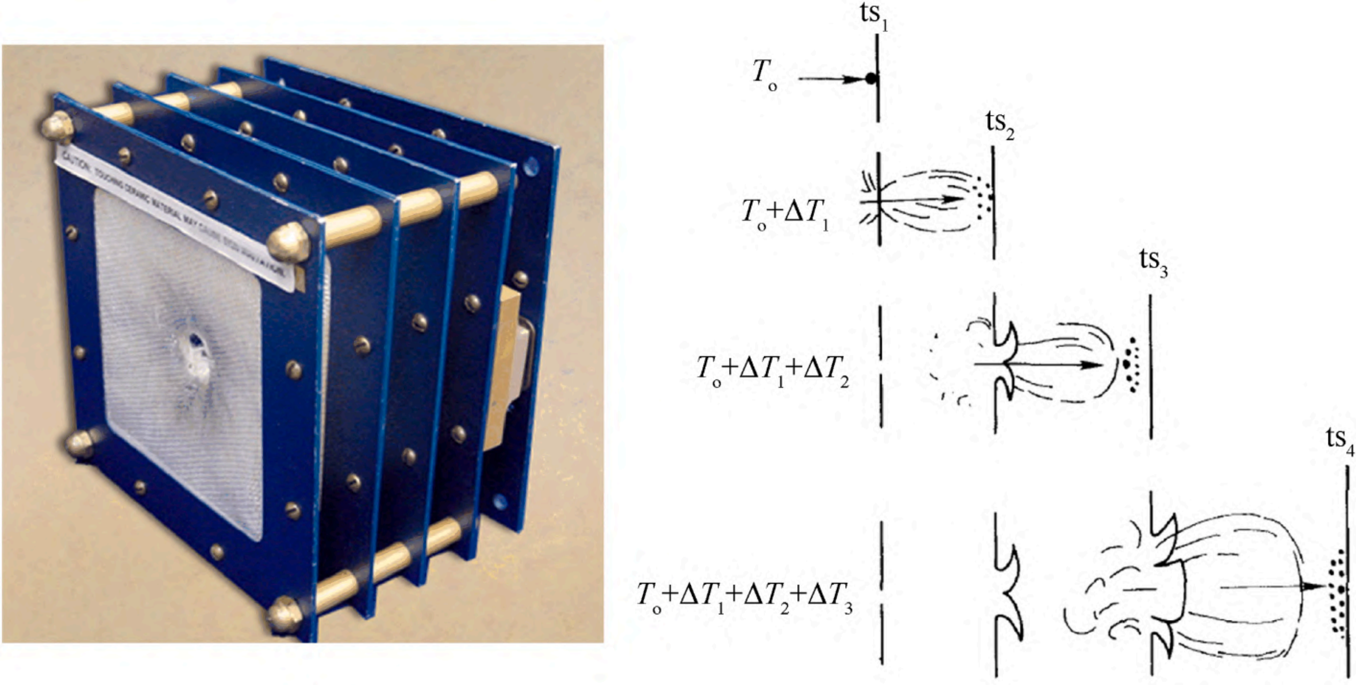
$ts_1$
$T_o$
$ts_2$
$T_o+\Delta T_1$
$ts_3$
$T_o+\Delta T_1+\Delta T_2$
$ts_4$
$T_o+\Delta T_1+\Delta T_2+\Delta T_3$

(a) (b)

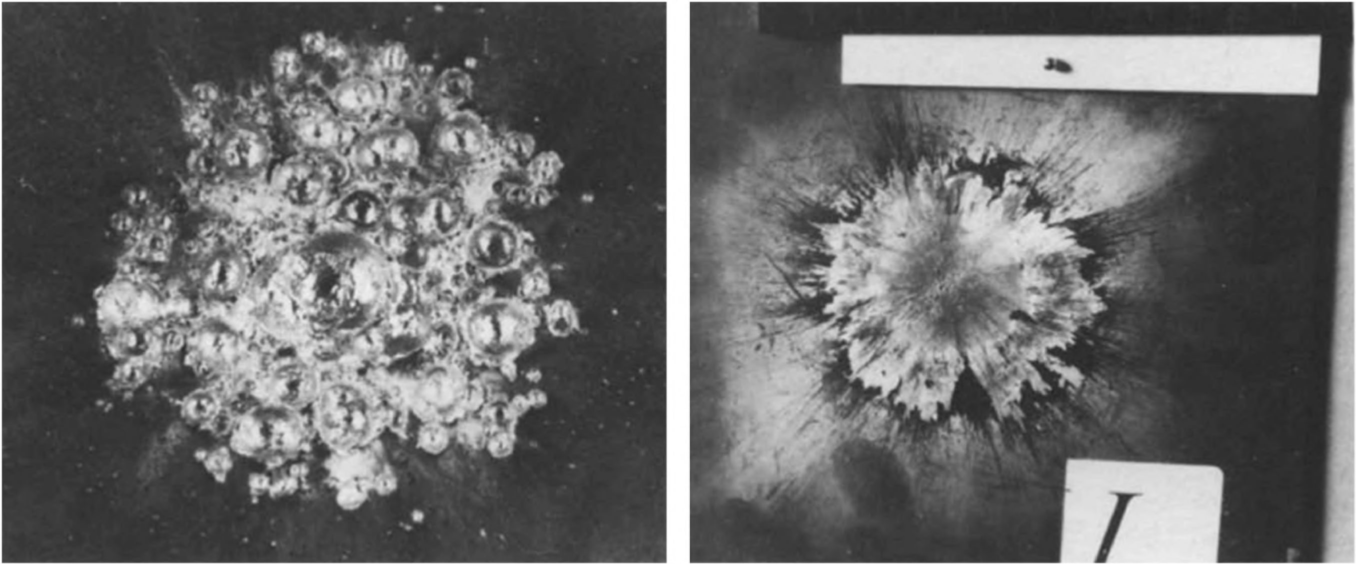

(a) (b)

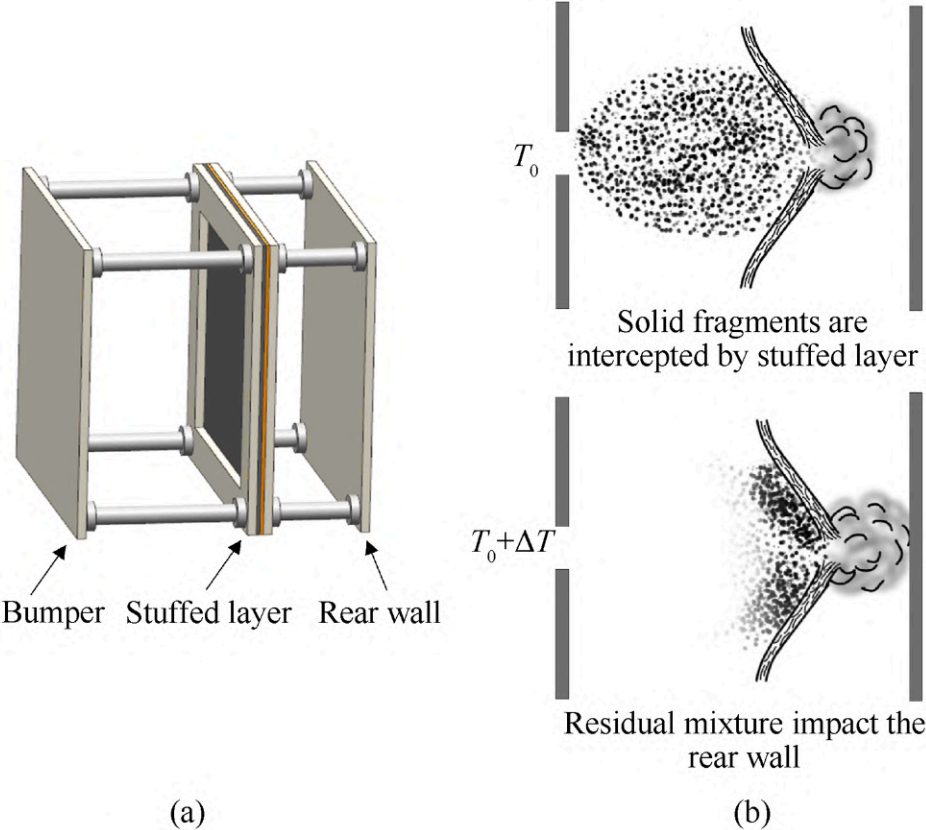

Bumper
Stuffed layer
Rear wall
(a)
$T_0$
Solid fragments are intercepted by stuffed layer
$T_0+\Delta T$
Residual mixture impact the rear wall
(b)

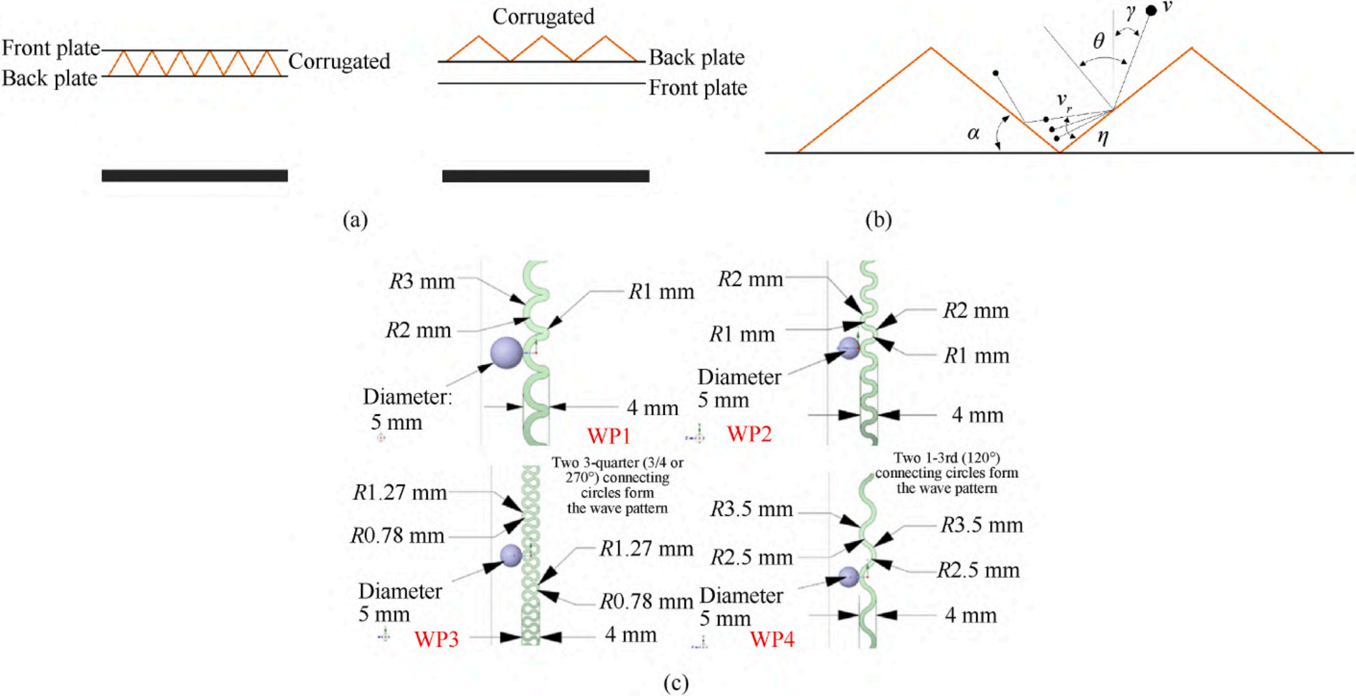

Front plate
Back plate
Corrugated
Corrugated
Back plate
Front plate
(a)
γ
v
θ
$v_r$
α
η
(b)
R3 mm
R1 mm
R2 mm
Diameter:
5 mm
4 mm
WP1
R2 mm
R2 mm
R1 mm
R1 mm
Diameter
5 mm
4 mm
WP2
Two 3-quarter (3/4 or 270°) connecting circles form the wave pattern
R1.27 mm
R0.78 mm
R1.27 mm
R0.78 mm
Diameter
5 mm
4 mm
WP3
Two 1-3rd (120°) connecting circles form the wave pattern
R3.5 mm
R3.5 mm
R2.5 mm
R2.5 mm
Diameter
5 mm
4 mm
WP4
(c)

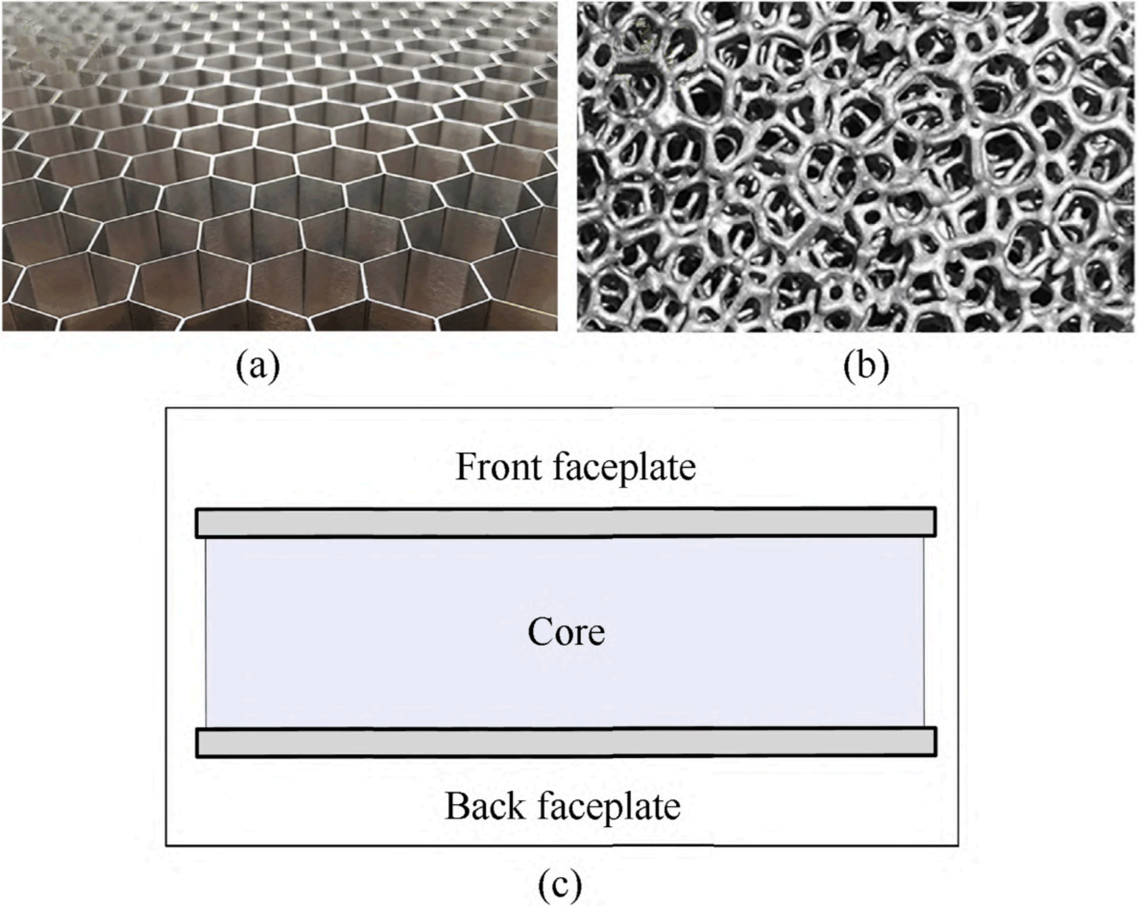
(a)
(b)
Front faceplate
Core
Back faceplate
(c)

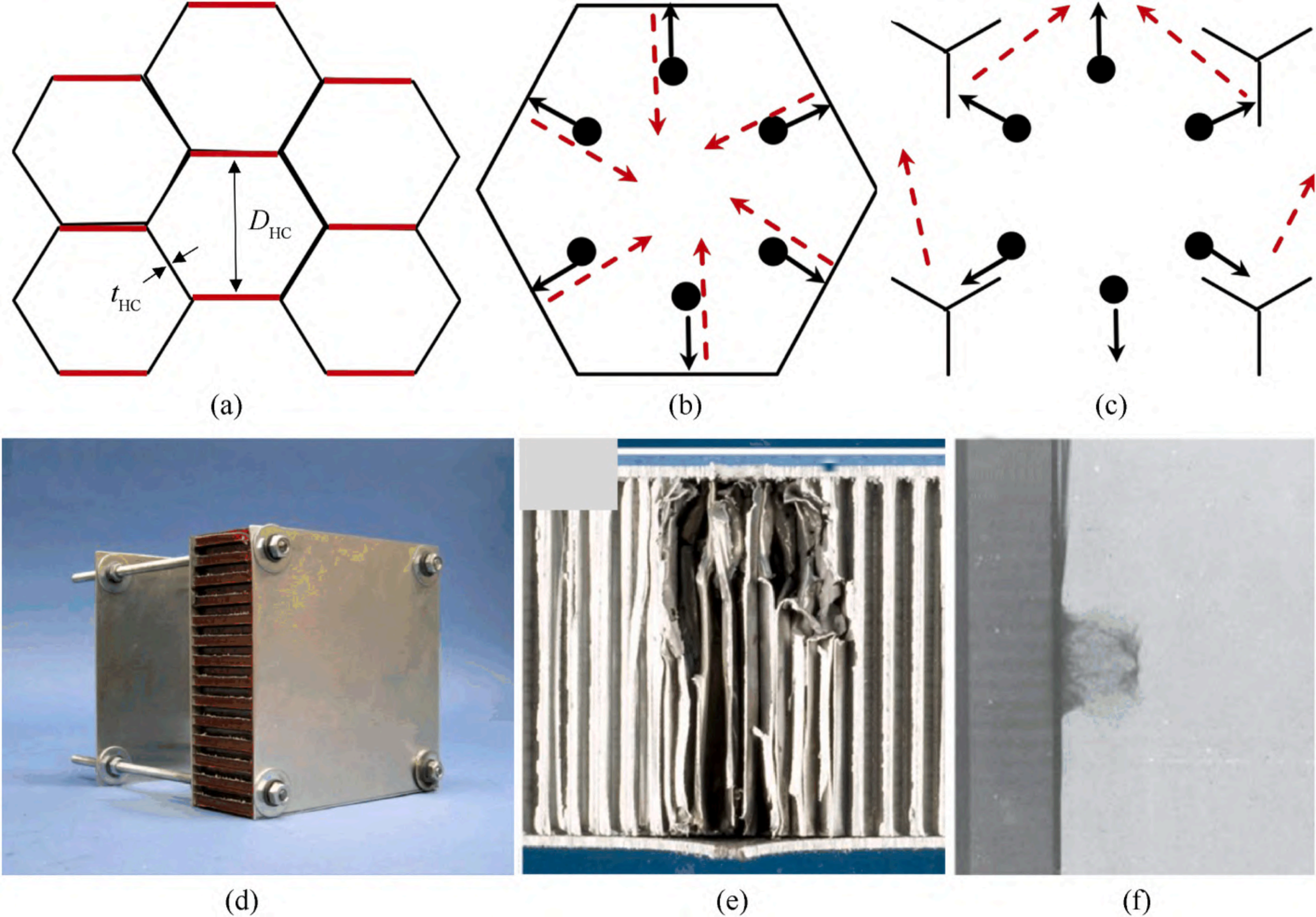

$D_{HC}$
$t_{HC}$
(a)
(b)
(c)
(d)
(e)
(f)

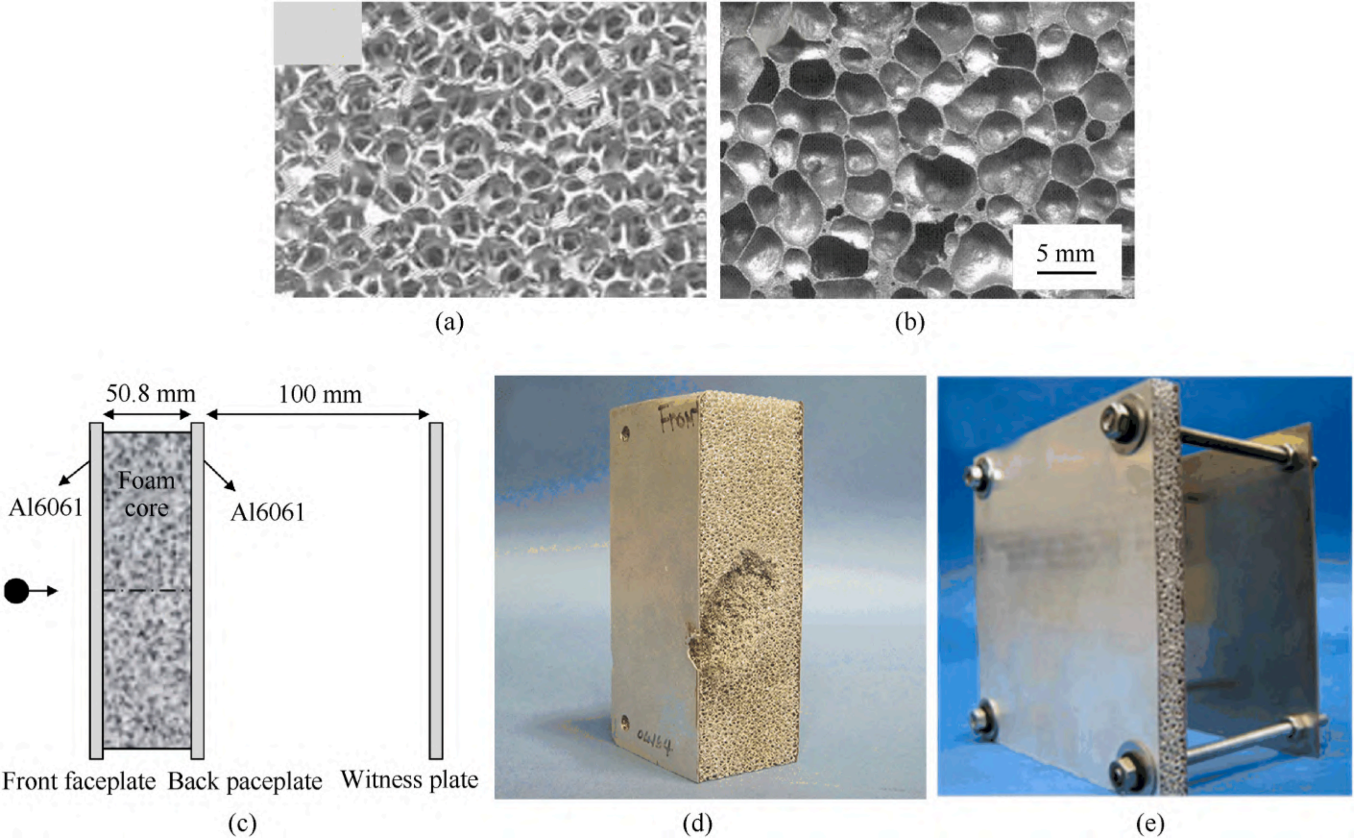

5 mm
(a)
(b)
50.8 mm
100 mm
Foam core
Al6061
Al6061
Front faceplate
Back paceplate
Witness plate
(c)
Front
(d)
(e)

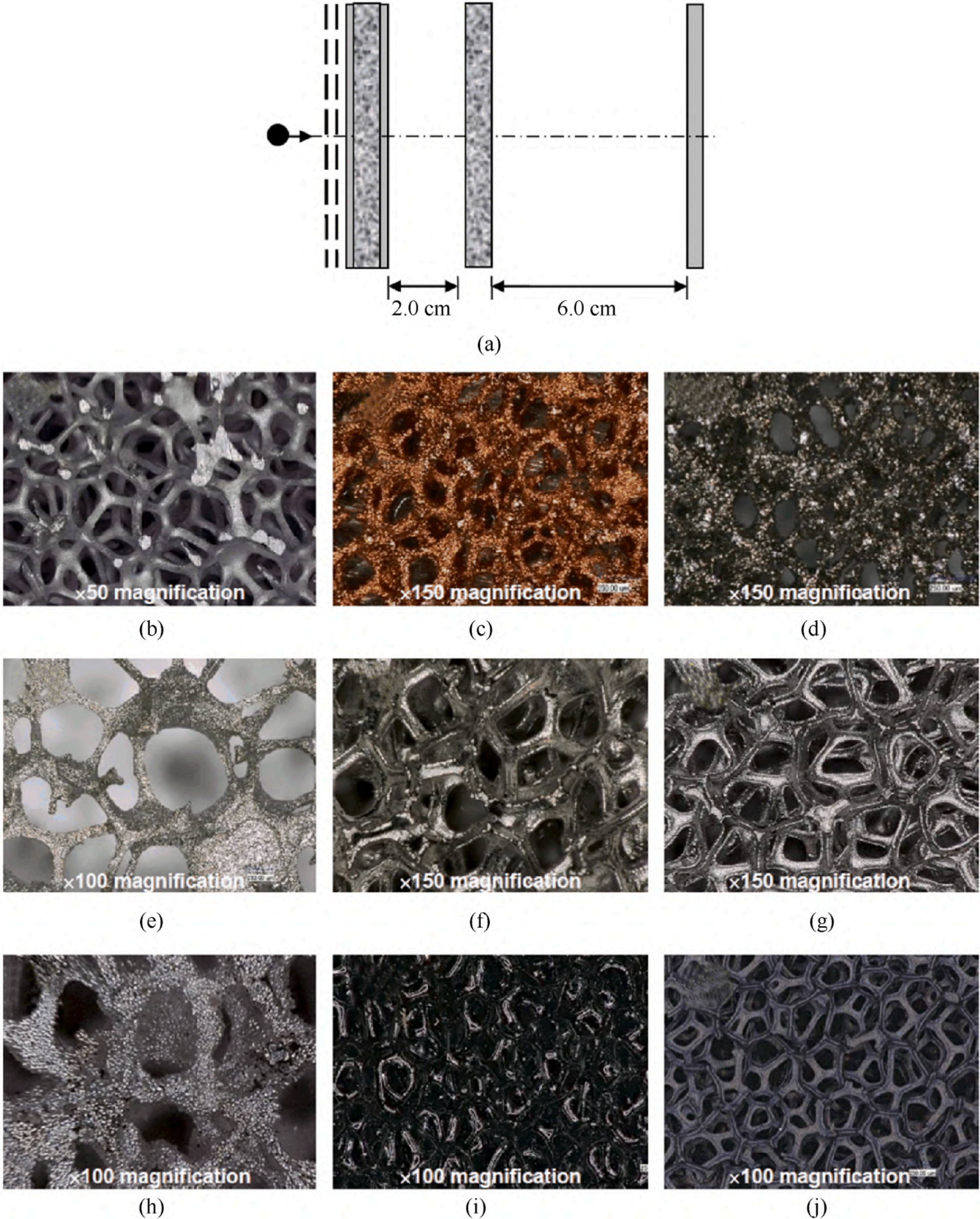
2.0 cm
6.0 cm
(a)
×50 magnification
(b)
×150 magnification
(c)
×150 magnification
(d)
×100 magnification
(e)
×150 magnification
(f)
×150 magnification
(g)
×100 magnification
(h)
×100 magnification
(i)
×100 magnification
(j)

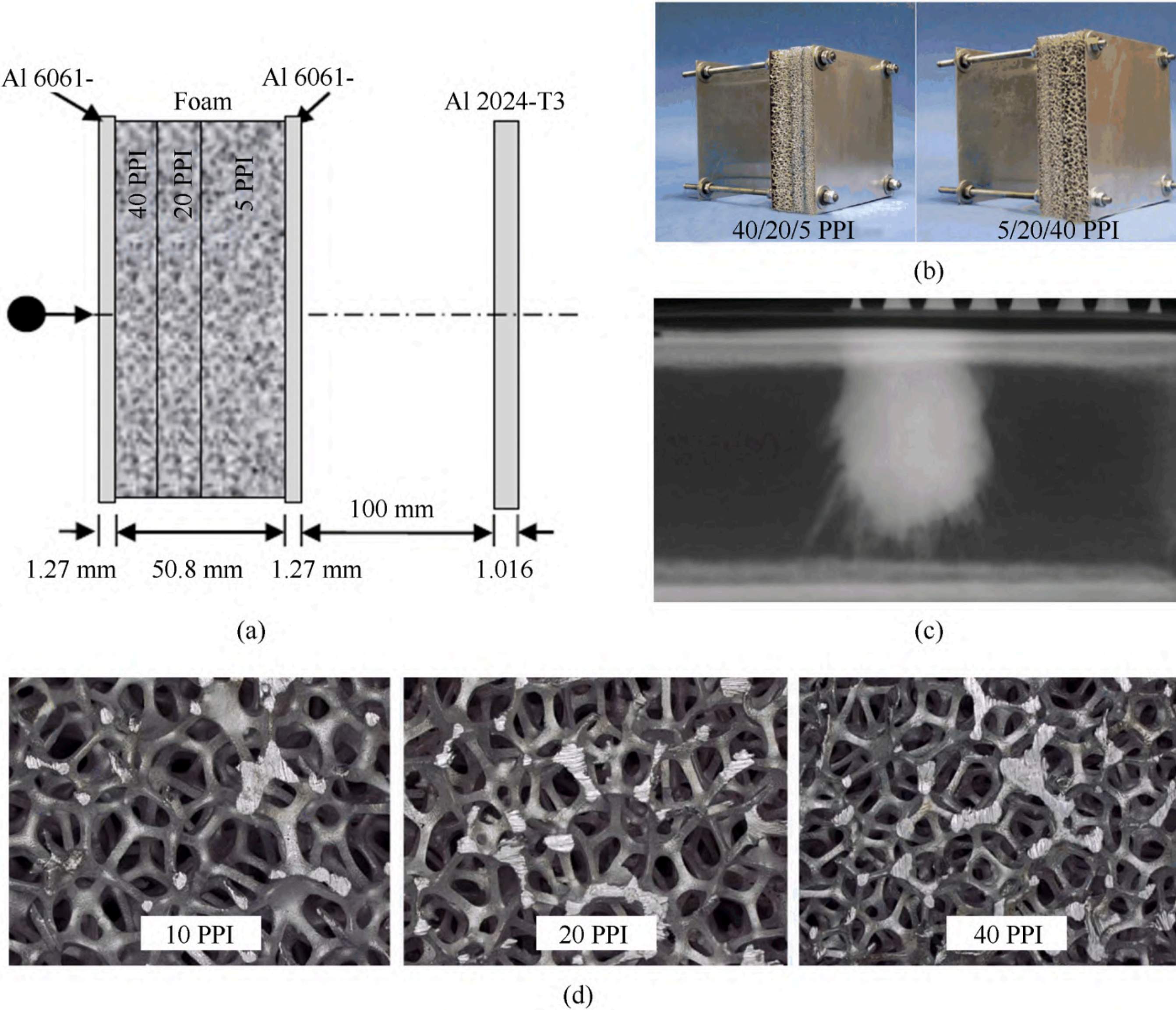

Al 6061-
Foam
Al 6061-
Al 2024-T3
40 PPI
20 PPI
5 PPI
100 mm
1.27 mm
50.8 mm
1.27 mm
1.016
(a)
40/20/5 PPI
5/20/40 PPI
(b)
(c)
10 PPI
20 PPI
40 PPI
(d)

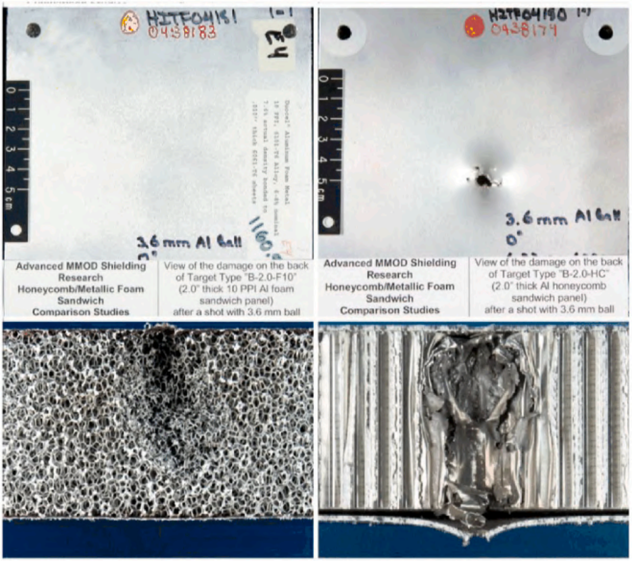

3.6 mm Al ball
Advanced MMOD Shielding Research Honeycomb/Metallic Foam Sandwich Comparison Studies
View of the damage on the back of Target Type "B-2.0-F10" (2.0" thick 10 PPI Al foam sandwich panel) after a shot with 3.6 mm ball
3.6 mm Al ball
Advanced MMOD Shielding Research Honeycomb/Metallic Foam Sandwich Comparison Studies
View of the damage on the back of Target Type "B-2.0-HC" (2.0" thick Al honeycomb sandwich panel) after a shot with 3.6 mm ball


(a)

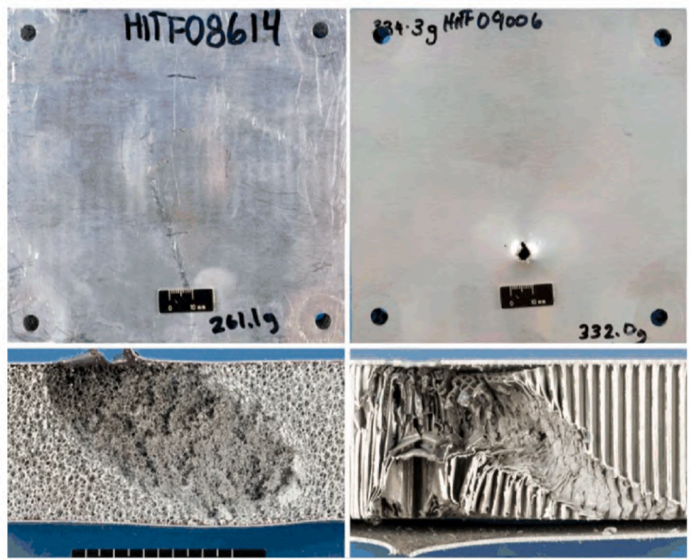

HITF08614
261.1g
HITF09006
332.0g


(b)

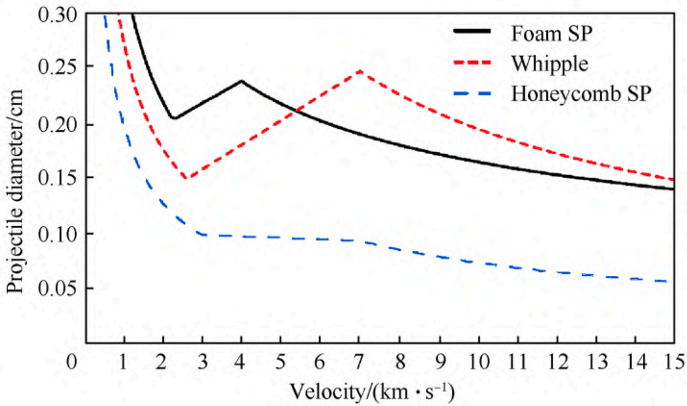

Foam SP
Whipple
Honeycomb SP
Projectile diameter/cm
Velocity/(km · s⁻¹)
0.30
0.25
0.20
0.15
0.10
0.05
0 1 2 3 4 5 6 7 8 9 10 11 12 13 14 15


(c)

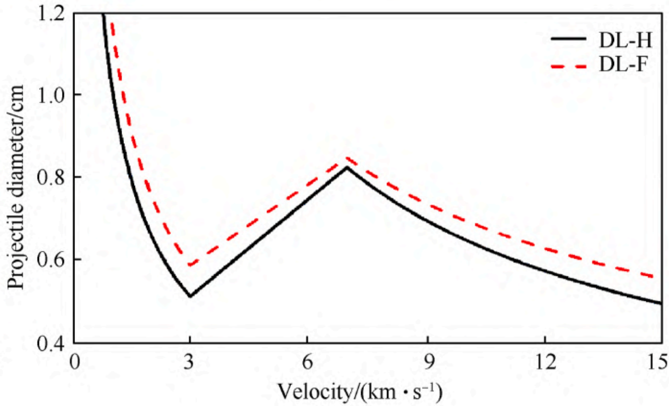

DL-H
DL-F
Projectile diameter/cm
Velocity/(km · s⁻¹)
1.2
1.0
0.8
0.6
0.4
0 3 6 9 12 15


(d)

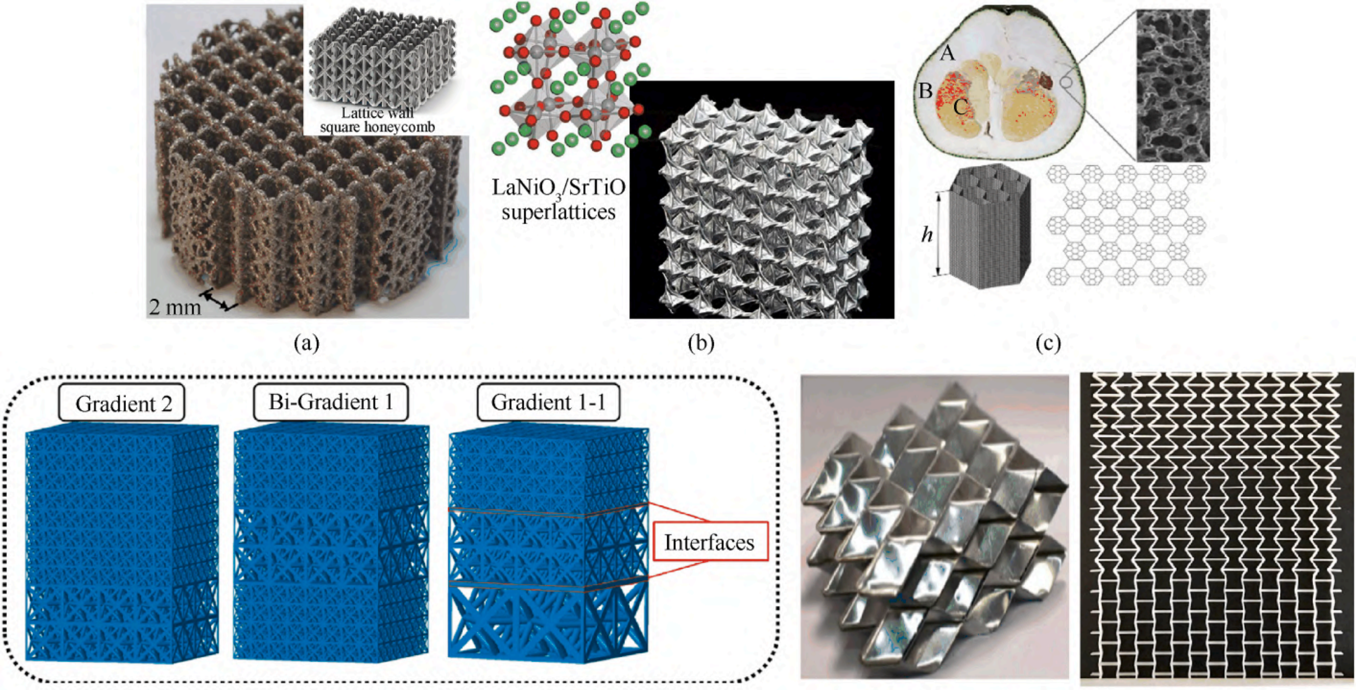

Lattice wall
square honeycomb
2 mm
LaNiO$_3$/SrTiO
superlattices
A
B
C
$h$
Gradient 2
Bi-Gradient 1
Gradient 1-1
Interfaces


(a) (b) (c)

(d) (e) (f)

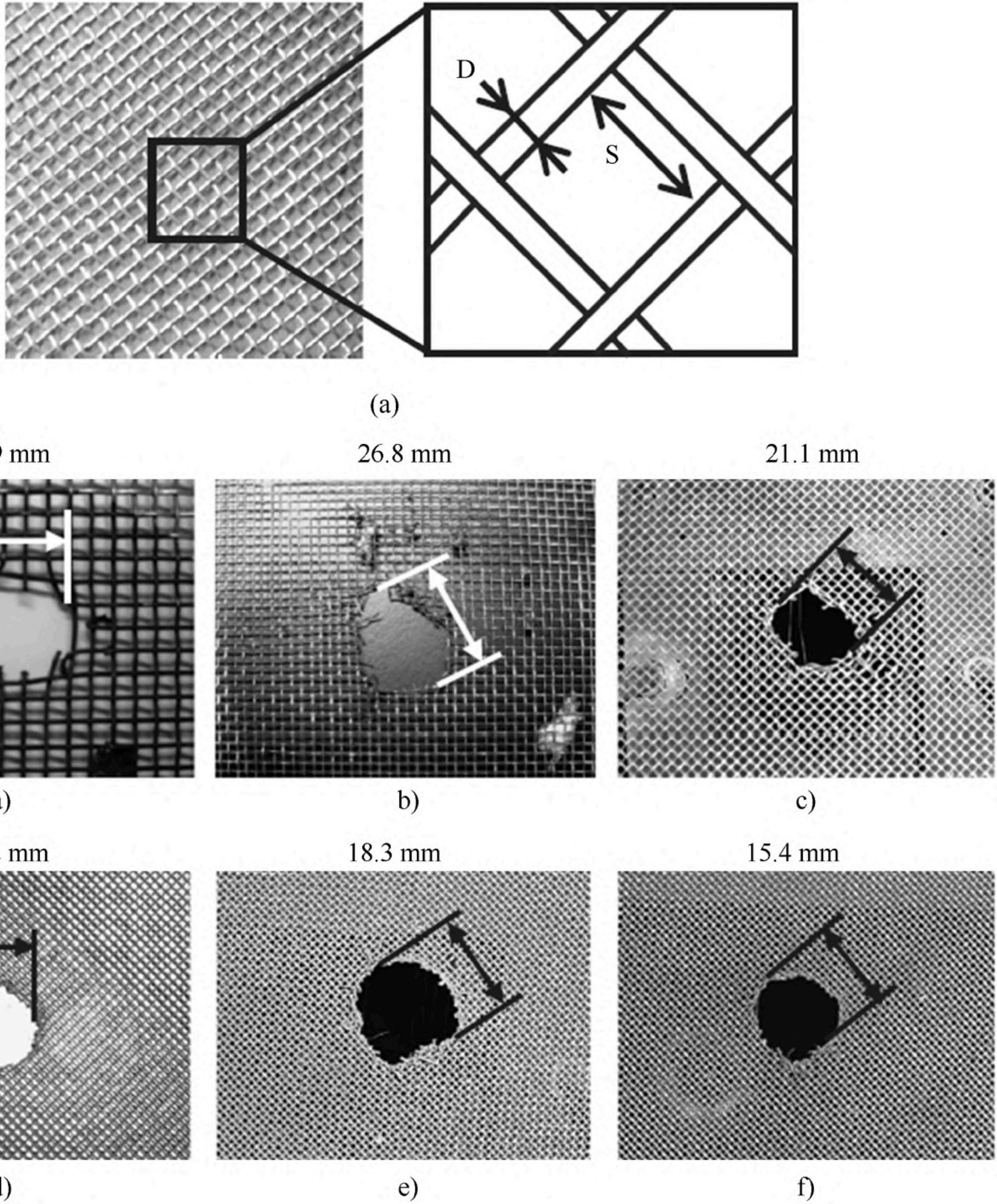


(b)

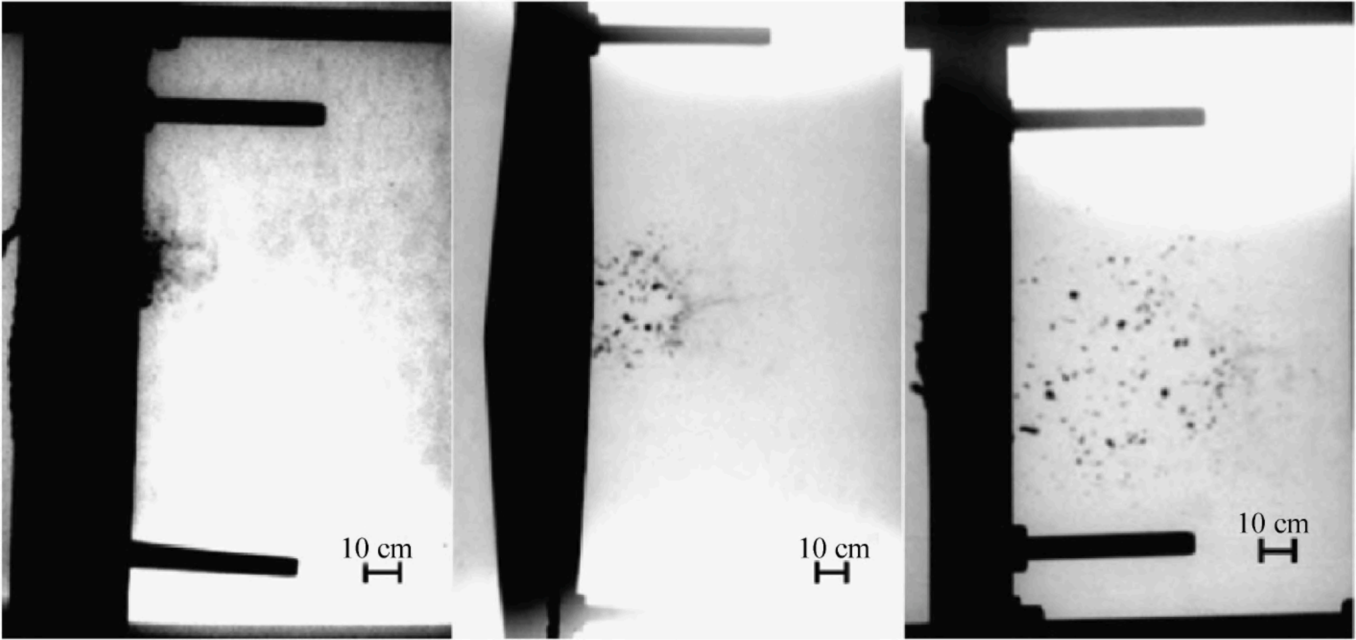
10 cm
10 cm
10 cm

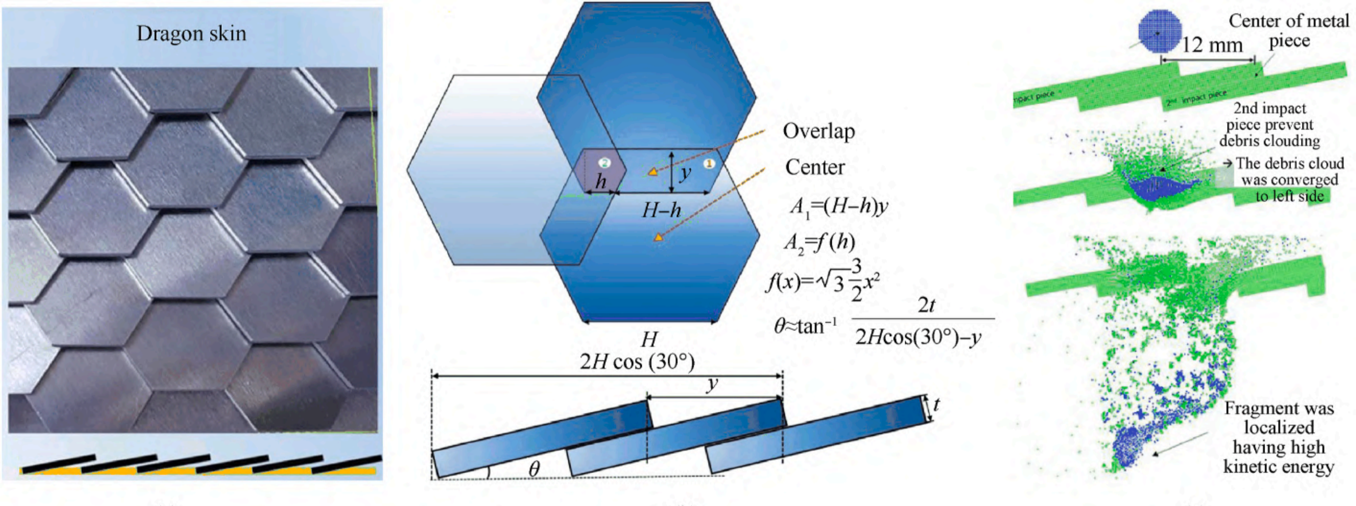

Dragon skin
Overlap
Center
y
h
H−h
$A_1=(H-h)y$
$A_2=f(h)$
$f(x)=\sqrt{3}\frac{3}{2}x^2$
$\theta \approx \tan^{-1}\frac{2t}{2H\cos(30°)-y}$
H
2H cos (30°)
y
t
θ
Center of metal piece
12 mm
2nd impact piece
2nd impact piece prevent debris clouding
The debris cloud was converged to left side
Fragment was localized having high kinetic energy


(a) (b) (c)

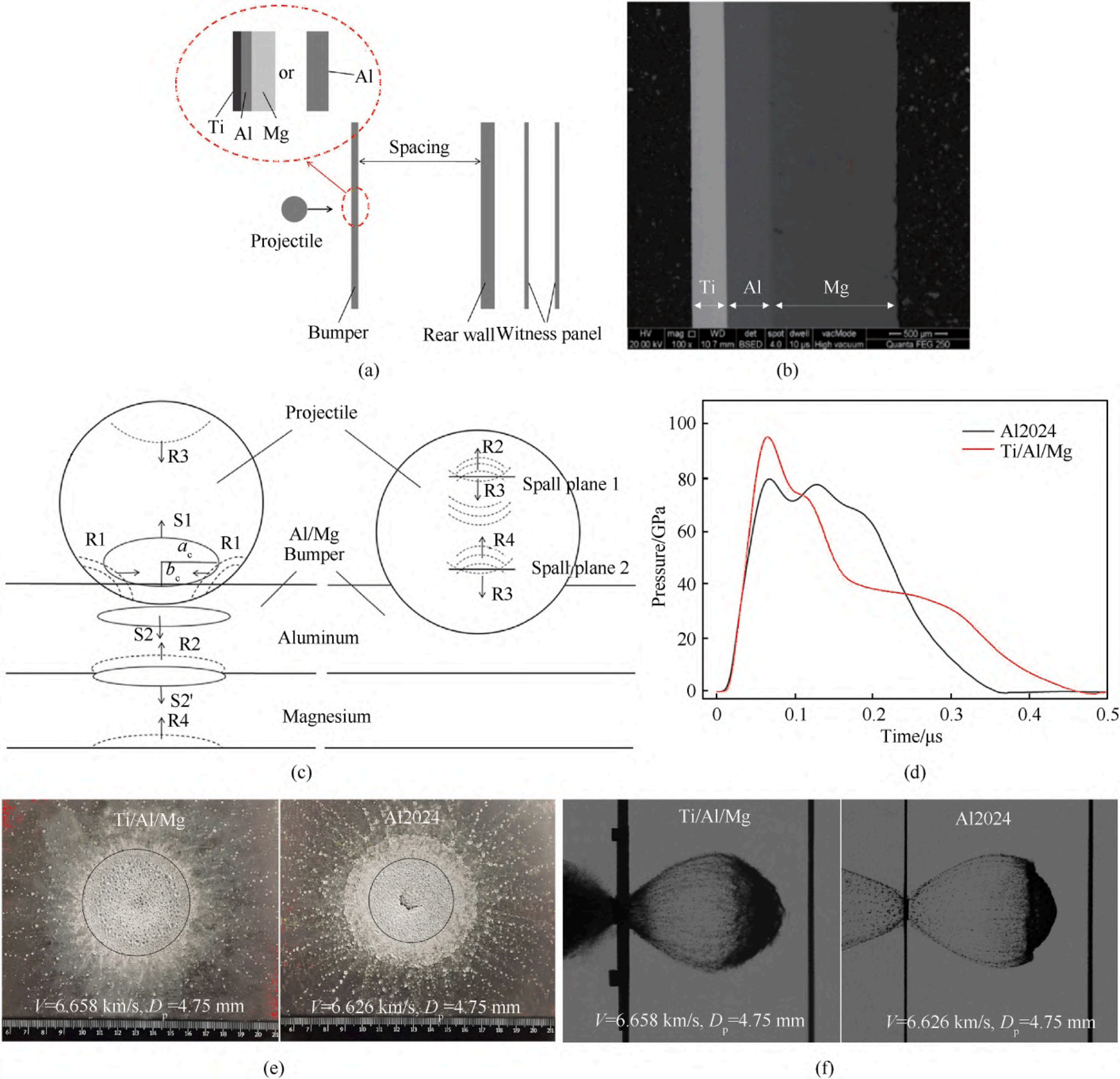

Ti
Al
Mg
or
Al
Spacing
Projectile
Bumper
Rear wall
Witness panel
(a)
Ti
Al
Mg
HV 20.00 kV
mag 100 x
WD 10.7 mm
det BSED
spot 4.0
dwell 10 μs
vacMode High vacuum
500 μm
Quanta FEG 250
(b)
Projectile
R3
S1
R1
R1
$a_c$
$b_c$
Al/Mg Bumper
S2
R2
Aluminum
S2'
R4
Magnesium
R2
R3
Spall plane 1
R4
Spall plane 2
R3
(c)
Pressure/GPa
Time/μs
Al2024
Ti/Al/Mg
100
80
60
40
20
0
0
0.1
0.2
0.3
0.4
0.5
(d)
Ti/Al/Mg
Al2024
V=6.658 km/s, $D_p$=4.75 mm
V=6.626 km/s, $D_p$=4.75 mm
(e)
Ti/Al/Mg
Al2024
V=6.658 km/s, $D_p$=4.75 mm
V=6.626 km/s, $D_p$=4.75 mm
(f)

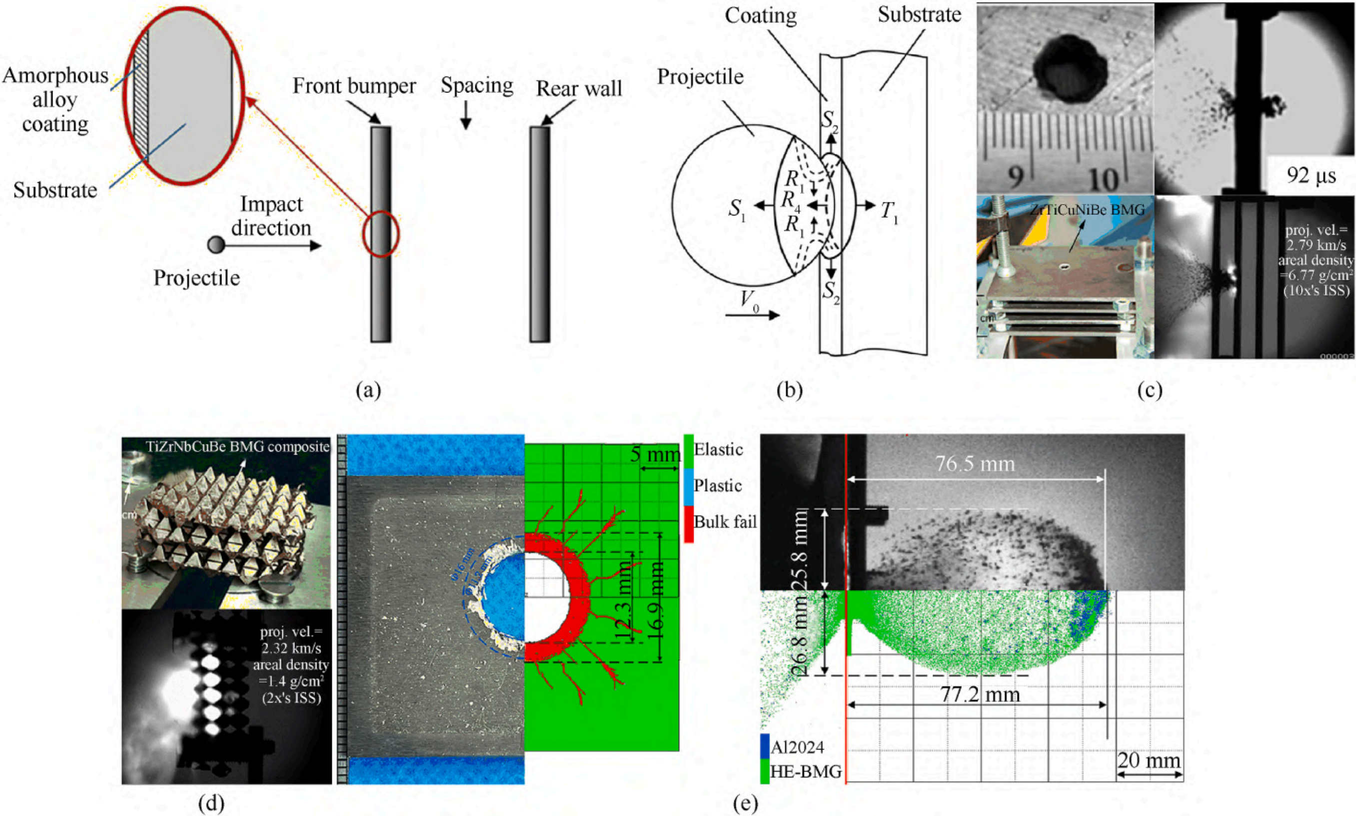

Amorphous alloy coating
Substrate
Front bumper
Spacing
Rear wall
Impact direction
Projectile
(a)
Coating
Substrate
Projectile
$S_2$
$R_1$
$R_4$
$R_1$
$S_1$
$T_1$
$S_2$
$V_0$
(b)
9
10
92 μs
ZrTiCuNiBe BMG
cm
proj. vel.= 2.79 km/s
areal density =6.77 g/cm²
(10x's ISS)
(c)
TiZrNbCuBe BMG composite
cm
proj. vel.= 2.32 km/s
areal density =1.4 g/cm²
(2x's ISS)
5 mm
Elastic
Plastic
Bulk fail
12.3 mm
16.9 mm
(d)
76.5 mm
25.8 mm
26.8 mm
77.2 mm
Al2024
HE-BMG
20 mm
(e)

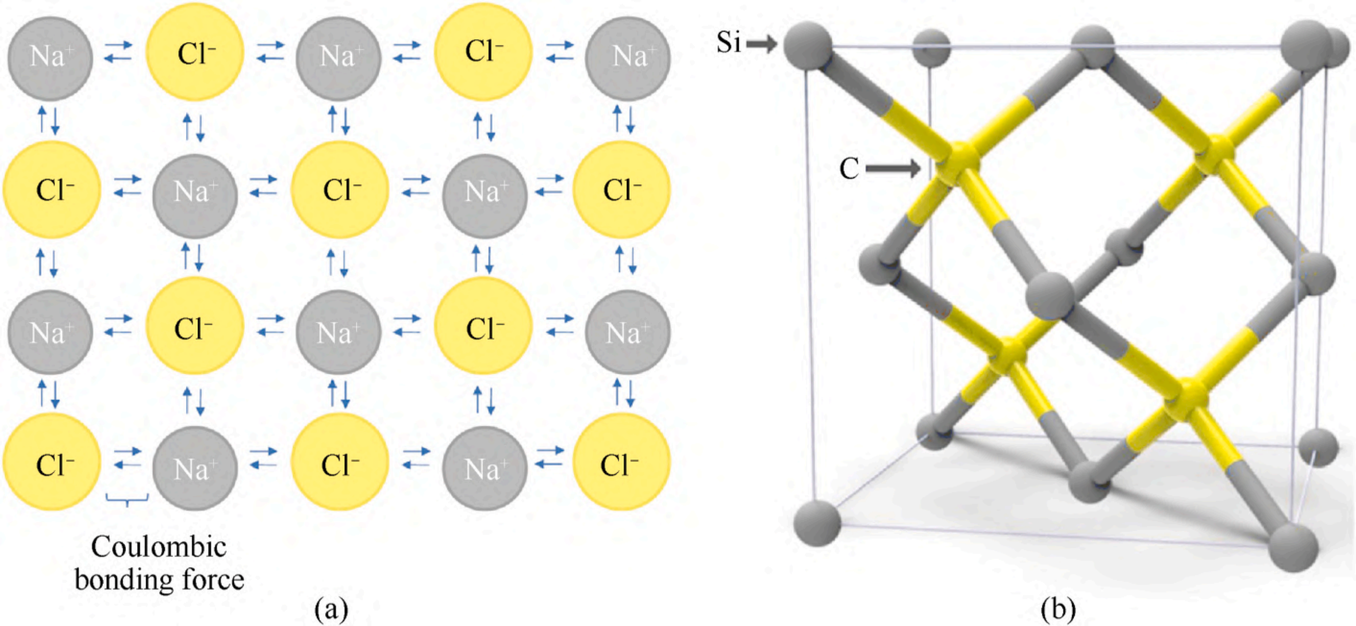
Na+
Cl-
Na+
Cl-
Na+
Cl-
Na+
Cl-
Na+
Cl-
Na+
Cl-
Na+
Cl-
Na+
Cl-
Na+
Cl-
Na+
Cl-
Coulombic bonding force
(a)
Si
C
(b)

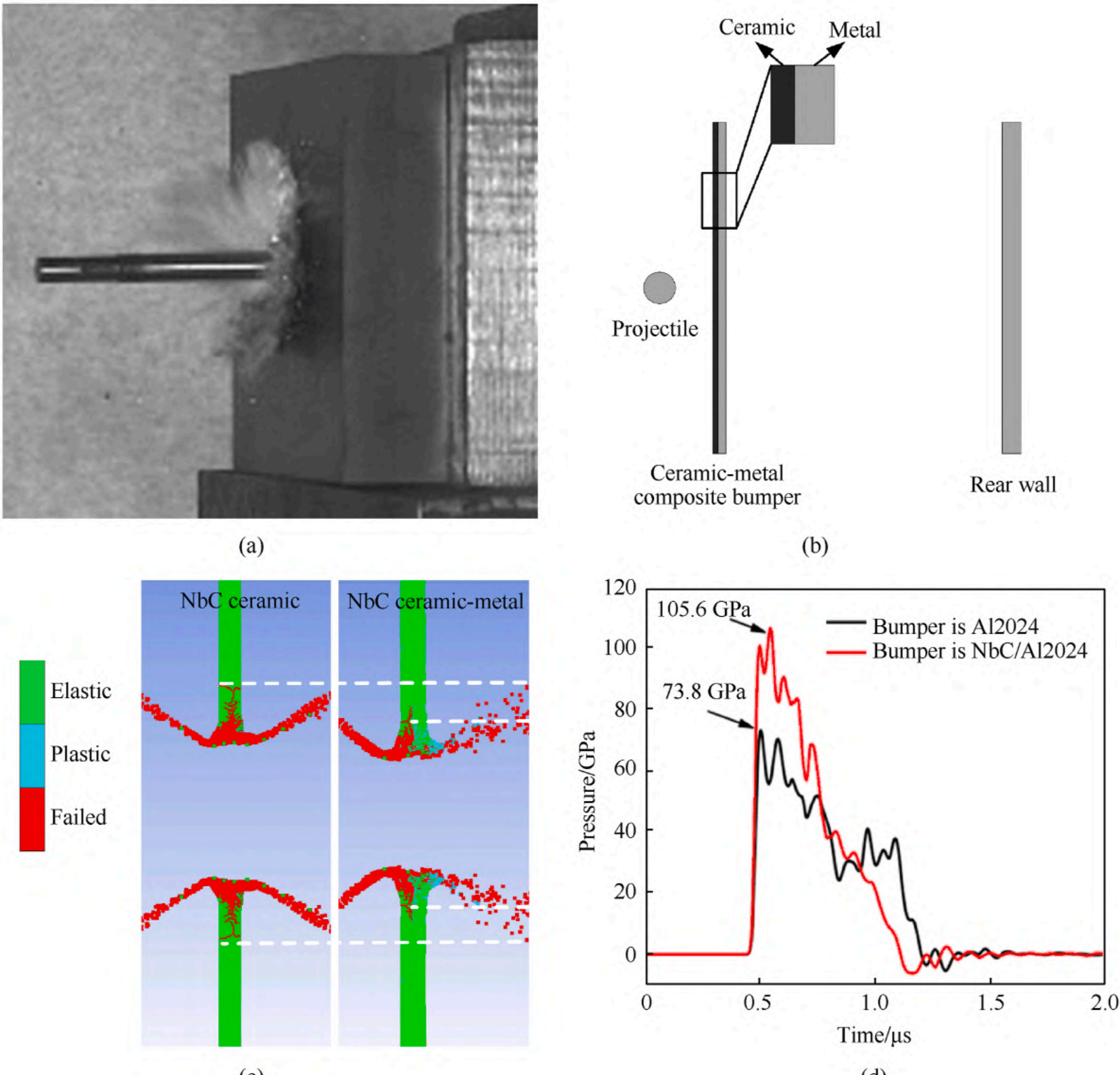

Ceramic
Metal
Projectile
Ceramic-metal composite bumper
Rear wall
NbC ceramic
NbC ceramic-metal
Elastic
Plastic
Failed
120
100
80
60
40
20
0
Pressure/GPa
105.6 GPa
73.8 GPa
Bumper is Al2024
Bumper is NbC/Al2024
0
0.5
1.0
1.5
2.0
Time/μs


(a)

(b)

(c)

(d)

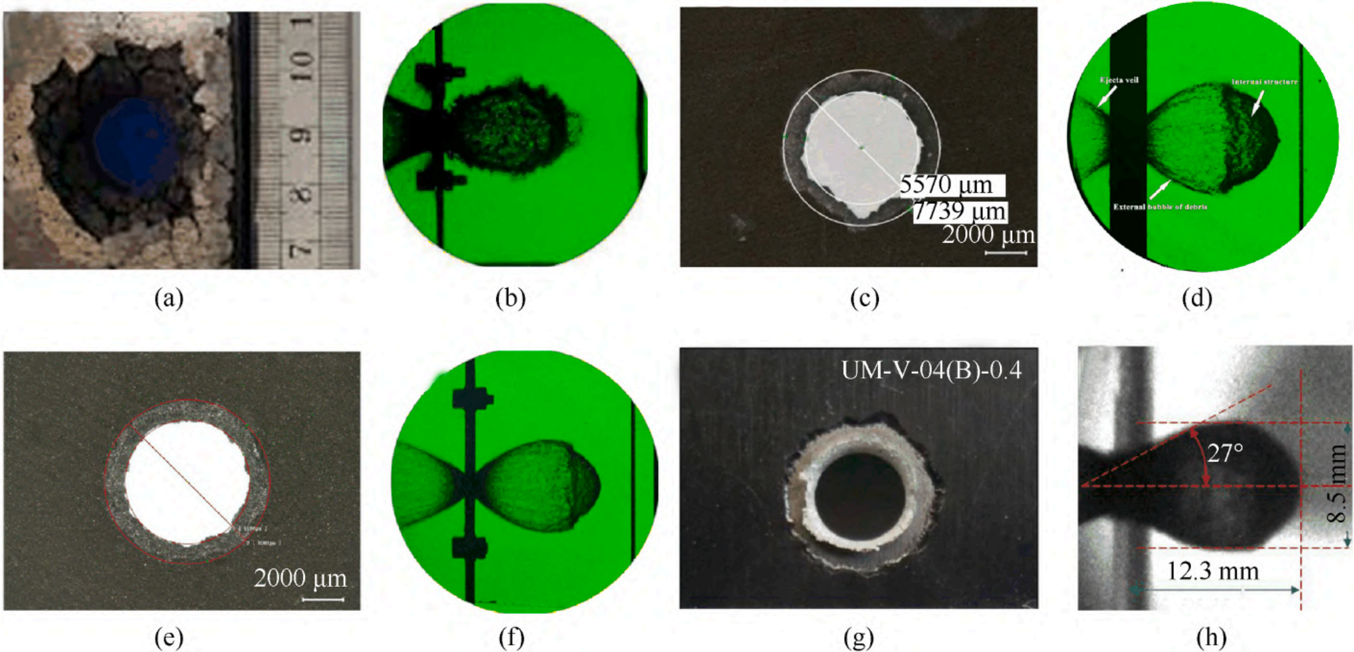
5570 µm
7739 µm
2000 µm
Ejecta veil
Internal structure
External bubble of debris
2000 µm
UM-V-04(B)-0.4
27°
8.5 mm
12.3 mm
(a)
(b)
(c)
(d)
(e)
(f)
(g)
(h)

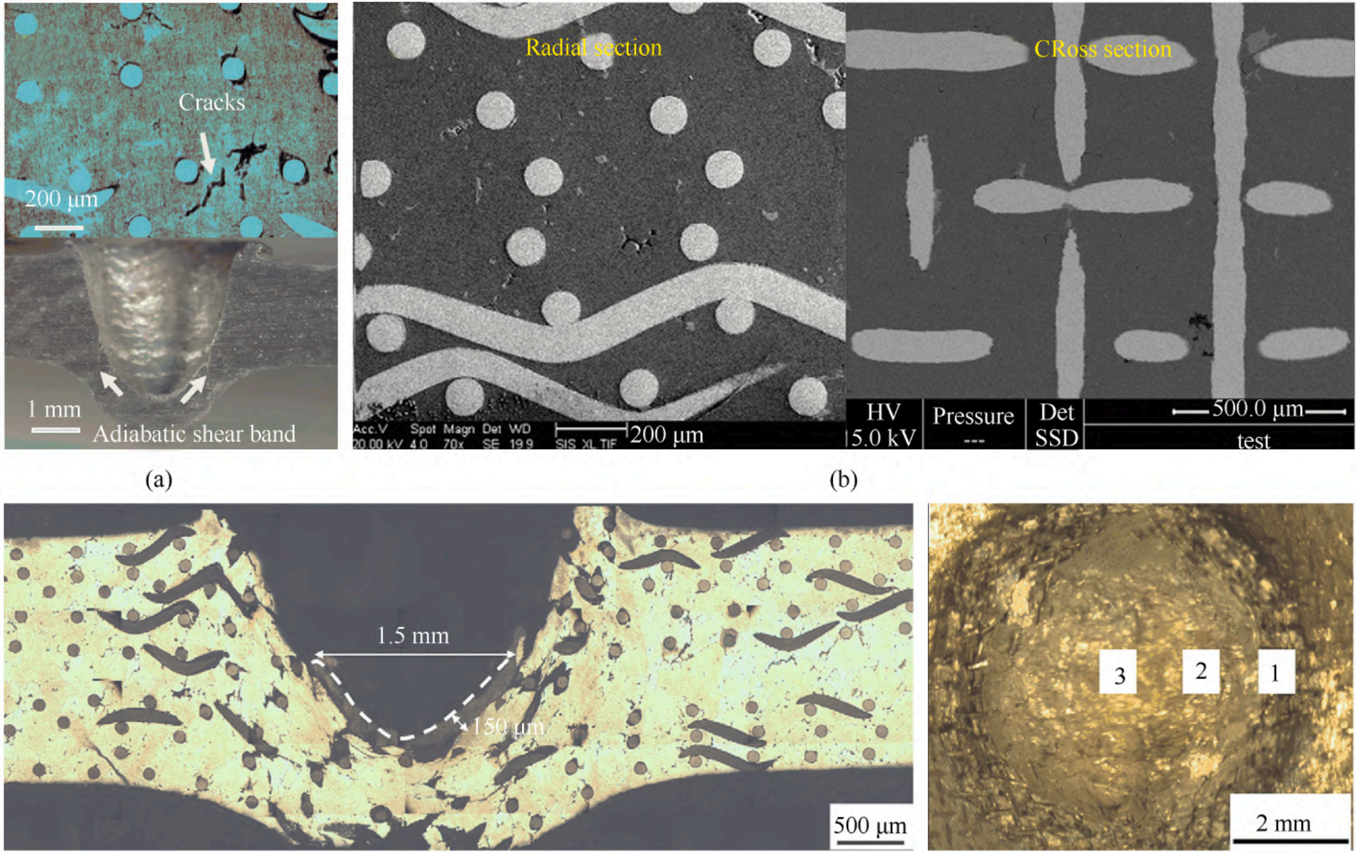
Cracks
200 μm
1 mm
Adiabatic shear band
Radial section
Acc.V Spot Magn Det WD
20.00 kV 4.0 70x SE 19.9
SIS XL TIF
200 μm
CRoss section
HV
15.0 kV
Pressure
---
Det
SSD
500.0 μm
test
1.5 mm
150 μm
500 μm
3
2
1
2 mm

(a) (b) (c) (d)

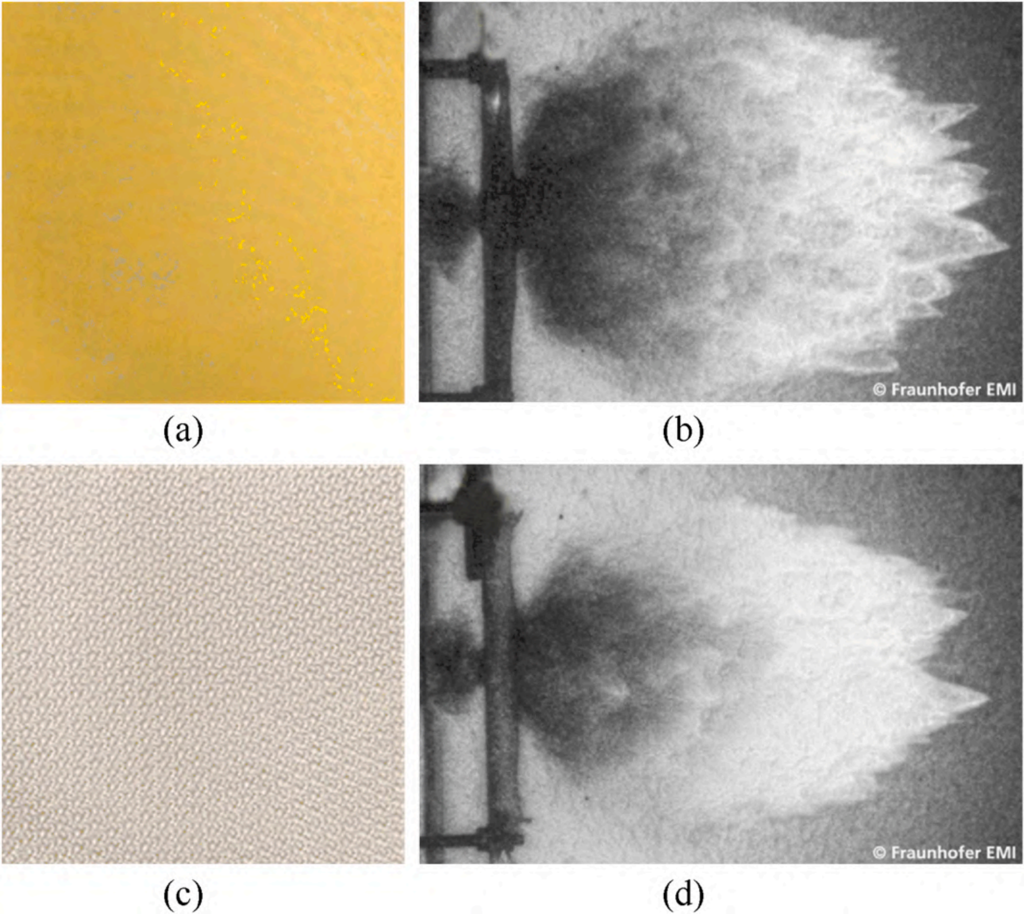
© Fraunhofer EMI
(a)
(b)
© Fraunhofer EMI
(c)
(d)

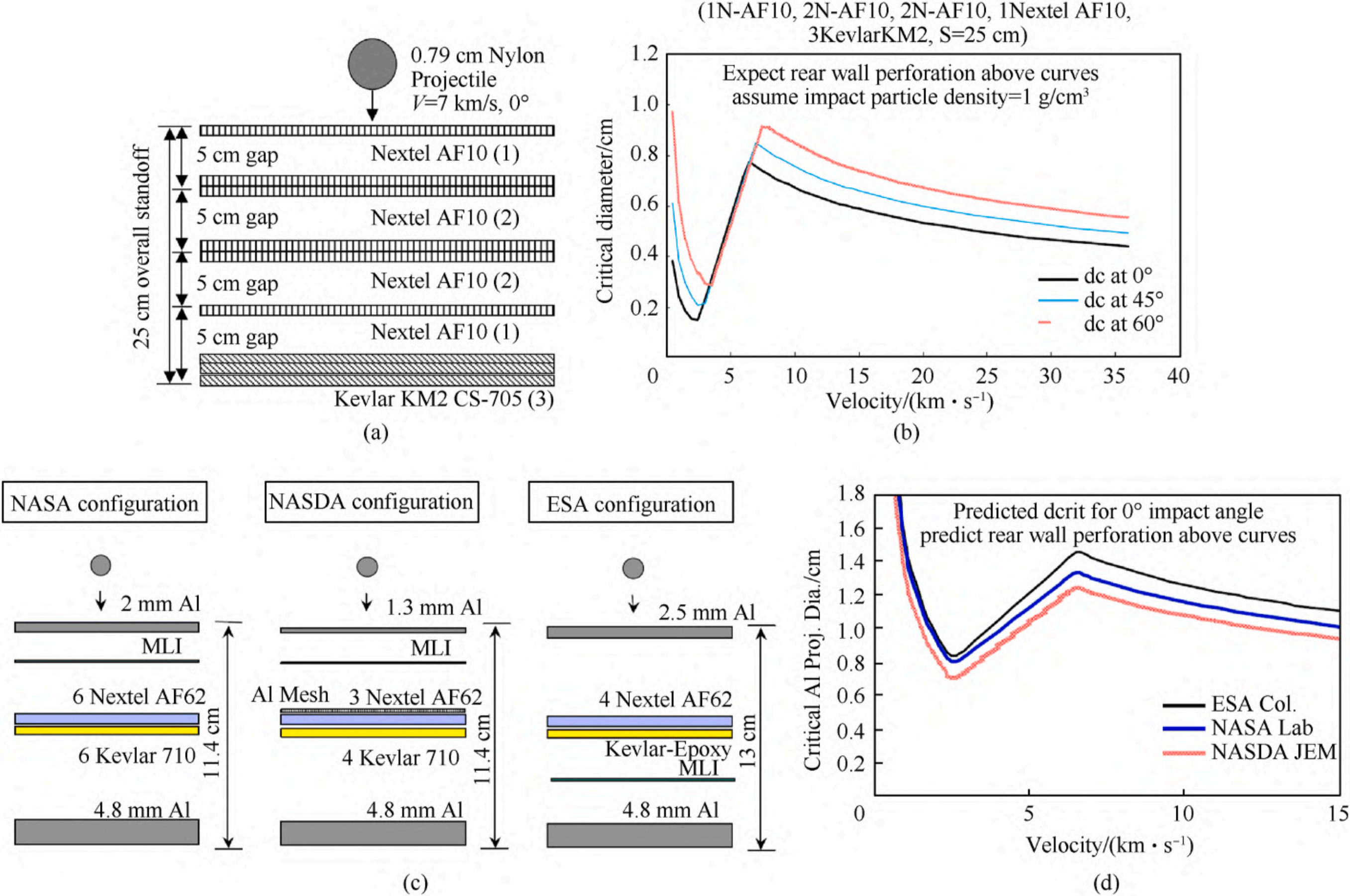
0.79 cm Nylon Projectile
V=7 km/s, 0°
25 cm overall standoff
5 cm gap
Nextel AF10 (1)
5 cm gap
Nextel AF10 (2)
5 cm gap
Nextel AF10 (2)
5 cm gap
Nextel AF10 (1)
Kevlar KM2 CS-705 (3)
(a)
(1N-AF10, 2N-AF10, 2N-AF10, 1Nextel AF10, 3KevlarKM2, S=25 cm)
Expect rear wall perforation above curves
assume impact particle density=1 g/cm³
Critical diameter/cm
Velocity/(km · s⁻¹)
dc at 0°
dc at 45°
dc at 60°
(b)
NASA configuration
2 mm Al
MLI
6 Nextel AF62
6 Kevlar 710
4.8 mm Al
11.4 cm
NASDA configuration
1.3 mm Al
MLI
Al Mesh
3 Nextel AF62
4 Kevlar 710
4.8 mm Al
11.4 cm
ESA configuration
2.5 mm Al
4 Nextel AF62
Kevlar-Epoxy
MLI
4.8 mm Al
13 cm
(c)
Predicted dcrit for 0° impact angle
predict rear wall perforation above curves
Critical Al Proj. Dia./cm
Velocity/(km · s⁻¹)
ESA Col.
NASA Lab
NASDA JEM
(d)

| | |
|---|---|
| External bumper (WS) | Al6061-T6, 2.5 mm |
| Intermediate bumper (stuffing) | Nextel 312 AF-62, 4 layers; Kevlar 129 Style 812 18 plies with Epoxy resin Brochier 914.6 mm |
| Back wall (BW) | Al 2219-T851, 4.8 mm |
| Intermediate spacing | 7 cm |
| Overall spacing | 13 cm |
| Overall area density | 3.2 g/cm$^2$ |

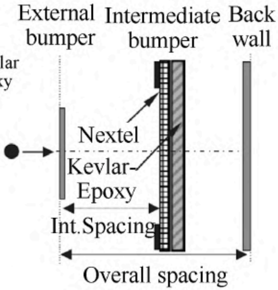


(a)

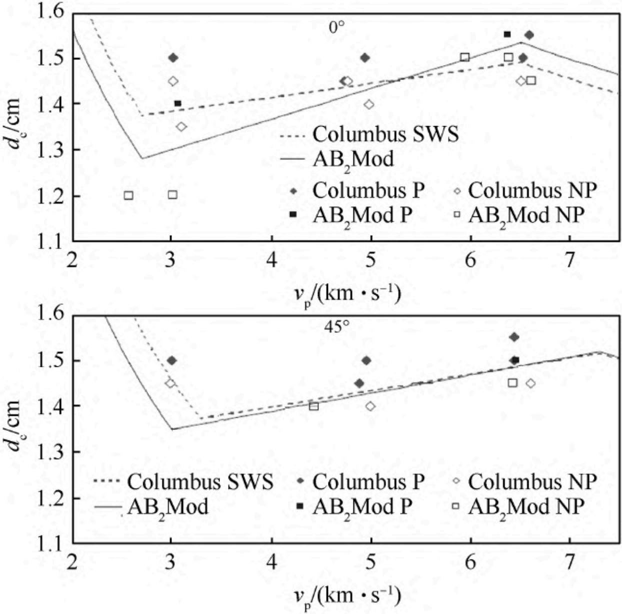


(b)

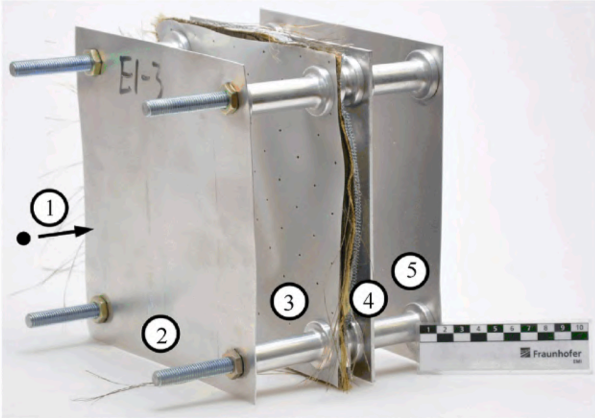

E1-3
1
2
3
4
5
1 2 3 4 5 6 7 8 9 10
Fraunhofer
EMI


(a)

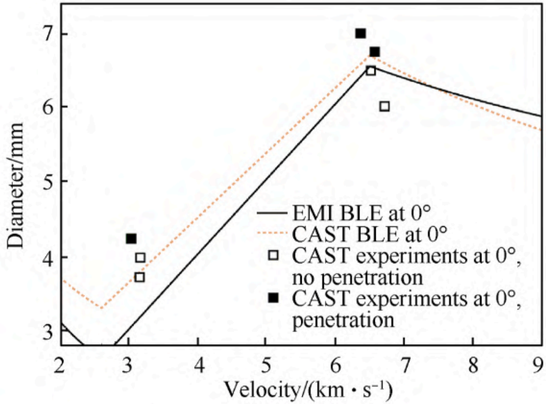

Diameter/mm
Velocity/(km · s⁻¹)
EMI BLE at 0°
CAST BLE at 0°
CAST experiments at 0°, no penetration
CAST experiments at 0°, penetration


(b)

(c)

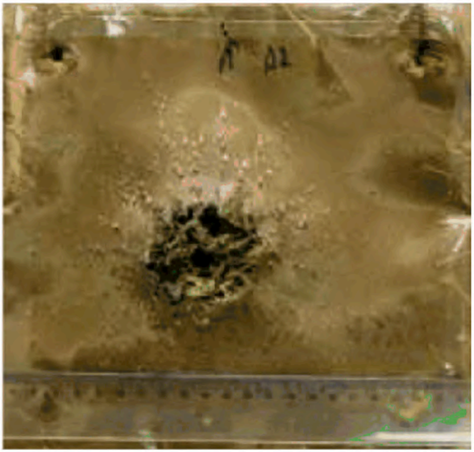

(d)

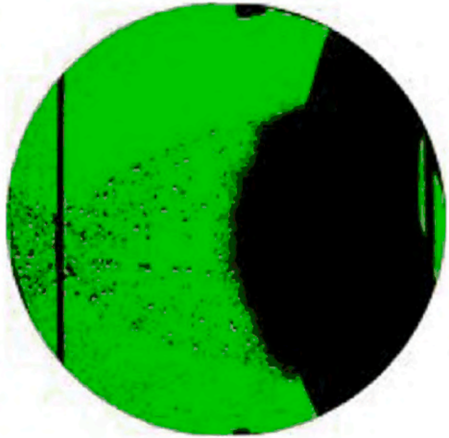

(e)

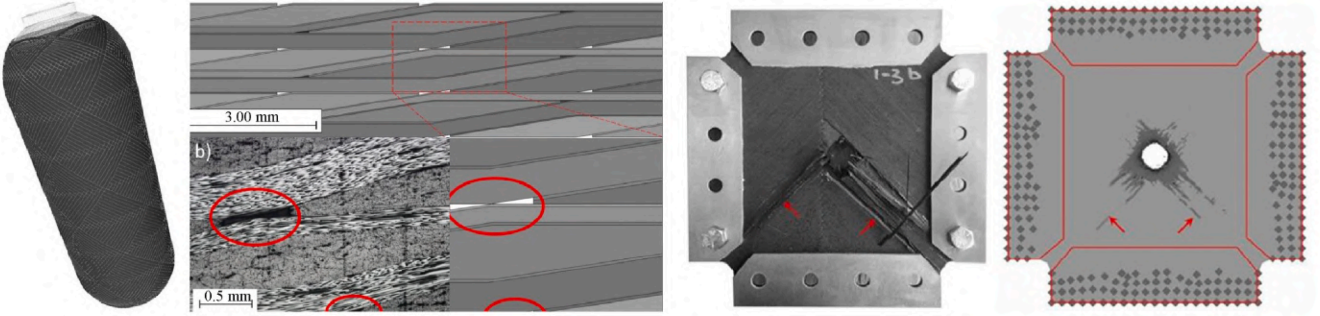

3.00 mm
b)
0.5 mm
1-3b


(a) (b) (c)

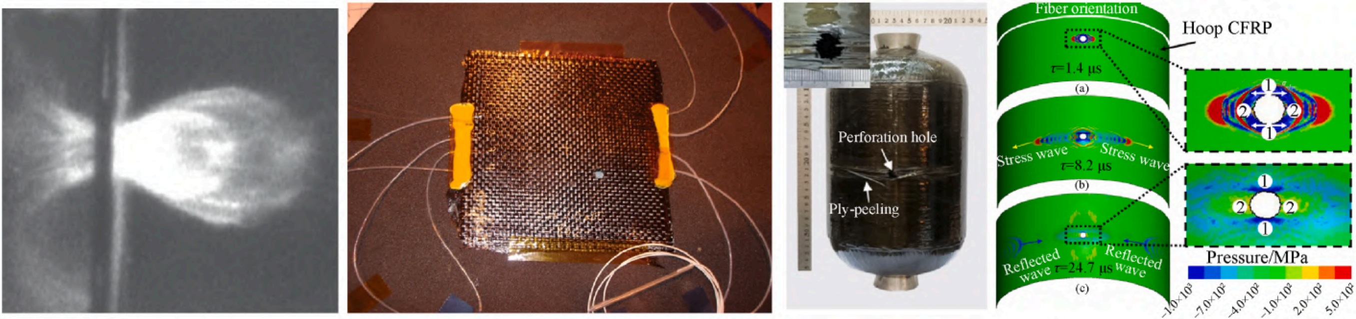

Perforation hole
Ply-peeling
Fiber orientation
Hoop CFRP
τ=1.4 μs
(a)
Stress wave
Stress wave
τ=8.2 μs
(b)
Reflected wave
Reflected wave
τ=24.7 μs
(c)
Pressure/MPa
−1.0×10³
−7.0×10²
−4.0×10²
−1.0×10²
2.0×10²
5.0×10²


(d) (e) (f)

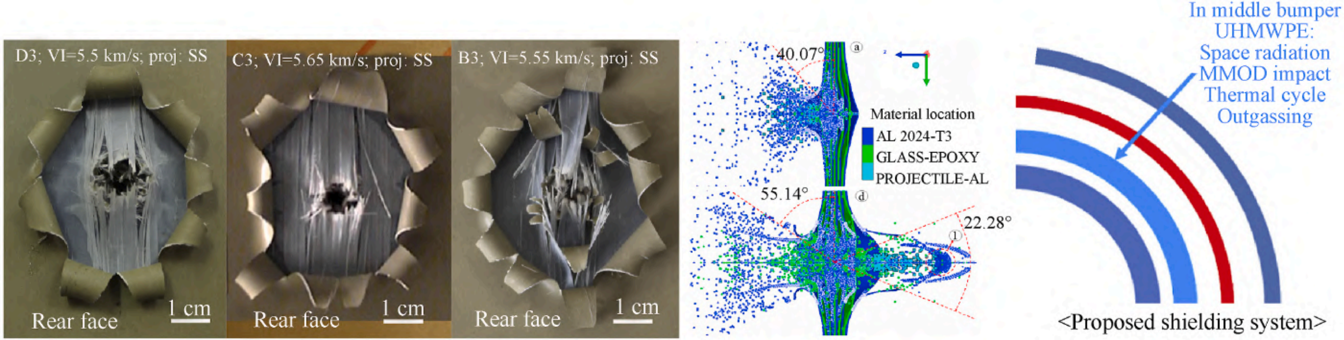
D3; VI=5.5 km/s; proj: SS
C3; VI=5.65 km/s; proj: SS
B3; VI=5.55 km/s; proj: SS
Rear face
1 cm
Rear face
1 cm
Rear face
1 cm
40.07°
55.14°
22.28°
Material location
AL 2024-T3
GLASS-EPOXY
PROJECTILE-AL
In middle bumper
UHMWPE:
Space radiation
MMOD impact
Thermal cycle
Outgassing
<Proposed shielding system>

(a) (b) (c)

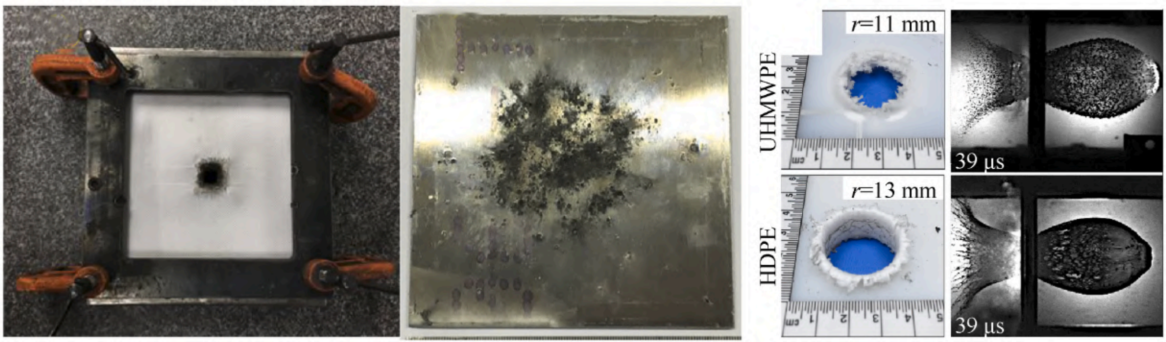
UHMWPE
r=11 mm
39 μs
HDPE
r=13 mm
39 μs

(d) (e) (f)

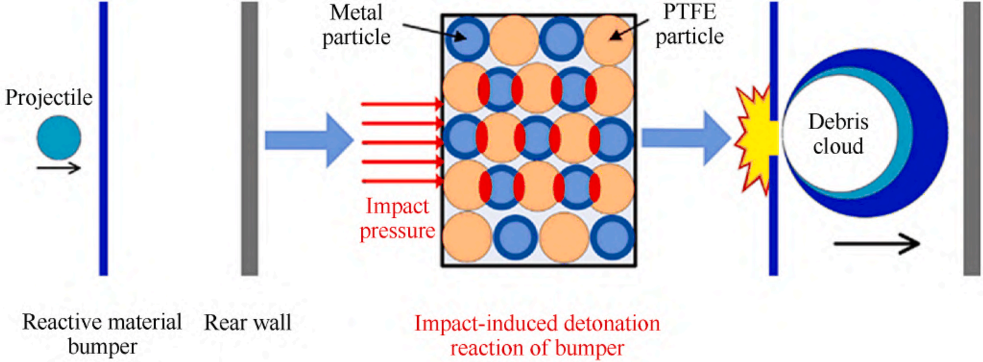
Metal particle
PTFE particle
Projectile
Impact pressure
Debris cloud
Reactive material bumper
Rear wall
Impact-induced detonation reaction of bumper

(a)

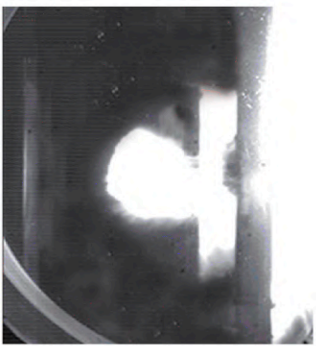

(b)

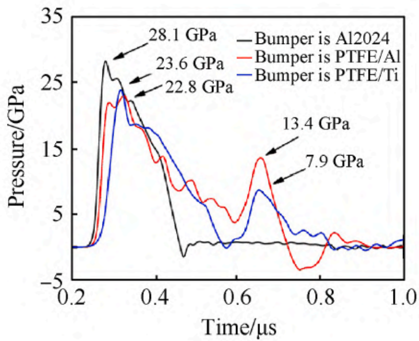
Pressure/GPa
Time/μs
28.1 GPa
23.6 GPa
22.8 GPa
13.4 GPa
7.9 GPa
Bumper is Al2024
Bumper is PTFE/Al
Bumper is PTFE/Ti
35
25
15
5
−5
0.2
0.4
0.6
0.8
1.0

(c)

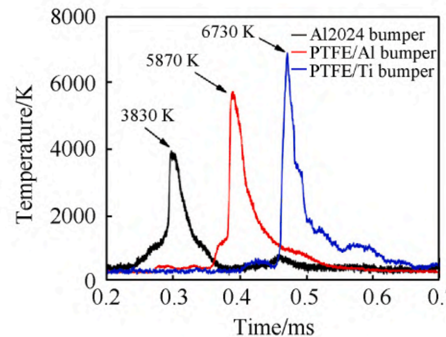
Temperature/K
Time/ms
6730 K
5870 K
3830 K
Al2024 bumper
PTFE/Al bumper
PTFE/Ti bumper
8000
6000
4000
2000
0
0.2
0.3
0.4
0.5
0.6
0.7

(d)

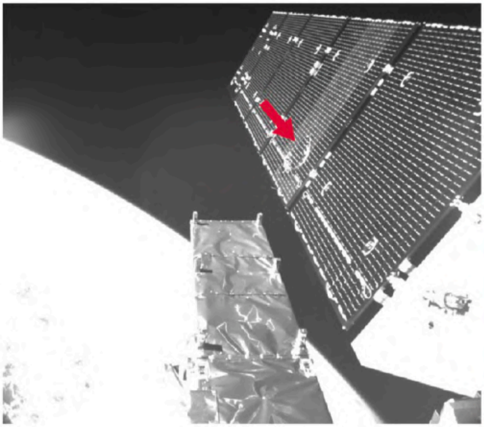

(a)

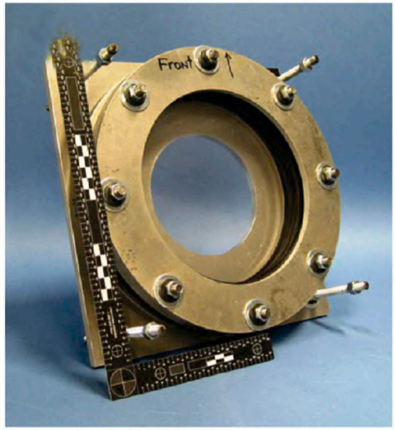


(b)

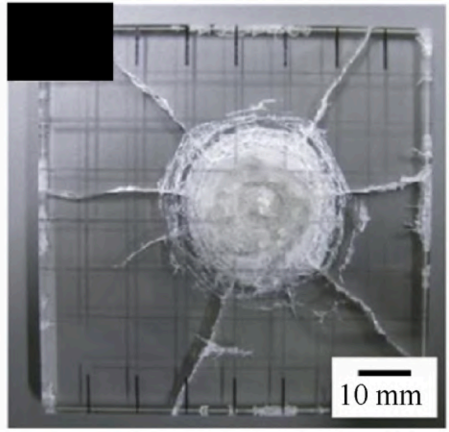


(c)

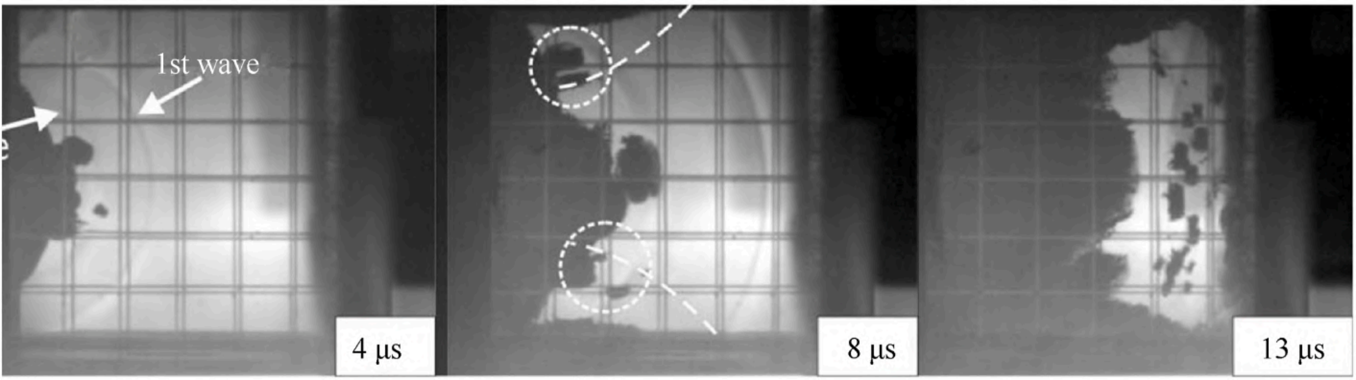


(d)

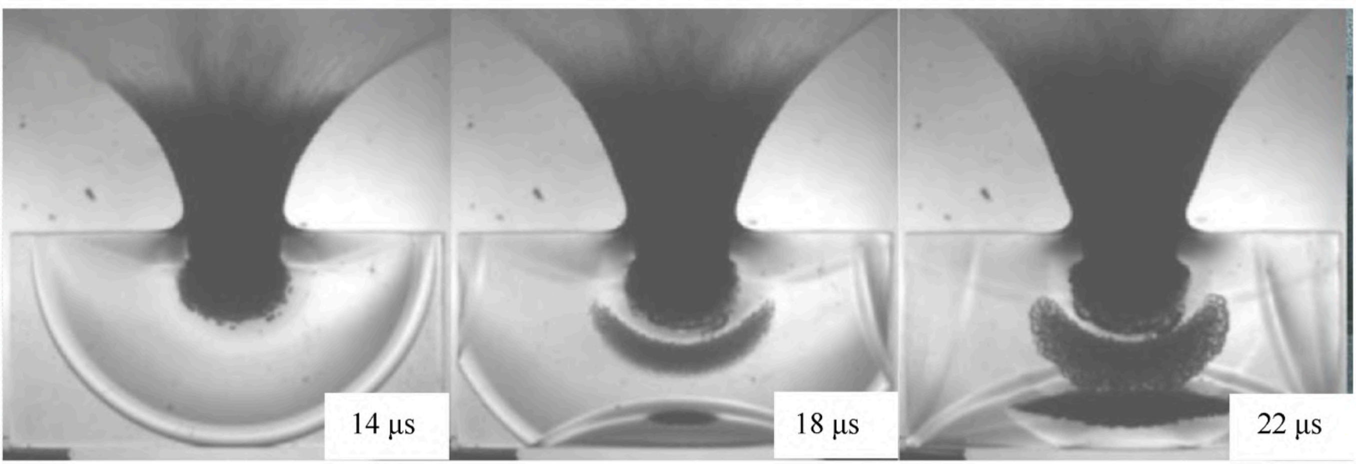


(e)

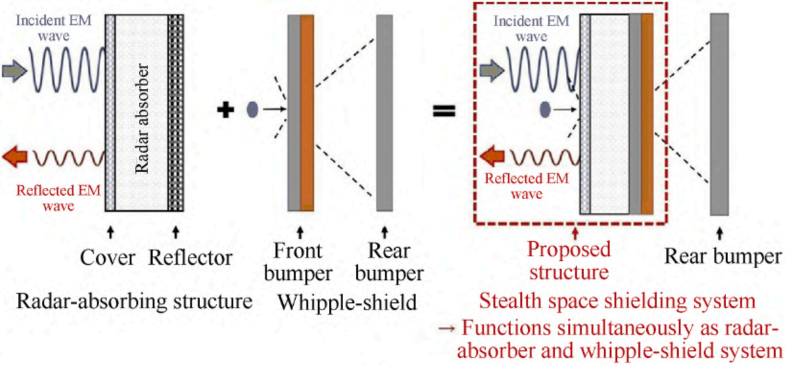
Incident EM wave
Radar absorber
Reflected EM wave
Cover
Reflector
Radar-absorbing structure
Front bumper
Rear bumper
Whipple-shield
Incident EM wave
Reflected EM wave
Proposed structure
Rear bumper
Stealth space shielding system
→ Functions simultaneously as radar-absorber and whipple-shield system

(a)

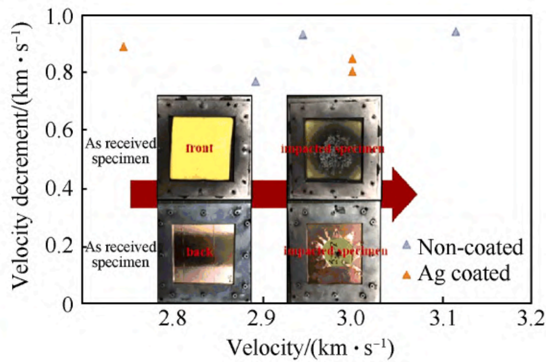
Velocity decrement/(km · s⁻¹)
1.0
0.8
0.6
0.4
0.2
0
As received specimen
front
impacted specimen
As received specimen
back
impacted specimen
Non-coated
Ag coated
2.8
2.9
3.0
3.1
3.2
Velocity/(km · s⁻¹)

(b)

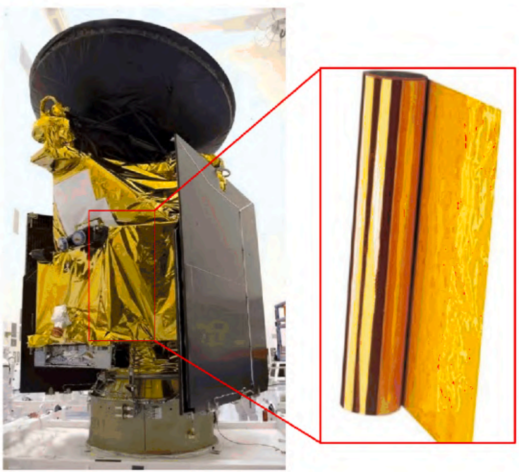

(c)

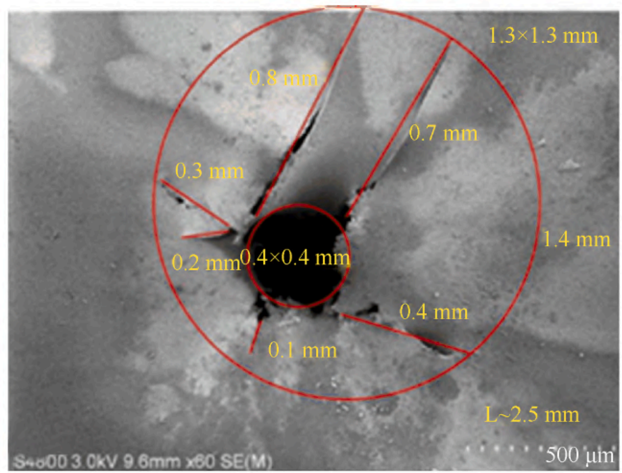
1.3×1.3 mm
0.8 mm
0.7 mm
0.3 mm
1.4 mm
0.2 mm
0.4×0.4 mm
0.4 mm
0.1 mm
L~2.5 mm
S4800 3.0kV 9.6mm x60 SE(M)
500 μm

(d)

| | Advantage | Disadvantage |
|---|---|---|
| Lagrange | ➢ Simple grid division<br>➢ High computational efficiency | ➢ Unable to form debris cloud<br>➢ Large grid distortion<br>➢ Energy and quality loss |
| Euler | ➢ Liquid computing<br>➢ High computational efficiency | ➢ Not applicable to solid impact |
| SPH | ➢ Solved grid distortion<br>➢ No energy and mass loss<br>➢ High calculation accuracy | ➢ Low efficiency in large-scale computing<br>➢ Difficult to identify fragment boundaries |
| FEM-SPH | ➢ High computational efficiency<br>➢ Easy to identify fragment boundaries | ➢ Set failure algorithm conversion<br>➢ Additional adaptive coupling algorithm |
| MPM | ➢ Solved grid distortion<br>➢ High computational efficiency<br>➢ Avoid dealing with convective terms | ➢ Noise induced by particle crossing the grid<br>➢ Slightly low computational accuracy |
| ALE | ➢ Solved grid distortion<br>➢ Fluid solid coupling calculation<br>➢ High calculation accuracy | ➢ Low computational efficiency<br>➢ Low calculation accuracy<br>➢ Difficult to identify fragment boundaries |

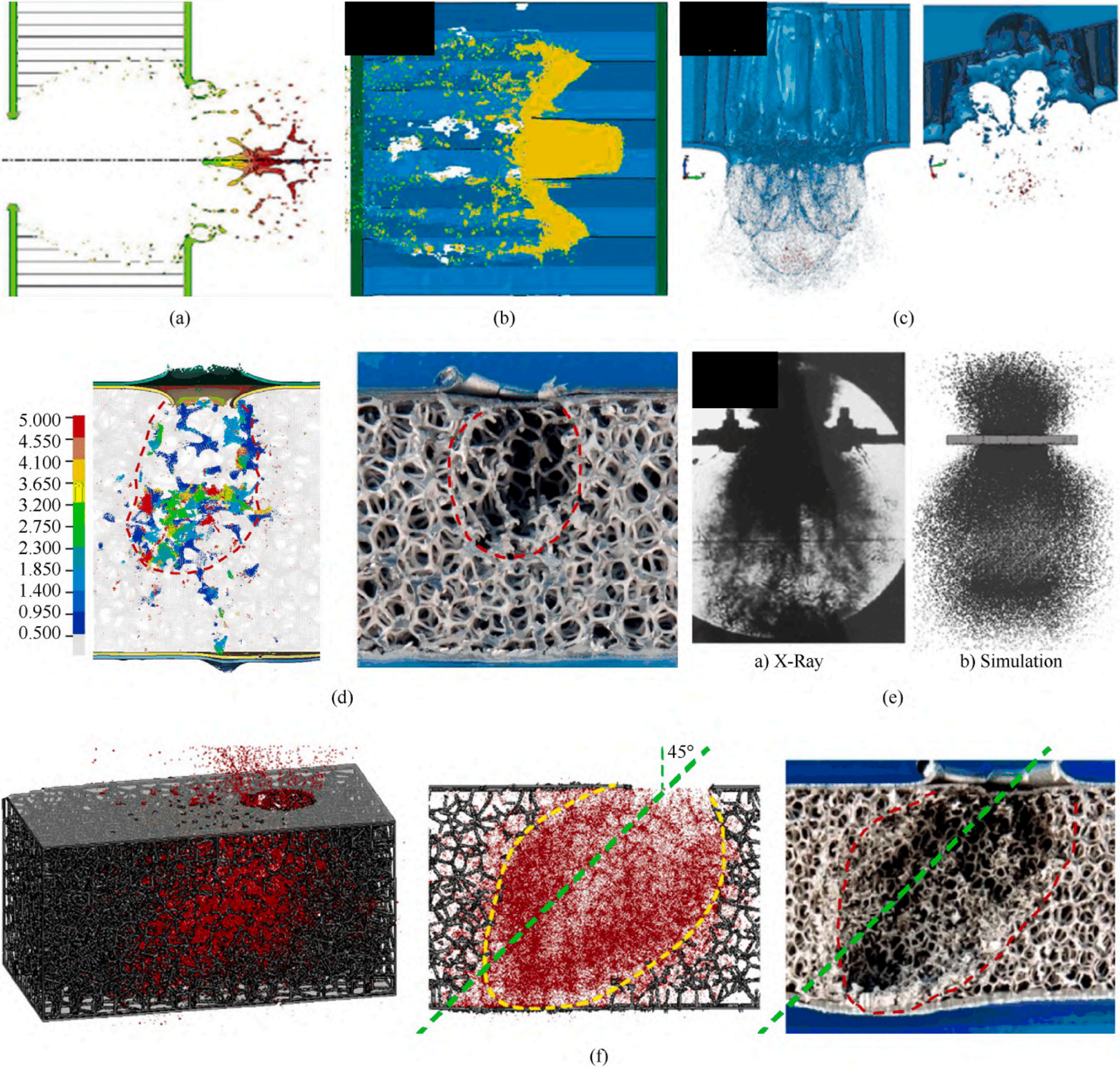

[redacted]
(a)
(b)
(c)
5.000
4.550
4.100
3.650
3.200
2.750
2.300
1.850
1.400
0.950
0.500
a) X-Ray
b) Simulation
(d)
(e)
45°
(f)

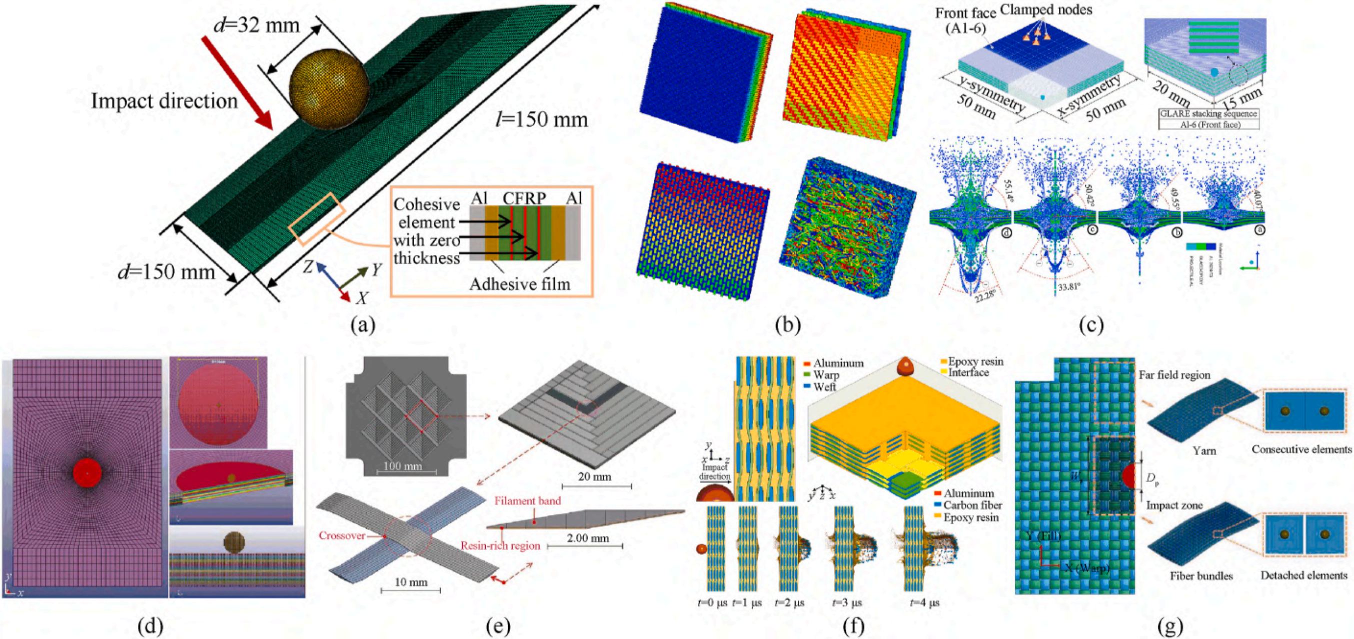

d=32 mm
Impact direction
l=150 mm
d=150 mm
Cohesive element with zero thickness
Al
CFRP
Al
Adhesive film
Z
Y
X
(a)
(b)
Front face (A1-6)
Clamped nodes
y-symmetry
50 mm
x-symmetry
50 mm
20 mm
15 mm
GLARE stacking sequence
Al-6 (Front face)
55.14°
50.42°
49.55°
40.07°
22.28°
33.81°
(c)
(d)
100 mm
20 mm
Filament band
Crossover
Resin-rich region
2.00 mm
10 mm
(e)
Aluminum
Warp
Weft
Epoxy resin
Interface
Impact direction
Aluminum
Carbon fiber
Epoxy resin
t=0 μs
t=1 μs
t=2 μs
t=3 μs
t=4 μs
(f)
Far field region
Yarn
Consecutive elements
Impact zone
Y (Fill)
X (Warp)
Fiber bundles
Detached elements
(g)

**Declaration of interests**

☒The authors declare that they have no known competing financialinterestsor personal relationships that could have appeared to influence the work reported in this paper.

☐The authors declare the following financial interests/personal relationships which may be considered as potential competing interests: